

# UC Santa Cruz

## UC Santa Cruz Electronic Theses and Dissertations

### Title

A multi-tracer approach to constraining hydrological and biogeochemical processes in aquatic environments of central California

### Permalink

<https://escholarship.org/uc/item/6dc286m8>

### Author

Richardson, Christina M

### Publication Date

2020

### Copyright Information

This work is made available under the terms of a Creative Commons Attribution-NonCommercial-NoDerivatives License, available at <https://creativecommons.org/licenses/by-nc-nd/4.0/>

Peer reviewed|Thesis/dissertation

UNIVERSITY OF CALIFORNIA  
SANTA CRUZ

**A MULTI-TRACER APPROACH TO CONSTRAINING HYDROLOGICAL  
AND BIOGEOCHEMICAL PROCESSES IN AQUATIC ENVIRONMENTS  
OF CENTRAL CALIFORNIA**

A dissertation submitted in partial satisfaction  
of the requirements of the degree of

DOCTOR OF PHILOSOPHY

in

EARTH SCIENCES

by

**Christina M. Richardson**

June 2020

This dissertation of Christina M. Richardson  
is approved:

---

Dr. Adina Paytan

---

Professor Andrew T. Fisher

---

Assistant Professor Margaret A. Zimmer

---

Quentin Williams  
Acting Vice Provost and Dean of Graduate Studies

Copyright © by  
Christina Michelle Richardson

## TABLE OF CONTENTS

ABSTRACT.....	x
ACKNOWLEDGEMENTS .....	xii
INTRODUCTION .....	1
Chapter 1 GEOLOGIC CONTROLS ON SOURCE WATER DRIVE BASEFLOW GENERATION AND CARBON GEOCHEMISTRY: EVIDENCE OF NON- STATIONARY BASEFLOW SOURCES ACROSS MULTIPLE SUBWATERSHEDS .....	8
Abstract .....	9
1.1 Introduction .....	10
1.2 Materials and Methods .....	14
1.2.1 Study area .....	14
1.2.2 Spatial analysis of subwatershed characteristics .....	15
1.2.3 Water sampling and stream gauging .....	16
1.2.4 Baseflow separation using endmember mixing analysis.....	17
1.2.5 Correlation analysis .....	21
1.3 Results .....	21
1.3.1 Analysis of subwatershed spatial characteristics.....	21
1.3.2 Baseflow magnitude and endmember contributions to streamflow .....	22
1.3.3 Relationship of baseflow magnitude and source to subwatershed characteristics .....	23
1.3.4 Stream water dissolved carbon geochemistry .....	24
1.4 Discussion .....	25
1.4.1 Geologic controls on non-stationarity in baseflow sources.....	25

1.4.2 Implications of shifting baseflow sources: an example using dissolved carbon geochemistry .....	28
1.5 Conclusions .....	32
Acknowledgements .....	34
References .....	35
Supplemental Index.....	52
 Chapter 2 LATERAL CARBON EXPORTS FROM DRAINED PEATLANDS: AN UNDERSTUDIED CARBON PATHWAY IN THE SACRAMENTO-SAN JOAQUIN DELTA, CALIFORNIA.....	 58
Abstract .....	59
2.1 Introduction .....	60
2.2 Methods.....	63
2.2.1 Study location.....	63
2.2.2 Geochemistry sample collection and analysis.....	65
2.2.3 Stable isotope sample collection and analysis.....	67
2.2.4 Discharge measurements, mass flux estimates, and net flux estimates.....	67
2.3 Results .....	71
2.3.1 Discharge trends from peat drainage outlets .....	71
2.3.2 Peat drainage geochemistry .....	72
2.3.3. Lateral C exports from drained peatlands .....	73
2.4 Discussion .....	75
2.4.1 Hydrological and biogeochemical controls on peat drainage C geochemistry.....	75
2.4.2 Transport driven lateral C losses from drained peatlands .....	81

2.4.3 Importance of lateral C exports in C budgets of drained peatlands .....	82
2.4.4 Annual variability in peat drainage C loads delivered to the Delta ecosystem .....	84
2.5 Conclusion.....	87
Acknowledgements .....	89
References .....	90
Supplemental Index.....	112
 Chapter 3 NUTRIENT AND TRACE METAL CONTRIBUTIONS FROM DRAINED ISLANDS IN THE SACRAMENTO-SAN JOAQUIN DELTA, CALIFORNIA .....	 120
Abstract .....	121
3.1 Introduction .....	122
3.2 Methods.....	128
3.2.1 Site description .....	128
3.2.2 Water analyses.....	129
3.2.3 Discharge, mass flux estimates, and net flux estimates.....	131
3.3 Results .....	135
3.3.1 Island drainage discharge and geochemistry .....	135
3.3.2 Island drainage nutrient and trace metal fluxes .....	137
3.4 Discussion .....	139
3.4.1 Controls on island drainage nutrient and trace metal composition .....	139
3.4.2 Island drainage nutrient and trace metal contributions to Delta waterways .....	144

3.4.3 Importance of island drainage nutrient contributions under a pre- and post-upgrade SRWTP scenario.....	148
3.4.4 Future recommendations .....	150
3.5 Summary .....	152
Acknowledgements .....	154
References .....	155
Supplemental Index.....	172
CONCLUSIONS.....	176

## LIST OF FIGURES AND TABLES

Figure 1-1. Geologic map of the San Lorenzo Watershed.....	42
Figure 1-2. San Lorenzo River specific discharge.....	43
Figure 1-3. Heatmap visualization of watershed characteristics. ....	43
Figure 1-4. Specific discharge for all streams. ....	44
Figure 1-5. Shallow subsurface water contributions to baseflow. ....	44
Figure 1-6. Shallow subsurface water and groundwater specific discharge through time. ....	45
Figure 1-7. Shallow subsurface water fractions versus bedrock permeability. ....	46
Figure 1-8. Groundwater fractions versus dissolved carbon geochemistry. ....	47
Figure 1-9. Conceptual diagram of baseflow generation processes. ....	48
Figure 1-10. DOC mixing relationships for each stream.....	49
Figure 1-11. Theoretical mixing of endmembers controlling dissolved carbon concentrations. ....	50
Table 1-1. Spearman’s rank of watershed characteristics and respective baseflow contributions. ....	51
Figure 2-1. Overview of the study area in the Delta.....	97
Figure 2-2. Monthly precipitation and discharge data from Delta islands. ....	98
Figure 2-3. $\text{Cl}^-$ and $\text{SiO}_4^{4-}$ concentrations versus water stable isotope values in peat drainage.....	99
Figure 2-4. Box plots of monthly peat drainage dissolved carbon geochemistry.....	100

Figure 2-5. Carbon stable isotope data for peat drainage. ....	101
Figure 2-6. Lateral carbon export relationships for each island. ....	102
Figure 2-7. Historical peat drainage carbon and groundwater elevation data. ....	103
Figure 2-8. Peat drainage carbon geochemistry.....	104
Figure 2-9. Conceptual diagram of seasonal changes in island hydrology and biogeochemistry.....	105
Figure 2-10. Regional comparison of carbon fluxes.....	106
Table 2-1. Mean annual river and peat drainage geochemistry. ....	107
Table 2-2. Seasonal means of peat drainage carbon geochemistry. ....	108
Table 2-3. Peat drainage carbon exports across two contrasting water years.....	109
Table 2-4. Comparison of lateral carbon exports to vertical carbon exports.....	110
Table 2-5. Delta wide island drainage C fluxes for WY 2017 and WY 2018. ....	111
Figure 3-1. Overview of the Delta and study islands.....	161
Figure 3-2. Box plots of monthly island drainage nutrient and trace metal concentrations. ....	162
Figure 3-3. Nitrogen stable isotope values for island drainage. ....	163
Figure 3-4. Monthly nitrogen fluxes from each island. ....	164
Figure 3-5. Breakdown of N species comprising total N in island drainage. ....	165
Figure 3-6. Trace metal geochemistry. ....	166
Figure 3-7. Pre- and post-upgrade regional dissolved N and P fluxes.....	167
Table 3-1. Mean annual river and island drainage geochemistry. ....	168

Table 3-2. Seasonal gross and net fluxes of nutrients and trace metals from island drainage.....	169
Table 3-3. Upscaled Delta-wide drainage nutrient and trace metal contributions....	170
Table 3-4. Upscaled Delta-wide seasonal gross and net island drainage fluxes into the Delta.....	171

## **ABSTRACT**

### **A Multi-Tracer Approach to Constraining Hydrological and Biogeochemical Processes in Aquatic Environments of Central California**

Christina M. Richardson

In California, local stressors on water quantity and quality are pervasive. This dissertation explores questions that can improve our understanding of water quality and quantity issues in two central California systems. Chapter 1 leverages the unique dry period of California's Mediterranean climate to better understand what water sources sustain critical low flow periods in a geologically complex watershed in central coastal California (San Lorenzo Watershed). Results from Chapter 1 show that both deep groundwater and shallow subsurface flow paths can contribute to baseflow during the summer dry down period, and that geology, specifically bedrock permeability, controls their relative contributions. This research adds to existing studies that are shifting traditional views on baseflow generation processes by showing low flow periods of hydrographs can be sustained by multiple water sources.

Chapter 2 and Chapter 3 investigate spatial and temporal variability of hydrological and biogeochemical processes in a highly altered estuary (the Sacramento-San Joaquin Delta). The Delta is comprised of over fifty peat islands that are drained for

commercial agriculture. Herein we refer to this outflow from Delta islands as peat drainage (Chapter 2) and island drainage (Chapter 3). Chapter 2 examines the magnitude of lateral carbon exports from peat drainage and possible controls on carbon release. Results from Chapter 2 can be used to account for a missing term in local carbon budgets. Chapter 3 explores nutrient and trace metal inputs from island drainage and the significance of island drainage mass fluxes relative to major inflows in the system. Results from Chapter 3 suggest that island drainage is an understudied source of nutrients and trace metals, with total nitrogen loads accounting for almost 1/6 of regional inputs during dry water years. Both Chapter 2 and Chapter 3 show that exports from Delta islands are water year and season dependent, highlighting the importance of accounting for multiple time scales in future assessments of mass fluxes in this system.

## **ACKNOWLEDGEMENTS**

I would like to thank my advisor, Dr. Adina Paytan, for her support and guidance throughout my studies. She gave me the freedom to explore a variety of my research interests, and I feel incredibly privileged to have worked with and alongside so many intelligent, strong, and driven women in science. I also thank my committee members and collaborators for their ongoing support and expertise. Finally, I thank my friends and family, who have all played an important role in shaping my ambitions and research interests. Jessica Smith helped lead me down this path, and this dissertation is in her memory.

## INTRODUCTION

Aquatic ecosystems face a growing number of challenges as anthropogenic stressors on freshwater resources increase worldwide. These stressors range in scale from local to global processes. Globally, climate change is altering water cycle processes, such as the amount and timing of precipitation, snowmelt, recharge, evapotranspiration, and river discharge (Bates et al., 2008). Locally, human impacts are driving a number of changes that impact both water quality and quantity. Over-extraction of groundwater and surface water has led to shortages in water supplies in many regions of the world, and these shortages are only expected to worsen in the face of climate change (Castle et al., 2014; Famiglietti, 2014; Wada & Bierkens, 2014). In addition to changes in water availability, widespread pollution of fresh waters is also driving environmental change in ecosystems around the world (Howarth et al., 2000; Woodward et al., 2012). Water-based conflicts can be traced back to early civilization (Priscoli, 2000), and modern-day water issues often occur at the crossroads of economic and ecologic needs (Layzer, 2013). This dissertation examines questions relating to both water quantity and quality in two central California systems that have important implications for both aquatic ecosystems and consumptive needs.

Ongoing water availability issues in California are expected to worsen from increases in precipitation volatility, with large annual swings that range from extreme drought to severe flooding (Polade et al., 2017; Wang et al., 2017). Extended dry periods are a

cornerstone of California's climate regime, both seasonally as part of its Mediterranean climate and annually to inter-annually from extended drought periods. Dry periods can persist for over six months of the year, and these extended dry periods allow for long-duration baseflow events in many Californian streams. Low flow periods are critically important to sustaining in-stream ecosystems and water needs for many communities of California. However, several questions remain about what water sources sustain stream flow during these dry down periods. Traditionally, low flow or baseflow periods of the hydrograph were assumed to be geochemically static components of streamflow that originate from a single groundwater source. More recent research on baseflow geochemistry and recession behavior suggests that multiple water sources may supply stream water during baseflow (Hale & McDonnell, 2016; Stoelzle et al., 2019; Zimmer et al., 2013). The first chapter of this dissertation provides supporting data that shows how geology, specifically bedrock permeability, controls water sources contributing to stream flow during low flow periods. These results, which shed light on water provenance during critical low flow periods, are informative for better understanding and predicting surface water availability in the face of increasing hydroclimatic variability projected for California and beyond (Swain et al., 2018).

Discussions of surface water availability in California center around the Sacramento-San Joaquin Delta, which supplies drinking water to over 27 million people and generates 1.6 billion dollars from agriculture (DPC, 2012). While the Delta is the hub

of California's water supply system, it also supports a range of ecosystem services that are declining in the face of widespread environmental change decade after decade (Cloern, 2019). The Delta is a complex and highly altered estuary comprised of over fifty drained peat islands. The Delta's drained peat islands are functionally similar to other degraded and drained peat systems, which are growing in number worldwide due to increasing human impacts. Drained peatlands can emit a substantial amount of greenhouse gasses, and many studies exist documenting vertical carbon emissions from the Delta's islands (Baldocchi et al., 2012; Hatala et al., 2012; Hemes et al., 2019; Hemes et al., 2018; Knox et al., 2015; Teh et al., 2011). The second chapter of this dissertation investigates lateral carbon fluxes from these islands, an important pathway for carbon loss that has been understudied in the Delta. This research builds on existing studies from other regions of the world that show degraded peatlands can export large amounts of carbon in dissolved and particulate forms (Limpens et al., 2008). Lateral carbon exports also have important implications for Delta water quality. High organic carbon concentrations in Delta water have been shown to lead to the formation of harmful disinfection by-products in drinking water exports (Fujii et al., 1998). Ecologically, carbon forms the base of the food web, and inventorying existing sources of organic matter in the Delta is also important to improving our understanding of why the Delta has seen widespread environmental changes that include a 74% decline in chlorophyll *a* concentrations since the 1970's (Cloern, 2019).

These dramatic ecological shifts in the Delta have also been accompanied by long-term water quality changes, including a fifty percent increase in  $\text{NH}_4^+$  and  $\text{NO}_3^-$  concentrations since 1975 (Cloern, 2019). The third chapter of this dissertation examines nutrient and trace metal exports from Delta islands to better understand the magnitude and regional significance of this understudied anthropogenic input. Nutrient concentrations in the Delta were historically thought to be at saturating levels for phytoplankton (Jassby et al., 2002), but more recent research has found that nutrient forms, ratios, and concentrations are important regulators of phytoplankton biomass, diversity, and primary productivity (Dugdale et al., 2015). This chapter's results provide new baseline estimates of Delta-wide drainage nutrient and trace metal fluxes that can be used to inform existing and future box models. More broadly, this research emphasizes the importance of explicitly examining mass fluxes at seasonal, annual, and interannual time scales in a system with direct water year dependence and in view of planned upgrades to the largest wastewater treatment plant discharging into the Delta.

Taken together, these three dissertation chapters show how constraining hydrologic processes in aquatic systems can help inform our understanding of biogeochemical processes. Exploring connections between hydrology and biogeochemical cycling can produce new insight into the fundamental role of water in carbon and nutrient transport, transformations, and fate. Improving our understanding of these coupled linkages is critically important for advancing both fields.

## References

- Baldocchi, D., Detto, M., Sonnentag, O., Verfaillie, J., Teh, Y. A., Silver, W., & Kelly, N. M. (2012). The challenges of measuring methane fluxes and concentrations over a peatland pasture. *Agricultural Forest Meteorology*, *153*, 177-187.
- Bates, B., Kundzewicz, Z., Wu, S., & Palutikof, J. (2008). Climate Change and Water Technical Paper of the Intergovernmental Panel on Climate Change VI.
- Castle, S. L., Thomas, B. F., Reager, J. T., Rodell, M., Swenson, S. C., & Famiglietti, J. S. (2014). Groundwater depletion during drought threatens future water security of the Colorado River Basin. *Geophysical Research Letters*, *41*(16), 5904-5911.
- Cloern, J. E. (2019). Patterns, pace, and processes of water-quality variability in a long-studied estuary. *Limnology and Oceanography*, *64*(S1), S192-S208.
- DPC. (2012). Economic Sustainability Plan for the Sacramento-San Joaquin Delta. A report prepared for the Delta Protection Commission.
- Dugdale, R., Wilkerson, F., & Parker, A. E. (2015). The “Ammonium Paradox”: A Summary of More than a Decade of Research into Phytoplankton Processes and Nitrogen Relationships in the Northern San Francisco Estuary. Suisun Synthesis II Report Section 2. Prepared for the San Francisco Bay Nutrient Management Strategy.
- Famiglietti, J. S. (2014). The global groundwater crisis. *Nature Climate Change*, *4*(11), 945-948.
- Fujii, R., Ranalli, A. J., Aiken, G. R., & Bergamaschi, B. A. (1998). Dissolved organic carbon concentrations and compositions, and trihalomethane formation potentials in waters from agricultural peat soils, Sacramento-San Joaquin Delta, California: Implications for drinking-water quality. *U.S. Geological Survey Water-Resources Investigations Report 98-4147*, 75 p.
- Hale, V. C., & McDonnell, J. J. (2016). Effect of bedrock permeability on stream base flow mean transit time scaling relations: 1. A multiscale catchment intercomparison. *Water Resources Research*, *52*(2), 1358-1374. <Go to ISI>://WOS:000373117300042
- Hatala, J., Detto, M., Sonnentag, O., Deverel, S., Verfaillie, J., & Baldocchi, D. (2012). Greenhouse gas (CO<sub>2</sub>, CH<sub>4</sub>, H<sub>2</sub>O) fluxes from drained and flooded

agricultural peatlands in the Sacramento-San Joaquin Delta. *Agriculture, Ecosystems & Environment*.

- Hemes, K. S., Chamberlain, S. D., Eichelmann, E., Anthony, T., Valach, A., Kasak, K., et al. (2019). Assessing the carbon and climate benefit of restoring degraded agricultural peat soils to managed wetlands. *Agricultural Forest Meteorology*, 268, 202-214.
- Hemes, K. S., Chamberlain, S. D., Eichelmann, E., Knox, S. H., & Baldocchi, D. D. (2018). A biogeochemical compromise: The high methane cost of sequestering carbon in restored wetlands. *Geophysical Research Letters*, 45(12), 6081-6091.
- Howarth, R. W., Anderson, D., Cloern, J. E., Elfring, C., Hopkinson, C. S., Lapointe, B., et al. (2000). Nutrient pollution of coastal rivers, bays, and seas. *Issues in Ecology*.
- Jassby, A. D., Cloern, J. E., & Cole, B. E. (2002). Annual primary production: Patterns and mechanisms of change in a nutrient-rich tidal ecosystem. *Limnology and Oceanography*, 47(3), 698-712.
- Knox, S. H., Sturtevant, C., Matthes, J. H., Koteen, L., Verfaillie, J., & Baldocchi, D. (2015). Agricultural peatland restoration: effects of land-use change on greenhouse gas (CO<sub>2</sub> and CH<sub>4</sub>) fluxes in the Sacramento-San Joaquin Delta. *Global Change Biology*, 21(2), 750-765.
- Layzer, J. A. (2013). Using science to restore California's Bay-Delta. *San Francisco Estuary and Watershed Science*, 11(3).
- Limpens, J., Berendse, F., Blodau, C., Canadell, J., Freeman, C., Holden, J., et al. (2008). Peatlands and the carbon cycle: from local processes to global implications—a synthesis. *Biogeosciences*, 5(5), 1475-1491.
- Polade, S. D., Gershunov, A., Cayan, D. R., Dettinger, M. D., & Pierce, D. W. (2017). Precipitation in a warming world: Assessing projected hydro-climate changes in California and other Mediterranean climate regions. *Scientific Reports*, 7(1), 1-10.
- Priscoli, J. D. (2000). Water and civilization: using history to reframe water policy debates and to build a new ecological realism. *Water Policy*, 1(6), 623-636.
- Stoelzle, M., Schuetz, T., Weiler, M., Stahl, K., & Tallaksen, L. M. (2019). Beyond binary baseflow separation: delayed flow index as a fresh perspective on streamflow contributions. *Journal of Hydrology and Earth System Sciences Discussions*, pp.1-30.

- Swain, D. L., Langenbrunner, B., Neelin, J. D., & Hall, A. (2018). Increasing precipitation volatility in twenty-first-century California. *Nature Climate Change*, 8(5), 427-+. <Go to ISI>://WOS:000431139900027
- Teh, Y. A., Silver, W. L., Sonnentag, O., Detto, M., Kelly, M., & Baldocchi, D. (2011). Large greenhouse gas emissions from a temperate peatland pasture. *Ecosystems*, 14(2), 311-325.
- Wada, Y., & Bierkens, M. F. (2014). Sustainability of global water use: past reconstruction and future projections. *Environmental Research Letters*, 9(10), 104003.
- Wang, S.-Y. S., Yoon, J.-H., Becker, E., & Gillies, R. (2017). California from drought to deluge. *Nature Climate Change*, 7(7), 465.
- Woodward, G., Gessner, M. O., Giller, P. S., Gulis, V., Hladyz, S., Lecerf, A., et al. (2012). Continental-scale effects of nutrient pollution on stream ecosystem functioning. *Science*, 336(6087), 1438-1440.
- Zimmer, M. A., Bailey, S. W., McGuire, K. J., & Bullen, T. D. (2013). Fine scale variations of surface water chemistry in an ephemeral to perennial drainage network. *Hydrological Processes*, 27(24), 3438-3451. <Go to ISI>://WOS:000325989300007

## **Chapter 1**

# **GEOLOGIC CONTROLS ON SOURCE WATER DRIVE BASEFLOW GENERATION AND CARBON GEOCHEMISTRY: EVIDENCE OF NON- STATIONARY BASEFLOW SOURCES ACROSS MULTIPLE SUBWATERSHEDS**

Richardson, C. M., M. A. Zimmer, J. K. Fackrell, and A. Paytan. 2020. Geologic controls on source water drive baseflow generation and carbon geochemistry: evidence of nonstationary baseflow sources across multiple subwatersheds. *Water Resources Research*.

## **Abstract**

The contributions and composition of baseflow sources across an extended recession period were quantified for six subwatersheds of varying size in a structurally complex watershed in coastal California using endmember mixing analysis and related to catchment characteristics (e.g., topography, geology, land use, and soil characteristics). Both shallow subsurface and deep groundwater reservoirs were important contributors for streamflow during low flow periods, and the composition of baseflow sources across subwatersheds was directly related to geologic indices. A binary classification of underlying bedrock permeability (e.g., low versus high) best explained the changes in shallow subsurface water and deeper groundwater inputs through the seasonal recession. Dissolved inorganic carbon (DIC), dissolved organic carbon (DOC), and specific UV absorbance at 254 nm ( $SUVA_{254}$ ) were used to provide additional insight into endmember characteristics and their contributions to baseflow. Stream water DIC concentrations were broadly controlled by mixing of groundwater and shallow subsurface water endmembers with relatively constant DIC concentrations, while stream water DOC concentrations reflected both spatial and temporal changes in shallow subsurface water DOC. Results from this study show (1) the importance of considering baseflow as a dynamic mixture of water from multiple sources, (2) the effect of geology on source composition at the subwatershed scale during low flow conditions, and (3) the impact of shifting baseflow sources on stream water dissolved carbon concentrations and the utility of using

dissolved carbon concentrations to obtain additional insight into temporal variability in baseflow sources.

## **1.1 Introduction**

Structural characteristics of watersheds (e.g., area, slope, bedrock type) have been used to aid in understanding and predicting streamflow generation in many systems (Jencso & McGlynn, 2011; McGuire et al., 2005; Price, 2011). Most work relating watershed characteristics to streamflow generation focuses on dynamic periods of the annual hydrograph (rainfall events or snowmelt periods), and knowledge gaps still exist regarding controls on baseflow. Baseflow is often characterized as a geochemically static component of streamflow that is sustained by regional groundwater (Klaus & McDonnell, 2013). This characterization of baseflow as temporally uniform and spatially homogenous may be inappropriate for many systems.

Previous work has documented significant spatial variability in stream geochemistry during low flow periods (Asano et al., 2009; Blumstock et al., 2015; Soulsby et al., 2007; Temnerud et al., 2010; Tetzlaff & Soulsby, 2008; Zimmer et al., 2013). Variability in stream geochemistry across stream networks during low flow periods is often indicative of multiple source waters, which typically have distinct endmember chemistry due to differences in routing and storage in the subsurface (Payn et al., 2012). Blumstock et al. (2015) found that stream water chemistry of a montane watershed became increasingly

heterogeneous as baseflow progressed, suggesting groundwater contributions from multiple geochemically distinct hydrological units. Others also found that several groundwater or shallow flow path sources can contribute to streamflow during baseflow (Costelloe et al., 2015; Smerdon et al., 2012).

Variability in recession curve behavior (e.g., slope, timing, and length) between and within watersheds also highlight that multiple sources and flow paths contribute to baseflow (Tallaksen, 1995). Baseflow is commonly considered to be comprised of delayed or slow flow path sources. These slow flow paths are not limited to deep groundwater reservoirs and may include shallow subsurface reservoirs (Anderson & Burt, 1980; Hewlett & Hibbert, 1963; McCallum et al., 2010; Smakhtin, 2001). To account for variability in recession behavior, Stoelzle et al. (2019) developed a new baseflow separation index that considers dynamic contributions from multiple sources during recession periods. Taken together, these studies on stream water geochemical variability and recession behavior during low flow periods raise critical questions about (1) the importance of runoff contributions from slow flow paths other than deep groundwater, and (2) how and why different water source contributions vary in time and space during baseflow.

Spatial variability in stream water sources within watersheds during baseflow may be predicted or explained by internal variability in catchment characteristics. Cohesive frameworks that integrate spatial predictors across space and time are needed (Sivapalan,

2003). In an effort to build on this need, a range of watershed characteristics, such as climate, topography, geology, soil, vegetation, and land use have been linked to streamflow generation processes (Buttle et al., 2004; Carlier et al., 2018; Emanuel et al., 2010; Jencso & McGlynn, 2011; Onda et al., 2006). Work focused exclusively on baseflow generation processes also shows connections to geology (Bloomfield et al., 2009; Price, 2011; Tague & Grant, 2004). Variability in water sources and their relative contributions to baseflow may be especially important in structurally complex watersheds, where flow pathways can vary at the subwatershed scale. Heterogeneous watersheds provide a unique opportunity to examine and integrate the importance of suggested hierarchal controls (e.g., climate, geology, soil, and vegetation) on hydrologic processes beyond commonly considered topographic indices (Bergstrom et al., 2016; Devito et al., 2005; Zimmer & Gannon, 2018). For example, Payn et al. (2012) used structurally diverse subwatersheds to relate topographic and geologic characteristics to baseflow generation processes and found that during baseflow recession, the importance of structural controls increased while the importance of topographic controls decreased.

Identification of sources using a multi-tracer approach may be useful for defining and distinguishing among the dominant contributors to baseflow. Geochemical differences between potential slow flow sources can be used to separate their relative contributions to baseflow as is frequently done for higher flow periods (Klaus & McDonnell, 2013).

Multi-tracer approaches can also be best leveraged in structurally complex watersheds where differences in source contributions may be largest.

In this study, we examine the spatial distribution and temporal evolution of baseflow sources in a structurally complex central coastal California watershed and their relationship to spatial controls (e.g., topography, geology, land use, and soil characteristics) based on four synoptic sampling events during the summer dry down season lasting ~6 months. We leverage the extended recession period typical of Mediterranean climate catchments to isolate the nature of contributions to baseflow in the absence of complicating rainfall events typical of many other systems. To do this, we used endmember mixing analysis (EMMA) to examine how source water contributions shift across the seasonal baseflow recession period in six geologically diverse subwatersheds. We relate the EMMA results to spatial characteristics of the subwatersheds to better understand hierarchal controls on source contributions to flow. Specifically, we aim to answer the following questions:

1. What water sources sustain baseflow at the subwatershed scale and do their proportions change with time and in space?
2. Are baseflow sources and magnitudes correlated to subwatershed spatial characteristics?
3. How do baseflow sources relate to variability in stream geochemistry, specifically dissolved carbon concentrations?

## **1.2 Materials and Methods**

### 1.2.1 Study area

The San Lorenzo River (SLR) drains the 360 km<sup>2</sup> San Lorenzo Watershed (SLW) in central coastal California (Fig. 1a). Discharge in the SLR is generally controlled by seasonal precipitation, which is characterized by winter maxima and summer minima typical of Mediterranean climates. This wet-dry seasonality often results in extended recession periods that start in late spring and persist through early fall. Average annual precipitation in the SLW was  $\sim 1090 \pm 527$  mm for Water Years (WY) 2011 to 2018, as measured at Station US1CASZ0024 in Felton, California (accessed via NOAA National Centers for Environmental Information Climate Data Online) (NCDC, 2019). The sampling period herein consists of the summer of WY 2018 (October 2017 to September 2018), a year with below average precipitation (692 mm).

The SLW consists of more than twenty subwatersheds, each draining primary tributaries that directly discharge into the mainstem SLR. This study focused on six subwatersheds in the SLW that vary in size from 3.7 to 69.5 km<sup>2</sup> (Fig. 1b-g). Boulder, Clear, and Fall creeks originate from western subwatersheds, while Bear, Love, and Zayante creeks drain eastern subwatersheds.

The watershed has complex lithology (Fig. 1). Regional groundwater inputs to surface waters arise from three potential water bearing units: Butano sandstone, Lompico

sandstone, and Santa Margarita sandstone (ETIC Engineering, 2006). The Santa Margarita sandstone is a high permeability, generally unconfined unit with exposures along Boulder, Love, and Zayante creeks. The Butano sandstone has surface exposures in areas along Bear, Boulder, Love, and Zayante creeks, but generally underlies the Lompico sandstone, which has surface exposures in all subwatersheds. Western subwatersheds of the SLW have high-grade metamorphic (e.g., schist) and igneous (e.g., granodiorite) bedrock, while eastern subwatersheds are underlain by primarily sedimentary bedrock. Soil parent material for the SLW is weathered sandstone and occasionally weathered granite; soils are generally well drained sandy loam mollisols. Vegetation in the SLW is dominated by evergreens, including native coastal redwoods (*Sequoia sempervirens*) and Douglas fir (*Pseudotsuga menziesii*).

### 1.2.2 Spatial analysis of subwatershed characteristics

Geologic, topographic, land use, and soil characteristics were aggregated for each subwatershed in ArcGIS. Land cover was based on the 30 m spatial resolution National Land Cover Database (NLCD) from 2011 (NLCD, 2011). Open space percentage includes the following NLCD classifications: “Developed, Open Space”, “Shrub”, “Grassland”, and “Pasture”. Forest percentages used in this study are the sum of “Evergreen Forest” and “Mixed Forest”. Classification definitions are available online from the NLCD database. Soil characteristics were extracted from the National Soil Conservation Service Soil Survey Geographic (SSURGO) database using the Web Soil

Survey tool (SSURGO, 2019). Topographic data was aggregated from a patched USGS 3 m DEM from Fisher (2016). Bedrock cover was analyzed using a digital geological map of Santa Cruz County based on Brabb et al. (1997). Bedrock permeability was classified in a binary manner by setting a threshold hydraulic conductivity value of  $10^{-9} \text{ m s}^{-1}$  (e.g., an intrinsic permeability of  $\sim 10^{-16} \text{ m}^2$ ), with values below this threshold considered low permeability. Aquifer test results compiled by Kennedy/Jenks (2015) were used to classify water bearing units. Non-water bearing units (e.g., granite, shale, and schist) were assumed to have hydraulic conductivity values of  $10^{-10}$  to  $10^{-13} \text{ m s}^{-1}$ , based on values given from Freeze and Cherry (1979).

### 1.2.3 Water sampling and stream gauging

Water samples were collected from six streams (Bear, Boulder, Clear, Fall, Love, and Zayante) during four single-day sampling events in April, May, June, and September of 2018, as mainstem discharge receded in the absence of major precipitation events (Fig. 2). Nearly 98% of rainfall in WY 2018 occurred between October and early April, prior to the sampling events. Groundwater samples were collected from eight established monitoring wells in the watershed during a separate sampling event in June 2018. All water samples were filtered to  $0.2 \text{ }\mu\text{m}$  and refrigerated immediately after sampling until geochemical analysis at the Marine Analytical Lab at the University of California at Santa Cruz (UCSC). Cation concentrations ( $\text{Na}^+$ ,  $\text{Ca}^{2+}$ ,  $\text{Mg}^{2+}$ ,  $\text{K}^+$ ) were measured using a Thermo iCAP 7400 Inductively Coupled Plasma Optical Emission Spectrometer. Anion

concentrations ( $\text{Cl}^-$ ,  $\text{SO}_4^{2-}$ ) were measured on a Dionex ICS-2000 Ion Chromatograph. Major dissolved inorganic nutrients ( $\text{NO}_3^-$ ,  $\text{PO}_4^{3-}$ ,  $\text{SiO}_4^{4-}$ ) were determined on a Lachat QuikChem 8000 Flow Injection Analyzer. Dissolved organic carbon (DOC) was measured as non-purgeable organic carbon (NPOC) on a Shimadzu TOC-VCPH TC/TN Analyzer, and dissolved inorganic carbon (DIC) was determined on a UIC Carbon Coulometer. Specific ultraviolet absorbance ( $\text{SUVA}_{254}$ ) at 254 nm, a measure of percent aromaticity considered to represent DOC reactivity, was measured on a Thermo Genesys 10S UV-Visible Spectrophotometer (Weishaar et al., 2003). Analytical precision and accuracy for all analytes was generally better than 5% (Table S1).

At the time of water sample collection, each stream was gauged just upstream of its confluence with the mainstem of the SLR using a Pygmy Price flow meter at 0.6 of the water depth. Flow was calculated using the velocity-area method according to Rantz (1982). Stream velocity was generally measured at intervals such that no more than 10% of streamflow was contained in one subsection ( $6.9 \pm 2.3\%$  in April,  $6.0 \pm 1.2\%$  in May,  $6.1 \pm 1.7\%$  in June, and  $8.2 \pm 1.8\%$  in September 2018).

#### 1.2.4 Baseflow separation using endmember mixing analysis

Endmember mixing analysis (EMMA) was used to divide inputs to streams into either groundwater (GW) or shallow subsurface water (SSW) (Christophersen & Hooper, 1992; Christophersen et al., 1990; Hooper et al., 1990). Ten tracers ( $\text{Na}^+$ ,  $\text{Ca}^{2+}$ ,  $\text{Mg}^{2+}$ ,  $\text{K}^+$ ,  $\text{Cl}^-$ ,

SO<sub>4</sub><sup>2-</sup>, NO<sub>3</sub><sup>-</sup>, PO<sub>4</sub><sup>3-</sup>, SiO<sub>4</sub><sup>4-</sup>, and specific conductivity) were considered for use and evaluated for conservative behavior. Tracers were defined as conservative if they exhibited at least one linear trend in bivariate solute-solute plots ( $R^2 > 0.5$ ,  $p < 0.01$ ) (Fig. S1). The final selected model indicated three endmembers and used eight tracers (Na<sup>+</sup>, Ca<sup>2+</sup>, Mg<sup>2+</sup>, Cl<sup>-</sup>, SO<sub>4</sub><sup>2-</sup>, NO<sub>3</sub><sup>-</sup>, PO<sub>4</sub><sup>3-</sup>, and specific conductivity). The model conformed to requirements of low residual structure (mean  $R^2 = 0.07 \pm 0.05$ ) and high cumulative variance in accordance with the ‘rule of 1’ ( $m=2$ , PC1= 73.9%, PC2=18.3%) (Table S2) (Hooper, 2003).

Since multiple water bearing units have the potential to contribute to baseflow in the SLW, we used results of the spatial analysis of subwatershed lithology combined with previous work indicating plausible groundwater contributions to the studied streams to inform all possible GW endmembers for each stream in EMMA (Table S3) (ETIC Engineering, 2006). The geochemistry of each GW endmember was based on the average concentrations of the collected water samples and corroborated with historical records (Table S4). NO<sub>3</sub><sup>-</sup> and PO<sub>4</sub><sup>3-</sup> concentrations used in EMMA were particularly useful for fingerprinting GW contributions from anthropogenically-impacted aquifers in the region (e.g., Santa Margarita and Lompico). All GW contributions herein are presented as the sum of GW fractions determined via EMMA.

Many studies exist showing large variability in soil water chemistry over relatively small scales in forested catchments (Grossmann & Kloss, 1994; Manderscheid & Matzner,

1995). Instead of direct sampling, which would be difficult to accomplish over the spatial scale of this study, we assumed a range in viable SSW endmember geochemistry based on a thorough examination of mixing dynamics across flow conditions in the SLR using historical and current water quality data from the California Environmental Protection Agency's Central Coastal Ambient Monitoring Program (CCAMP, 2019). Principal component analysis (PCA) of available water quality data ( $\text{Cl}^-$ ,  $\text{Na}^+$ ,  $\text{PO}_4^{3-}$ ,  $\text{NO}_3^-$ , and specific conductivity) was completed using mainstem SLR data for three water years for which both discharge and geochemical data were available (WY 2005, 2011, and 2017) at USGS 11160500. The PCA revealed two distinct data clusters that separated out as a function of flow conditions: low to intermediate discharge periods, and intermediate to high discharge periods (Fig. S2). These clusters, which shed light on how water sources to the SLR operate seasonally, regardless of antecedent conditions, were confirmed with k-means cluster analysis (Fig. S2). At low flows, PCA results indicated a transition in dominant source contributions, likely representing diminished inputs from SSW and increases in GW contributions. Given knowledge of GW endmember geochemistry for the region, the SSW source must be a low conductivity, low ionic strength endmember that more closely resembles geochemistry observed during mid- to high-discharge periods. As such, the stream with the lowest conductivity and cation/anion concentrations during the first sampling event in March 2018 was used as the upper boundary of SSW geochemistry. To compliment this upper boundary geochemistry estimate, we assumed the lowest concentration SSW endmember was close to regional rainwater chemistry (e.g., equivalent to the shortest possible residence time with no significant interaction

with subsurface strata). We used a 5-year average (2013-2017) rainwater geochemical profile from National Trends Network (Site CA 66), which is part of the National Atmospheric Deposition Program (NTN, 2019) to estimate the lowest concentration SSW endmember.

These endmember estimates assume that SSW geochemistry, with respect to the parameters used in EMMA, is relatively uniform across the watershed, an assumption we believe to be reliable for the needs of this study based on (1) spatial analyses of soil characteristics that show general homogeneity in soil types across the watershed examined, (2) supporting DIC data independent of the EMMA model as presented in the Discussion, and (3) expectations that intra-source geochemical variability of the SSW endmember is likely low with respect to across source variability (relative to GW endmembers) from large differences in residence times. We recognize that the fractions generated in EMMA are biased by our endmember approximation, but believe that the resulting estimate is sufficient for the goals of this paper as both SSW endmembers represent geochemical extremes, but even at their upper and lower boundaries, the resulting shifts in contributions from the SSW endmember, as determined via EMMA, were generally small ( $5.6 \pm 4.5\%$ , see Fig. 5).

### 1.2.5 Correlation analysis

Cross correlations of spatial characteristics were analyzed using Pearson's correlation coefficient (R) after confirming that the distributions were not significantly different from normal using a Kolmogorov-Smirnov normality test. Relationships between spatial characteristics and derived quantities from streamflow and source fractions were analyzed using the non-parametric Spearman's rank correlation coefficient ( $r_s$ ). Average values are denoted herein as " $\bar{x}$ " and typically presented with their 1-sigma standard deviation.

## **1.3 Results**

### 1.3.1 Analysis of subwatershed spatial characteristics

There was a clear gradient in spatial characteristics across the subwatersheds (Fig. 3, Table S5), and the majority of the considered characteristics were correlated (Fig. S3). For example, smaller subwatersheds were generally steeper with shorter flow paths and greater spatial extents of low permeability bedrock compared to larger subwatersheds. Larger subwatersheds also had greater fractions of their area underlain by aquifers ( $R^2 = 0.87$ ,  $p < 0.05$ ). Land use cover across the subwatersheds was relatively uniform with forests covering 75 to 88% of the subwatersheds, though these slight differences were strongly negatively correlated with other characteristics such as open space cover, subwatershed area, length/gradient, aquifer area, and soil sand/clay content (Fig. S3). The secondary dominant land cover for all subwatersheds was open space, which ranged from

10 to 20%. Physical characteristics of soils were also relatively uniform in terms of sand content ( $61\pm 3\%$ ) and clay content ( $17\pm 2\%$ ). Soil organic matter (SOM) content varied slightly across the study area, with eastern subwatersheds containing slightly higher SOM ( $2.2\pm 0.2\%$ ) relative to western subwatersheds ( $1.3\pm 0.2\%$ ; Table S6).

### 1.3.2 Baseflow magnitude and endmember contributions to streamflow

Discharge normalized by watershed area, defined as specific discharge ( $Q$ ), decreased in all streams across the study period (Fig. 4). Specific discharge from all streams averaged  $0.94 \pm 0.41 \text{ mm d}^{-1}$  in April,  $0.51\pm 0.28 \text{ mm d}^{-1}$  in May,  $0.25\pm 0.17 \text{ mm d}^{-1}$  in June, and  $0.12\pm 0.10 \text{ mm d}^{-1}$  in September of 2018. Between April and September of 2018, specific discharge decreased on average by  $0.83\pm 0.36 \text{ mm d}^{-1}$ , or  $88\pm 10\%$ , in all streams. Western streams (Boulder, Clear and Fall) had higher specific discharges initially relative to eastern streams (Bear, Love, and Zayante;  $1.15$  to  $1.54 \text{ mm d}^{-1}$  versus  $0.53$  to  $0.69 \text{ mm d}^{-1}$ , respectively). Of the three western streams with high initial specific discharge, Fall and Clear creeks maintained the highest specific discharges through the entire recession period, and initial spatial differences observed in specific discharge across most streams were similar through the dry down period.

The fraction of shallow subsurface water ( $f_{\text{SSW}}$ ) generally decreased through time in all streams, though not all transitioned to GW dominance, which we define here as a  $f_{\text{GW}}$  greater than 0.5 (Fig. 5). In April 2018, four (Boulder, Clear, Fall, Love) of the six

streams were SSW dominated (defined as  $f_{SSW}$  greater than 0.5). Of the four initial SSW dominated streams, only Boulder Creek transitioned to GW dominance by September 2018.  $f_{SSW}$  decreased on average by  $0.15 \pm 0.07$  in all streams across the recession period. The largest and smallest decreases in  $f_{SSW}$  occurred in Boulder Creek (-0.26) and Zayante Creek (-0.08), respectively (Fig. 5).

Specific discharge from SSW ( $Q_{SSW}$ ) ranged from 0.16 to 1.19 mm d<sup>-1</sup> in April ( $\bar{x} = 0.57 \pm 0.39$  mm d<sup>-1</sup>), 0.05 to 0.64 mm d<sup>-1</sup> in May ( $\bar{x} = 0.29 \pm 0.23$  mm d<sup>-1</sup>), 0.02 to 0.29 mm d<sup>-1</sup> in June ( $\bar{x} = 0.13 \pm 0.12$  mm d<sup>-1</sup>), and 0.002 to 0.13 mm d<sup>-1</sup> in September of 2018 ( $\bar{x} = 0.06 \pm 0.06$  mm d<sup>-1</sup>) (Fig. 6a).  $Q_{SSW}$  decreased on average by  $91 \pm 8\%$  in all streams during the summer dry down period, and the largest decreases in  $Q_{SSW}$  generally occurred in western streams (Boulder, Clear, and Fall).  $Q_{GW}$  ranged from 0.26 to 0.46 mm d<sup>-1</sup> in April ( $\bar{x} = 0.38 \pm 0.07$  mm d<sup>-1</sup>), 0.15 to 0.30 mm d<sup>-1</sup> in May ( $\bar{x} = 0.23 \pm 0.06$  mm d<sup>-1</sup>), 0.07 to 0.20 mm d<sup>-1</sup> in June ( $\bar{x} = 0.12 \pm 0.05$  mm d<sup>-1</sup>), and 0.007 to 0.11 mm d<sup>-1</sup> in September of 2018 ( $\bar{x} = 0.06 \pm 0.05$  mm d<sup>-1</sup>) (Fig. 6b).  $Q_{GW}$  decreased on average by  $85 \pm 12\%$  in all streams during the study period.

### 1.3.3 Relationship of baseflow magnitude and source to subwatershed characteristics

The relationship between specific discharge,  $f_{SSW}$ ,  $Q_{SSW}$ , and  $Q_{GW}$  were examined with respect to subwatershed characteristics to evaluate potential first order spatial predictors (Table 1). Specific discharge was not correlated to any of the spatial predictors

considered in this study. The binary index of bedrock permeability was the best standalone predictor of  $f_{SSW}$  ( $r_s=0.94$  to  $1.00$ ,  $p<0.05$ ) (Fig. 7).  $Q_{SSW}$  was best predicted by the fraction of the catchment with low permeability bedrock initially ( $r_s=0.94$ ,  $p<0.05$ ), though this correlation's significance decreased through the recession period. There were no statistically significant correlations for  $Q_{GW}$ .

#### 1.3.4 Stream water dissolved carbon geochemistry

Stream water DIC, DOC, and  $SUVA_{254}$  values generally followed similar trends with time, though absolute changes in concentrations among the streams varied in magnitude (Fig. 8). Across all subwatersheds, stream water DIC concentrations and  $SUVA_{254}$  values generally increased, and stream water DOC concentrations decreased as  $f_{GW}$  increased through the recession period. Stream water DIC concentrations and  $SUVA_{254}$  values increased on average by  $450\pm 300$   $\mu\text{M}$  and  $1.8\pm 0.3$   $\text{L mg}^{-1} \text{m}^{-1}$ , respectively, while stream water DOC concentrations decreased on average by  $120\pm 50$   $\mu\text{M}$  through the dry season.

Spatial differences in stream water DOC concentrations and  $SUVA_{254}$  values across subwatersheds were also apparent. Stream water DOC concentrations ranged from 130 to 390  $\mu\text{M}$  ( $\bar{x} = 250\pm 100$   $\mu\text{M}$ ) at the start of the dry season (April 2018) and decreased to 60 to 200  $\mu\text{M}$  ( $\bar{x} = 130\pm 70$   $\mu\text{M}$ ) by the end of the study period (September 2018) (Fig. 8b).  $SUVA_{254}$  values in stream water were spatially variable as well and ranged as follows: 1.2 to 2.3  $\text{L mg}^{-1} \text{m}^{-1}$  in April ( $\bar{x} = 1.9\pm 0.5$   $\text{L mg}^{-1} \text{m}^{-1}$ ), 2.3 to 3.2  $\text{L mg}^{-1} \text{m}^{-1}$  in May ( $\bar{x} =$

2.6±0.3 L mg<sup>-1</sup> m<sup>-1</sup>), 2.1 to 3.7 L mg<sup>-1</sup> m<sup>-1</sup> in June ( $\bar{x} = 3.1 \pm 0.6$  L mg<sup>-1</sup> m<sup>-1</sup>), and 3.4 to 4.1 L mg<sup>-1</sup> m<sup>-1</sup> in September of 2018 ( $\bar{x} = 3.6 \pm 0.3$  L mg<sup>-1</sup> m<sup>-1</sup>) (Fig. 8c).

## **1.4 Discussion**

### 1.4.1 Geologic controls on non-stationarity in baseflow sources

Many studies on streamflow generation mechanisms have focused exclusively on topographic indices as spatial predictors. This approach is well suited for structurally homogeneous systems where geology is generally uniform (McGuire et al., 2005). In more structurally complex landscapes, geologic controls may override topographic predictors of streamflow generation processes. Subwatersheds of the SLW were primarily distinguished by differences in bedrock permeability. By leveraging these spatial differences in geology during the summer dry down period, we were able to show that the relative contribution of shallow subsurface water and deep groundwater to streamflow was best explained by subwatershed scale differences in bedrock permeability (Table 1). This finding is in line with previous work that has suggested that bedrock permeability is an important control on subsurface flow pathways and transit times (Pfister et al., 2017; Uchida et al., 2006), especially during baseflow (Hale & McDonnell, 2016; Hale et al., 2016; Jencso & McGlynn, 2011; Tague & Grant, 2004). These spatial differences in bedrock permeability translated to physical distinctions in available subsurface water storage capacity (Fig. 9). In subwatersheds with greater areal extents of high permeability bedrock, relative contributions of groundwater to streamflow were highest. High

permeability bedrock allows for vertical movement of water, via infiltration and deeper recharge of groundwater reservoirs, which limits the extent of water accumulation in shallow subsurface storage and, subsequently, downslope shallow subsurface water contributions to baseflow (Fig. 9c,d). In contrast, subwatersheds with low permeability bedrock transmitted water primarily through shallow subsurface pathways (Fig. 9a). Streams in these subwatersheds received up to an order of magnitude more shallow subsurface water than their more permeable counterparts and remained compositionally dominated by shallow subsurface water through the entire recession period considered, even as specific discharge decreased across all streams (Fig. S4). Hale and McDonnell (2016) found similar differences in subsurface flow paths in catchments with contrasting underlying geology; in areas with low permeability volcanic rock, storage was limited to shallow soils, and mean transit times in these areas were short (~1.8 years) relative to more sedimentary catchments with deeper groundwater reservoirs (~6.2 years). Such permeability contrasts at soil-bedrock contacts are known to initiate shallow downslope subsurface flow (Harr, 1977), and early studies on recession flows show that these shallow flowpaths can be active, long-duration contributors to streamflow in the absence of rainfall (Hewlett & Hibbert, 1963; Mosley, 1979). Additionally, while no work exists showing the extent of bedrock fracturing in the studied subwatersheds, it is possible that the shallow subsurface stores are influenced by exfiltration of bedrock groundwater into overlying soil layers (Fig. 9b); catchments with significant fracturing of bedrock can receive 50 to 95% of baseflow contributions from bedrock groundwater (Uchida et al., 2003). The exact routing of water, from initial infiltration to final discharge from shallow

subsurface storage, through the low permeability subwatersheds is unclear without more detailed field-based work on flow paths.

Interestingly, the subwatersheds with the greatest areal extent of low permeability bedrock were generally able to maintain the highest specific discharges through the recession period (from sustained shallow subsurface water contributions) even though their specific discharges decreased the most in absolute terms. The drainage characteristics of shallow subsurface water-dominated streams implies that subwatersheds with greater percentages of low permeability bedrock can accumulate more water per area for initial rapid release from dynamic storage in the soil mantle and that this compartment drains faster, but less efficiently than deep groundwater stores. This “inefficiency” ties back to early experimental work by Hewlett and Hibbert (1963), which shows sustained soil mantle drainage can last over 140 days in the absence of rainfall. The finding of shallow subsurface water dominated streams is especially important in the context of emerging hydroclimatic variability. Shallow subsurface water dominated streams may be more sensitive to seasonal and annual changes in precipitation as these stores depend on relatively recent precipitation (within the water year) for recharge, while primary aquifers are often better buffered against interannual precipitation variability (Nippgen et al., 2016; Zimmer & Gannon, 2018).

Similar to past work on scaling properties of structurally diverse catchments (Carlier et al., 2018; Hale & McDonnell, 2016; Hale et al., 2016; Tague & Grant, 2004), our finding of the importance of bedrock permeability in baseflow source partitioning emphasizes the value of including geologic indices in development of a hydrologic classification system (McDonnell & Woods, 2004; Wagener et al., 2007). Systems with strong correlations of topographic indices to properties of catchment function may actually represent finer scale controls on water cycling and fit into studies such as this one, which leverages structural heterogeneity to delineate the higher spatial order control of geology. Such intercomparisons hint at the importance of geologic controls on catchment storage and release functions during low flow periods in geologically diverse, mountainous watersheds.

#### 1.4.2 Implications of shifting baseflow sources: an example using dissolved carbon geochemistry

Spatial and temporal differences in water sources contributing to baseflow have consequences for observed stream biogeochemistry. Variability in concentrations of biologically relevant compounds, such as dissolved carbon, across and within structurally complex watersheds during baseflow may arise primarily from differences in water sources rather than in-stream biogeochemical processing. We found that dissolved carbon concentrations and associated SUVA<sub>254</sub> values shifted in line with changes in dominant source contributions (Fig. 8). Though the exact concentrations of dissolved carbon in

streams in this study are more geochemically complex than binary mixing of GW and SSW endmembers (e.g., dependent on contributions from multiple aquifers), general trends through time and in space in stream water dissolved carbon were used to provide supplemental insight and independent confirmation of mixing dynamics.

The observed shifts in stream water dissolved carbon geochemistry across subwatersheds (see Fig. 8, from high DOC and low DIC/SUVA<sub>254</sub> to low DOC and high DIC/SUVA<sub>254</sub>) evaluated together with the transition in groundwater endmember contributions to streamflow (from low to high  $f_{GW}$ ) through time supports our classification of the SSW endmember as a shallow, short residence time source relative to the GW endmembers. Streamflow DOC concentrations generally decreased and DIC concentrations increased as  $f_{GW}$  increased in all subwatersheds through time. The observed decreases in DOC concentrations in individual streams occurred at the same time as increases in  $f_{GW}$ , which is consistent with (1) measured GW endmember DOC concentrations, which were low and highly uniform across all well samples ( $38 \pm 6 \mu\text{M}$ ), and (2) previous work showing significant differences in dissolved organic matter (DOM) content in soil versus GW reservoirs from abiotic (e.g., sorption) and biotic (e.g., remineralization) processing (Chapelle et al., 2016; Shen et al., 2015).

DOM quantity and quality shift during transport through the subsurface; in soils, bioavailability of DOM is typically reduced with increasing depth as microbes preferentially remineralize labile OM and leave behind more refractory DOM (Shen et

al., 2015). Subsequent recharge of water containing this highly recycled soil DOM often leads to substantial differences in DOM concentration, composition, and bioavailability between soil water and GW (Chapelle et al., 2016; Shen et al., 2015). The high SUVA<sub>254</sub> values associated with higher  $f_{GW}$  in this study is consistent with an expected decrease in DOM reactivity with greater source contributions from GW. All well samples from the San Lorenzo Watershed had high SUVA<sub>254</sub> values ( $4.0 \pm 1.8 \text{ L mg}^{-1} \text{ m}^{-1}$ ), indicative of recycled (e.g., refractory) DOM.

Initial DOC concentrations in streams were also spatially variable, which suggested SSW endmember DOC geochemistry was distinct across subwatersheds as GW DOC concentrations were highly uniform. The uniformity in GW endmember DOC concentrations, which is common to many groundwater systems (Chapelle et al., 2016), allowed us to establish conservative mixing lines for approximation of SSW endmember DOC concentrations using individual projections through the stream water and GW endmember DOC data. SSW endmember DOC concentrations in western streams projected out to a lower DOC concentration SSW endmember than their eastern counterparts (Fig. 10a). The lower SOM content in western subwatersheds relative to eastern subwatersheds can explain the spatial distinction in estimated SSW endmember DOC concentrations ( $r_s = 0.79$ ), while allowing SSW DIC concentrations to remain relatively uniform otherwise (Fig. 10b). The mixing lines also highlight that the rate of change in DOC concentrations with respect to  $f_{GW}$  shifts with time; changes in slope indicate a shift in process or behavior that may be best explained as intra-source

variability in SSW endmember DOC concentrations, not only in space, but also with time. The extrapolated decreases in SSW endmember DOC concentrations with time in subwatersheds is consistent with drainage of water in shallow water storage zones (whether that water is primarily transported via downslope drainage and/or as exfiltrating bedrock groundwater that enters the shallow zone before final discharge into proximal streams). Work by Bishop et al. (2004) showed that DOC geochemistry can be depth dependent in soils, and SOM data extracted from SSURGO confirmed this depth-dependency in SOM content in SLW soils (Table S6).

Conceptually, this change in SSW endmember DOC geochemistry with time and in space can be contrasted with endmember mixing dynamics controlling stream water DIC concentrations. Slopes of regressions between  $f_{GW}$  and stream water DIC concentrations were generally consistent with time, though mixing lines were not established as GW endmember DIC concentrations were not uniform, and DIC concentrations in streams are affected by gas evasion, which can lower DIC concentrations considerably (Doctor et al., 2008; Öquist et al., 2009). Both factors would have a significant effect on mixing line projections. Nonetheless, a visual examination of stream water DIC concentrations indicates that (1) most data fall on lines with y-intercepts (e.g., theoretical SSW endmember DIC concentrations) that are reasonable (e.g., positive and low DIC concentration consistent with shallow subsurface waters from other forested watersheds), and (2) GW endmember DIC concentrations within the range of DIC concentrations observed for GW in the area (aside from Love Creek) (Kindler et al., 2011). These

general consistencies in regression behavior in DIC concentrations imply a relative stasis in both GW and SSW endmember DIC contributions through the dry down period.

Taken together, we suspect that shallow subsurface flow paths contributing to baseflow in individual subwatersheds shift spatially during the dry season as shown for other systems (Nippgen et al., 2015; Uchida et al., 2006), and that this spatial evolution of contributing areas differentially affects dissolved carbon geochemistry (Laudon et al., 2011; Zimmer & McGlynn, 2018). As sources shift, DIC concentrations change relatively uniformly in space and time, acting very broadly as a qualitative indicator of watershed scale source transitions in this system at low flows (e.g. low to high as a proxy for SSW to GW dominance) (Fig. 11a). In contrast, DOC concentrations are indicators of subwatershed scale SSW intra-source endmember variability as shallow subsurface water storage is depleted through the seasonal baseflow recession (Fig. 11b).

## **1.5 Conclusions**

Source contributions to baseflow in a structurally complex central coastal California watershed were quantified using EMMA during the summer dry down period and related to spatial indices at the subwatershed scale to gain insight into the drivers of baseflow generation. Relative contributions of groundwater and shallow subsurface water to baseflow were spatially and temporally variable across subwatersheds. While some streams transitioned to groundwater dominance, several streams remained dominated by

shallow subsurface water contributions through the baseflow recession period. Watershed controls on groundwater versus shallow subsurface water dominated streams appeared to arise from subwatershed scale differences in lithology, which dictates where water can be stored and transported in the subsurface. This, in turn, influences the residence time of flow paths, and the timing of streamflow contributions. At the subwatershed scale, dissolved carbon geochemistry was consistent with shifting source waters, even as contributing areas associated with each source within subwatersheds likely changed through time. Stream water DIC concentrations were broad, qualitative indicators of watershed level transitions in dominant source waters, while DOC concentrations and  $SUVA_{254}$  values were assumed to better reflect intra-source changes consistent with expected shifts in organic matter content as soil layers at different depths drained. Our findings show that using a multi-tracer approach for identification of source contributions to baseflow in structurally diverse watersheds can provide new insight into baseflow dynamics. These results have broad implications for our understanding of baseflow generation, and more work is needed to better understand when and where assumptions of stationarity in baseflow sources may be inappropriate.

## **Acknowledgements**

The authors thank Nate Gillespie at the San Lorenzo Valley Water District and Ross Albert at the Scotts Valley Water District for providing historical water quality data and access to monitoring wells for sampling, and Rob Franks, Kaylee Glenney, and Carolyn Brady for field and/or lab assistance. We thank Andrew Fisher for providing material support. We thank Jason Parke and Barry Hecht at Balance Hydrologics, and John Ricker at the County of Santa Cruz, Environmental Health Department for useful discussions. We thank the associate editor and editor as well as three anonymous reviewers for valuable feedback that significantly improved the quality of this manuscript. Data used in this study are available from the Hydroshare data repository (<https://www.hydroshare.org/resource/8b054e66289743f7b930358907e48f8e/>). This research was supported by the Geological Society of America (GSA) through two student research grants with additional support from the National Science Foundation Graduate Research Fellowship Program (DGE-1329626).

## References

- Anderson, M. G., & Burt, T. P. (1980). Interpretation of recession flow. *Journal of Hydrology*, 46(1-2), 89-101. <Go to ISI>://WOS:A1980JJ63400006
- Asano, Y., Uchida, T., Mimasu, Y., & Ohte, N. (2009). Spatial patterns of stream solute concentrations in a steep mountainous catchment with a homogeneous landscape. *Water Resources Research*, 45. <Go to ISI>://WOS:000271136000001
- Bergstrom, A., Jencso, K., & McGlynn, B. (2016). Spatiotemporal processes that contribute to hydrologic exchange between hillslopes, valley bottoms, and streams. *Water Resources Research*, 52(6), 4628-4645. <Go to ISI>://WOS:000380100200023
- Bishop, K., Seibert, J., Koher, S., & Laudon, H. (2004). Resolving the Double Paradox of rapidly mobilized old water with highly variable responses in runoff chemistry. *Hydrological Processes*, 18(1), 185-189. <Go to ISI>://WOS:000188506700013
- Bloomfield, J. P., Allen, D. J., & Griffiths, K. J. (2009). Examining geological controls on baseflow index (BFI) using regression analysis: An illustration from the Thames Basin, UK. *Journal of Hydrology*, 373(1-2), 164-176. <Go to ISI>://WOS:000268074900015
- Blumstock, M., Tetzlaff, D., Malcolm, I., Nuetzmann, G., & Soulsby, C. (2015). Baseflow dynamics: Multi-tracer surveys to assess variable groundwater contributions to montane streams under low flows. *Journal of Hydrology*, 527, 1021-1033.
- Brabb, E. E., Wentworth, C., Knifong, D., Graymer, R., & Blissenbach, J. (1997). Geologic map of Santa Cruz County, California: A digital database. In: USGS.
- Buttle, J. M., Dillon, P. J., & Eerkes, G. R. (2004). Hydrologic coupling of slopes, riparian zones and streams: an example from the Canadian Shield. *Journal of Hydrology*, 287(1-4), 161-177. <Go to ISI>://WOS:000220153300010
- Carlier, C., Wirth, S. B., Cochand, F., Hunkeler, D., & Brunner, P. (2018). Geology controls streamflow dynamics. *Journal of Hydrology*, 566, 756-769. <Go to ISI>://WOS:000449901100057
- CCAMP. (2019). *Central Coastal Ambient Monitoring Program, Environmental Protection Agency*. Available online at [www.ceden.org](http://www.ceden.org). Accessed January 2019.

- Chapelle, F. H., Shen, Y., Strom, E. W., & Benner, R. (2016). The removal kinetics of dissolved organic matter and the optical clarity of groundwater. *Hydrogeology Journal*, 24(6), 1413-1422. <Go to ISI>://WOS:000382049400007
- Christophersen, N., & Hooper, R. P. (1992). Multivariate-analysis of stream water chemical-data - the use of principal components-analysis for the end-member analysis mixing problem. *Water Resources Research*, 28(1), 99-107. <Go to ISI>://WOS:A1992GY77200010
- Christophersen, N., Neal, C., Hooper, R. P., Vogt, R. D., & Andersen, S. (1990). Modeling streamwater chemistry as a mixture of soilwater end-members - a step towards 2nd-generation acidification models *Journal of Hydrology*, 116(1-4), 307-320. <Go to ISI>://WOS:A1990DX38100021
- Costelloe, J., Peterson, T., Halbert, K., Western, A., & McDonnell, J. (2015). Groundwater surface mapping informs sources of catchment baseflow. *J Hydrology and Earth System Sciences*.
- Devito, K., Creed, I., Gan, T., Mendoza, C., Petrone, R., Silins, U., & Smerdon, B. (2005). A framework for broad-scale classification of hydrologic response units on the Boreal Plain: is topography the last thing to consider? *Hydrological Processes*, 19(8), 1705-1714. <Go to ISI>://WOS:000229232800010
- Doctor, D. H., Kendall, C., Sebestyen, S. D., Shanley, J. B., Ohte, N., & Boyer, E. W. (2008). Carbon isotope fractionation of dissolved inorganic carbon (DIC) due to outgassing of carbon dioxide from a headwater stream. *Hydrological Processes*, 22(14), 2410-2423.
- Emanuel, R. E., Epstein, H. E., McGlynn, B. L., Welsch, D. L., Muth, D. J., & D'Odorico, P. (2010). Spatial and temporal controls on watershed ecohydrology in the northern Rocky Mountains. *Water Resources Research*, 46. <Go to ISI>://WOS:000284711600002
- ETIC Engineering, I. (2006). Groundwater modeling study of the Santa Margarita Groundwater Basin. A report prepared for Scotts Valley Water District. In.
- Fisher, A., Lozano, S., Beganskas, S., Teo, E., Young, K., Weir, W., Harmon, R. (2016). Regional Managed Aquifer Recharge and Runoff Analyses in Santa Cruz and northern Monterey Counties, California. A report prepared for the California State Coastal Conservancy, Project 13-118. In.
- Freeze, R., & Cherry, J. A. (1979). *Groundwater* (Vol. Vol. 7632, 604). Englewood Cliffs: Prentice-Hall Inc.

- Grossmann, J., & Kloss, R. (1994). Variability of water quality in a spruce stand. *Plant Nutrition and Soil Science*, 157(1), 47-51.
- Hale, V. C., & McDonnell, J. J. (2016). Effect of bedrock permeability on stream base flow mean transit time scaling relations: 1. A multiscale catchment intercomparison. *Water Resources Research*, 52(2), 1358-1374. <Go to ISI>://WOS:000373117300042
- Hale, V. C., McDonnell, J. J., Stewart, M. K., Solomon, D. K., Doolittle, J., Ice, G. G., & Pack, R. T. (2016). Effect of bedrock permeability on stream base flow mean transit time scaling relationships: 2. Process study of storage and release. *Water Resources Research*, 52(2), 1375-1397. <Go to ISI>://WOS:000373117300043
- Harr, R. (1977). Water flux in soil and subsoil on a steep forested slope. *Journal of Hydrology*, 33, 37-58.
- Hewlett, J. D., & Hibbert, A. R. (1963). Moisture and Energy Conditions within a Sloping Soil Mass during Drainage. *Journal of Geophysical Research*, 68(4), 1081.
- Hooper, R. P. (2003). Diagnostic tools for mixing models of stream water chemistry. *Water Resources Research*, 39(3). <Go to ISI>://WOS:000182213100003
- Hooper, R. P., Christophersen, N., & Peters, N. E. (1990). Modeling streamwater chemistry as a mixture of soilwater end-members - an application to the Panola Mountain Catchment, Georgia, USA. *Journal of Hydrology*, 116(1-4), 321-343. <Go to ISI>://WOS:A1990DX38100022
- Jencso, K. G., & McGlynn, B. L. (2011). Hierarchical controls on runoff generation: Topographically driven hydrologic connectivity, geology, and vegetation. *Water Resources Research*, 47. <Go to ISI>://WOS:000297650900001
- Katsura, S., Kosugi, K., Mizutani, T., Okunaka, S., & Mizuyama, T. (2008). Effects of bedrock groundwater on spatial and temporal variations in soil mantle groundwater in a steep granitic headwater catchment. *Water Resources Research*, 44(9).
- Kennedy/Jenks. (2015). Santa Margarita Basin Groundwater Modeling Technical Study. A report prepared for Scotts Valley Water District. .
- Kindler, R., Siemens, J., Kaiser, K., Walmsley, D. C., Bernhofer, C., Buchmann, N., et al. (2011). Dissolved carbon leaching from soil is a crucial component of the net ecosystem carbon balance. *Global Change Biology*, 17(2), 1167-1185. <Go to ISI>://WOS:000285878000040

- Klaus, J., & McDonnell, J. J. (2013). Hydrograph separation using stable isotopes: Review and evaluation. *Journal of Hydrology*, 505, 47-64. <Go to ISI>://WOS:000328806400005
- Laudon, H., Berggren, M., Agren, A., Buffam, I., Bishop, K., Grabs, T., et al. (2011). Patterns and Dynamics of Dissolved Organic Carbon (DOC) in Boreal Streams: The Role of Processes, Connectivity, and Scaling. *Ecosystems*, 14(6), 880-893. <Go to ISI>://WOS:000294683300002
- Manderscheid, B., & Matzner, E. (1995). Spatial and temporal variation of soil solution chemistry and ion fluxes through the soil in a mature Norway spruce (*Picea abies* (L.) Karst.) stand. *Biogeochemistry*, 30(2), 99-114.
- McCallum, J. L., Cook, P. G., Brunner, P., & Berhane, D. (2010). Solute dynamics during bank storage flows and implications for chemical base flow separation. *Water Resources Research*, 46. <Go to ISI>://WOS:000280591200003
- McDonnell, J. J., & Woods, R. (2004). On the need for catchment classification. *Journal of Hydrology*, 299, 2-3.
- McGuire, K. J., McDonnell, J. J., Weiler, M., Kendall, C., McGlynn, B. L., Welker, J. M., & Seibert, J. (2005). The role of topography on catchment-scale water residence time. *Water Resources Research*, 41(5). <Go to ISI>://WOS:000229149900004
- Mosley, M. P. (1979). Streamflow generation in a forested watershed, New Zealand. *Water Resources Research*, 15(4), 795-806.
- NCDC. (2019). National Centers for Environmental Information Climate Data Online. Available online at <https://www.ncdc.noaa.gov/>. Accessed January 2019.
- Nippgen, F., McGlynn, B. L., & Emanuel, R. E. (2015). The spatial and temporal evolution of contributing areas. *Water Resources Research*, 51(6), 4550-4573. <Go to ISI>://WOS:000358301200036
- Nippgen, F., McGlynn, B. L., Emanuel, R. E., & Vose, J. M. (2016). Watershed memory at the Coweeta Hydrologic Laboratory: The effect of past precipitation and storage on hydrologic response. *Water Resources Research*, 52(3), 1673-1695.
- NLCD. (2011). National Land Cover Database, Multi-Resolution Land Characteristics Consortium. Available online at <https://www.mrlc.gov/data>. Accessed January 2019. <https://www.mrlc.gov/data>

- NTN. (2019). National Trends Network, National Atmospheric Deposition Program. Available online at <http://nadp.slh.wisc.edu/>. Accessed January 2019.
- Onda, Y., Tsujimura, M., Fujihara, J. I., & Ito, J. (2006). Runoff generation mechanisms in high-relief mountainous watersheds with different underlying geology. *Journal of Hydrology*, 331(3-4), 659-673. <Go to ISI>://WOS:000242697700023
- Öquist, M. G., Wallin, M., Seibert, J., Bishop, K., & Laudon, H. (2009). Dissolved inorganic carbon export across the soil/stream interface and its fate in a boreal headwater stream. *Environmental Science and Technology*, 43(19), 7364-7369.
- Payn, R. A., Gooseff, M. N., McGlynn, B. L., Bencala, K. E., & Wondzell, S. M. (2012). Exploring changes in the spatial distribution of stream baseflow generation during a seasonal recession. *Water Resources Research*, 48. <Go to ISI>://WOS:000303124700003
- Pfister, L., Martinez-Carreras, N., Hissler, C., Klaus, J., Carrer, G. E., Stewart, M. K., & McDonnell, J. J. (2017). Bedrock geology controls on catchment storage, mixing, and release: A comparative analysis of 16 nested catchments. *Hydrological Processes*, 31(10), 1828-1845. <Go to ISI>://WOS:000400854700001
- Price, K. (2011). Effects of watershed topography, soils, land use, and climate on baseflow hydrology in humid regions: A review. *Progress in Physical Geography*, 35(4), 465-492. <Go to ISI>://WOS:000292888900003
- Rantz, S. E. (1982). *Measurement and computation of streamflow* (Vol. 2175): US Department of the Interior, USGS.
- Shen, Y., Chapelle, F. H., Strom, E. W., & Benner, R. (2015). Origins and bioavailability of dissolved organic matter in groundwater. *Biogeochemistry*, 122(1), 61-78. <Go to ISI>://WOS:000346163800005
- Sivapalan, M. (2003). Process complexity at hillslope scale, process simplicity at the watershed scale: is there a connection? *Hydrological Processes*, 17(5), 1037-1041. <Go to ISI>://WOS:000181829600013
- Smakhtin, V. U. (2001). Low flow hydrology: a review. *Journal of Hydrology*, 240(3-4), 147-186. <Go to ISI>://WOS:000166327000001
- Smerdon, B. D., Gardner, W. P., Harrington, G. A., & Tickell, S. J. (2012). Identifying the contribution of regional groundwater to the baseflow of a tropical river (Daly River, Australia). *Journal of Hydrology*, 464, 107-115.

- Soulsby, C., Tetzlaff, D., van den Bedem, N., Malcolm, I. A., Bacon, P. J., & Youngson, A. F. (2007). Inferring groundwater influences on surface water in montane catchments from hydrochemical surveys of springs and streamwaters. *Journal of Hydrology*, 333(2-4), 199-213. <Go to ISI>://WOS:000244160900003
- SSURGO. (2019). Soil Survey Staff, Natural Resources Conservation Service, United States Department of Agriculture. Web Soil Survey. Available online at <https://websoilsurvey.nrcs.usda.gov/>. Accessed January 2019. <https://websoilsurvey.nrcs.usda.gov/>
- Stoelzle, M., Schuetz, T., Weiler, M., Stahl, K., & Tallaksen, L. M. (2019). Beyond binary baseflow separation: delayed flow index as a fresh perspective on streamflow contributions. *Journal of Hydrology and Earth System Sciences Discussions*, pp.1-30.
- Tague, C., & Grant, G. E. (2004). A geological framework for interpreting the low-flow regimes of Cascade streams, Willamette River Basin, Oregon. *Water Resources Research*, 40(4). <Go to ISI>://WOS:000221327200002
- Tallaksen, L. (1995). A review of baseflow recession analysis. *Journal of Hydrology*, 165(1-4), 349-370.
- Temnerud, J., Folster, J., Buffam, I., Laudon, H., Erlandsson, M., & Bishop, K. (2010). Can the distribution of headwater stream chemistry be predicted from downstream observations? *Hydrological Processes*, 24(16), 2269-2276. <Go to ISI>://WOS:000280142100007
- Tetzlaff, D., & Soulsby, C. (2008). Sources of baseflow in larger catchments - Using tracers to develop a holistic understanding of runoff generation. *Journal of Hydrology*, 359(3-4), 287-302. <Go to ISI>://WOS:000259831300008
- Uchida, T., Asano, Y., Ohte, N., & Mizuyama, T. (2003). Seepage area and rate of bedrock groundwater discharge at a granitic unchanneled hillslope. *Water Resources Research*, 39(1).
- Uchida, T., McDonnell, J. J., & Asano, Y. (2006). Functional intercomparison of hillslopes and small catchments by examining water source, flowpath and mean residence time. *Journal of Hydrology*, 327(3-4), 627-642. <Go to ISI>://WOS:000239870900028
- Wagener, T., Sivapalan, M., Troch, P., & Woods, R. (2007). Catchment classification and hydrologic similarity. *Geography Compass*, 1(4), 901-931.

- Weishaar, J. L., Aiken, G. R., Bergamaschi, B. A., Fram, M. S., Fujii, R., & Mopper, K. (2003). Evaluation of specific ultraviolet absorbance as an indicator of the chemical composition and reactivity of dissolved organic carbon. *Environmental Science and Technology*, 37(20), 4702-4708.
- Zimmer, M. A., Bailey, S. W., McGuire, K. J., & Bullen, T. D. (2013). Fine scale variations of surface water chemistry in an ephemeral to perennial drainage network. *Hydrological Processes*, 27(24), 3438-3451. <Go to ISI>://WOS:000325989300007
- Zimmer, M. A., & Gannon, J. P. (2018). Run-off processes from mountains to foothills: The role of soil stratigraphy and structure in influencing run-off characteristics across high to low relief landscapes. *Hydrological Processes*, 32(11), 1546-1560. <Go to ISI>://WOS:000434115300003
- Zimmer, M. A., & McGlynn, B. L. (2018). Lateral, Vertical, and Longitudinal Source Area Connectivity Drive Runoff and Carbon Export Across Watershed Scales. *Water Resources Research*, 54(3), 1576-1598. <Go to ISI>://WOS:000430364900010

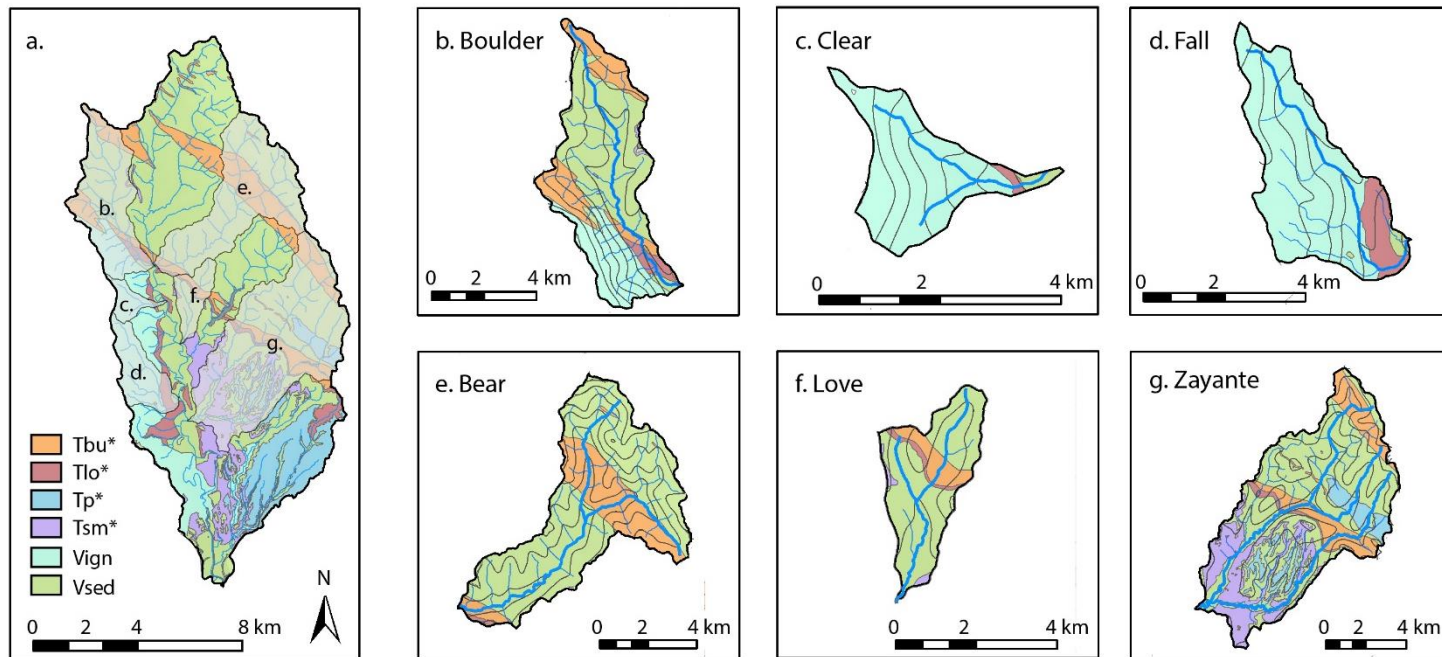


**Figure 1-1. Geologic map of the San Lorenzo Watershed.**

(a) Geologic map of the San Lorenzo Watershed in Santa Cruz County, California. Asterisks indicate water bearing units. Tbu, tertiary Butano sandstone; Tlo, tertiary Lompico sandstone; Tp, tertiary Purisima Formation; Tsm, tertiary Santa Margarita sandstone; Vign, various non-water bearing igneous and metamorphic facies; Vsed, various non-water bearing sedimentary units. Gray-shaded regions depict the studied subwatersheds. (b-g) Geologic maps of the subwatersheds. Contour lines represent 100 m changes in elevation.

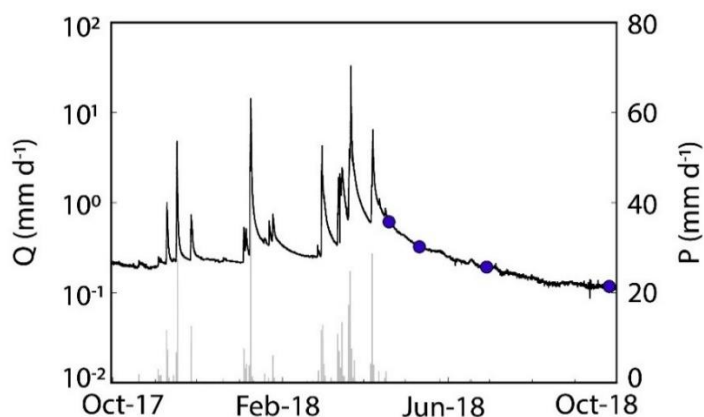


**Figure 1-2. San Lorenzo River specific discharge.**

San Lorenzo River mainstem specific discharge (Q) at USGS 11160500 and daily precipitation (P) for the 2018 water year at NCDC Station US1CASZ0024. Synoptic sampling events are indicated by blue markers on the hydrograph.

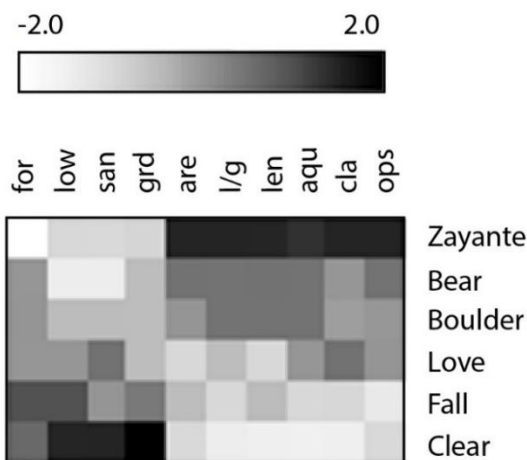


**Figure 1-3. Heatmap visualization of watershed characteristics.**

Heatmap visualization of subwatershed characteristics. Characteristics were centered by the mean and scaled by the standard deviation. FOR, %forest; low, %low permeability bedrock; san, %sand in soil; grd, mean stream gradient; ops, %open space; cla, %clay in soil; aqu, %aquifer; l/g, stream length/mean gradient; are, watershed area; len, stream length. See Table S5 for the actual values.

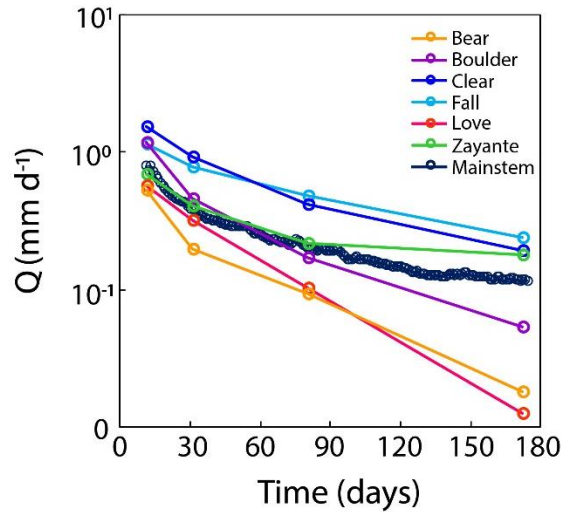


**Figure 1-4. Specific discharge for all streams.**

Time (days) versus specific discharge,  $Q$ , ( $\text{mm d}^{-1}$ ) for all streams. Mainstem  $Q$  is shown for USGS 11160500. Markers represent the sampling events.

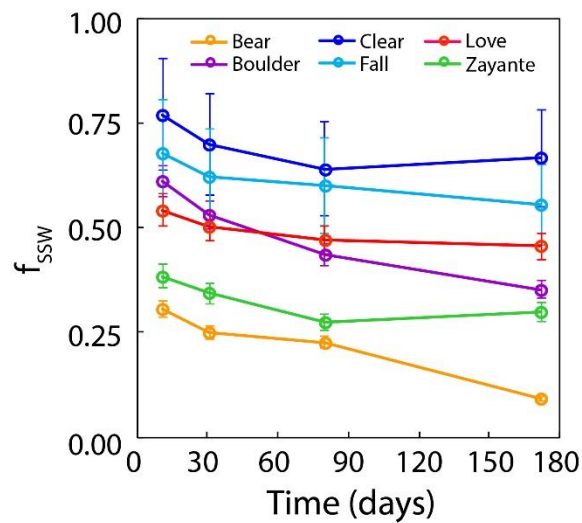


**Figure 1-5. Shallow subsurface water contributions to baseflow.**

Time (days) versus fraction of stream water baseflow from SSW ( $f_{SSW}$ ) for all streams. Error bars represent the range of fractions produced using the upper and lower estimates of SSW endmember geochemistry. Markers represent the sampling events.

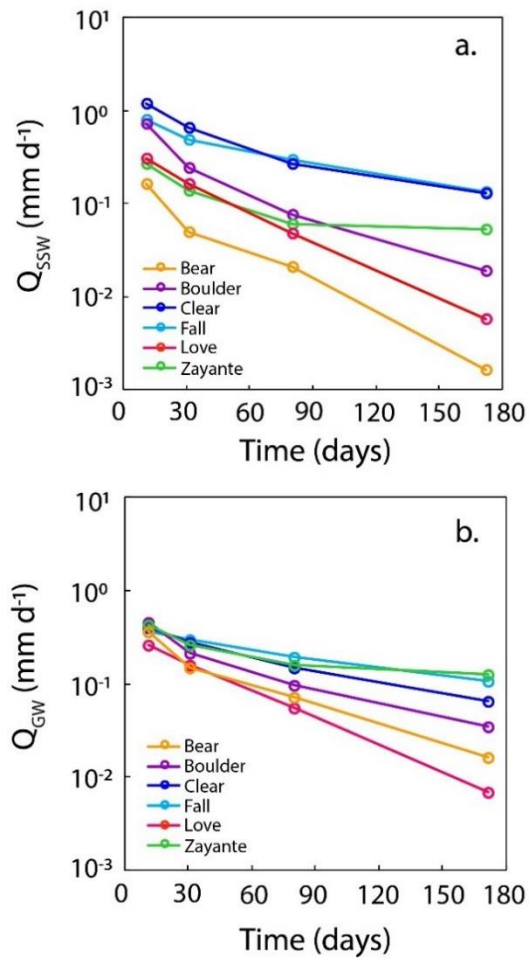


**Figure 1-6. Shallow subsurface water and groundwater specific discharge through time.**

Time (days) versus (a) specific discharge ( $\text{mm d}^{-1}$ ) from SSW ( $Q_{SSW}$ ) and (b) specific discharge from GW ( $Q_{GW}$ ) for all streams. Markers represent the sampling events.

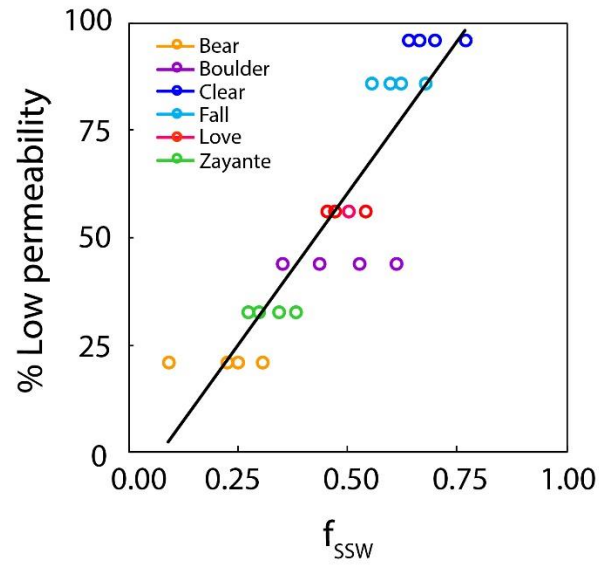


**Figure 1-7. Shallow subsurface water fractions versus bedrock permeability.**

Fraction of stream water baseflow from SSW ( $f_{SSW}$ ) versus percent of subwatershed with low permeability bedrock. Markers represent the sampling events ( $r_s = 0.93$ , see Table 1).

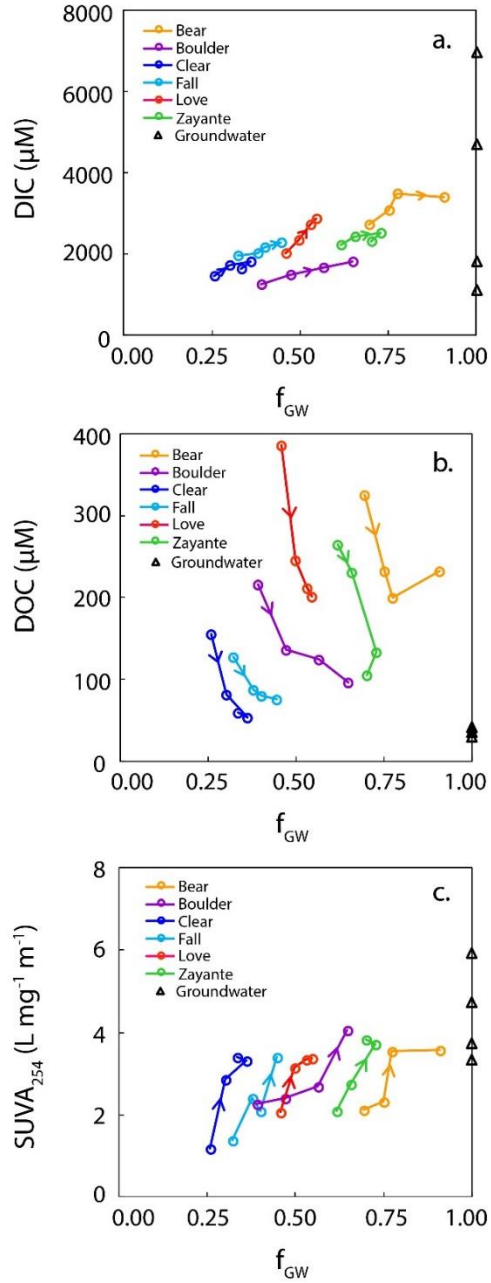


**Figure 1-8. Groundwater fractions versus dissolved carbon geochemistry.**

Fraction of stream water baseflow from GW ( $f_{GW}$ ) versus (a) DIC concentration, (b) DOC concentration, and (c)  $\text{SUVA}_{254}$ . Markers represent the sampling events with time progressing in the direction of the arrow. Black triangles represent the range in GW endmember concentrations or values.

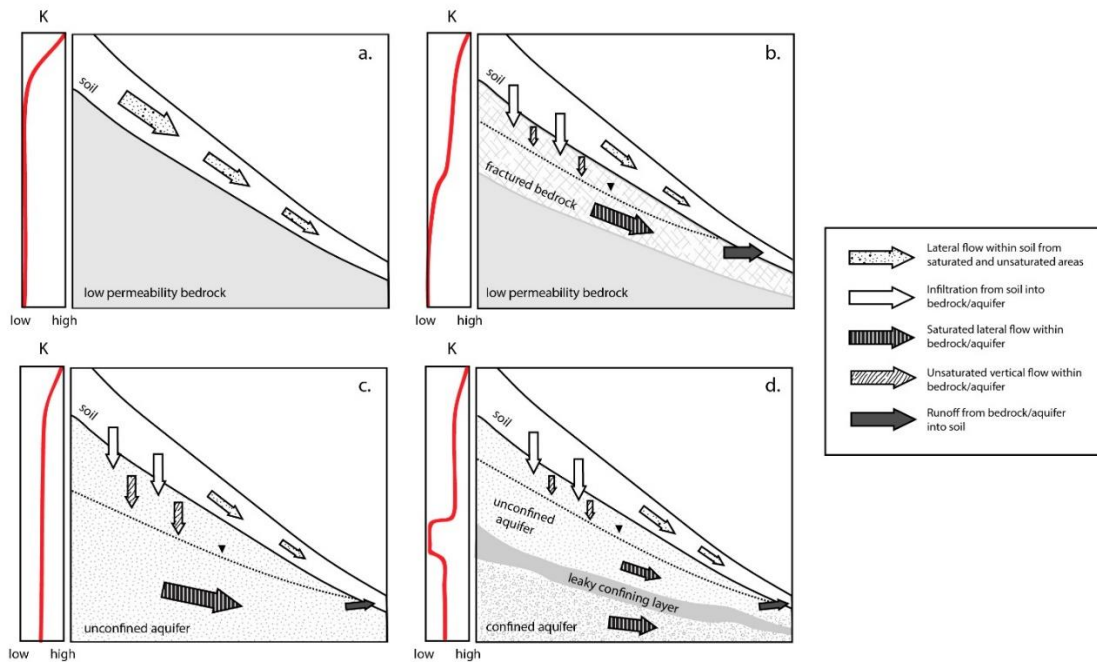


**Figure 1-9. Conceptual diagram of baseflow generation processes.**

Conceptual diagram of baseflow generation processes in a range of geologic settings showing how various flow paths can contribute to baseflow. Each subfigure shows hillslope depictions of baseflow dominated by (a) shallow subsurface water contributions, (b) bedrock groundwater emerging as shallow subsurface water contributions, (c) groundwater contributions, and (d) groundwater contributions from multiple aquifers. All lateral arrows represent flow paths that can eventually contribute to runoff. Sideplots accompanying each subfigure show possible changes in hydraulic conductivity,  $K$ , (as an indicator of permeability) with depth. Figure is not to scale and is modified from Katsura et al. (2008).

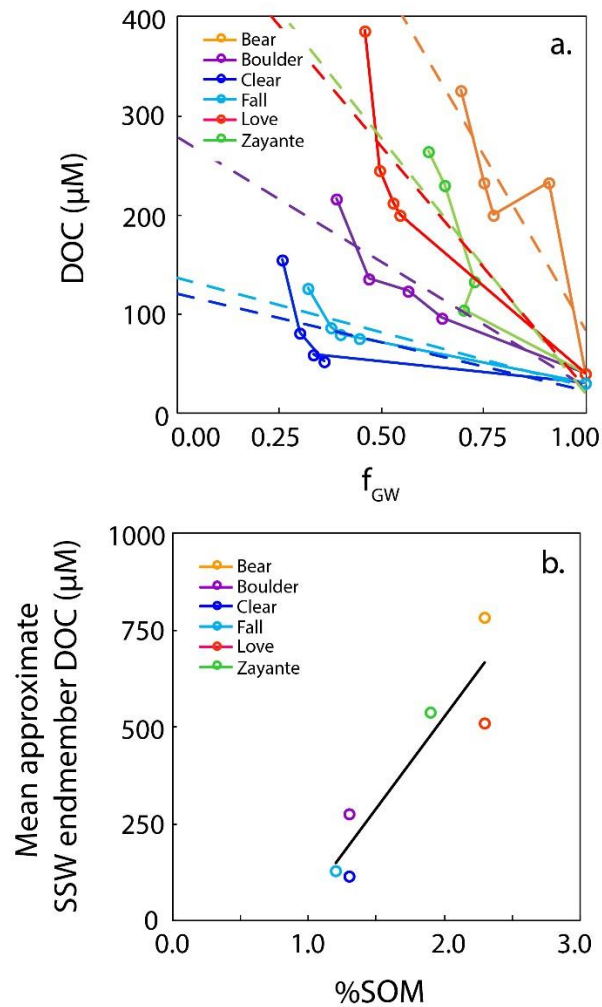


**Figure 1-10. DOC mixing relationships for each stream.**

(a) Stream water DOC concentration versus the fraction of stream water baseflow from GW ( $f_{GW}$ ) with mixing lines displayed for each stream using GW endmember DOC and stream DOC concentrations, and (b) percent soil organic matter (%SOM) in each subwatershed versus the back-calculated SSW endmember DOC concentration for each subwatershed ( $r_s=0.79$ ).

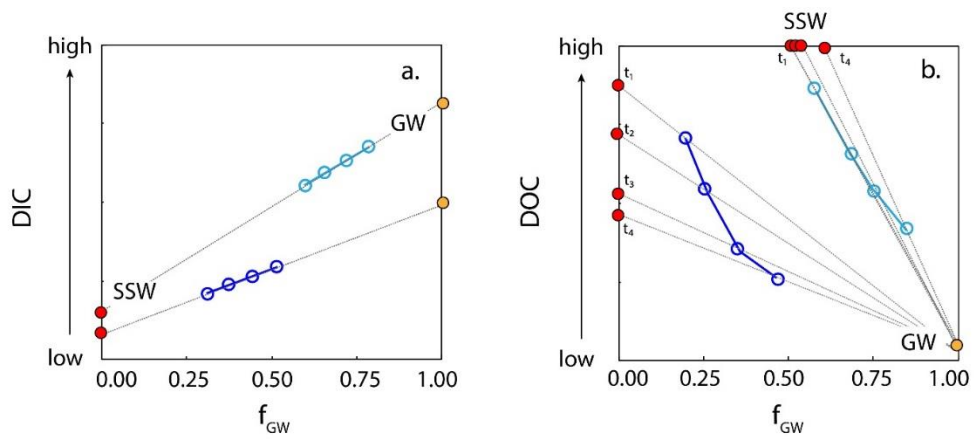


**Figure 1-11. Theoretical mixing of endmembers controlling dissolved carbon concentrations.**

Generalization of hypothetical stream water dissolved carbon mixing dynamics controlled by (a) SSW and GW endmembers with relatively uniform DIC geochemistry through the summer dry down period and (b) a spatially variable SSW endmember with shifting DOC geochemistry and static GW DOC concentrations through the summer dry down period.

**Table 1-1. Spearman’s rank of watershed characteristics and respective baseflow contributions.**

Spearman’s rank correlation coefficients ( $r_s$ ) between subwatershed characteristics and specific discharge (Q), fraction of streamflow from shallow subsurface water ( $f_{ssw}$ ), specific discharge from SSW ( $Q_{ssw}$ ), and specific discharge from GW ( $Q_{gw}$ ).

	Geology		Topography				Land use		Soil	
	%Aquifer	%Low permeability	Area	Length	Gradient	L/G	%Forest	%Open Space	%Clay	%Sand
<b>Q</b>										
Apr-2018	-0.49	0.71	-0.49	-0.49	0.31	-0.37	0.64	-0.66	-0.71	0.60
May-2018	-0.64	0.83	-0.54	-0.54	0.49	-0.54	0.75	-0.77	-0.77	0.66
Jun-2018	-0.49	0.71	-0.31	-0.31	0.37	-0.43	0.64	-0.66	-0.54	0.49
Sept-2018	-0.49	0.71	-0.31	-0.31	0.37	-0.43	0.64	-0.66	-0.54	0.49
<i>Cumulative</i>	-0.14	0.07	-0.04	-0.04	0.26	-0.17	0.10	-0.06	-0.21	0.01
<b><math>f_{ssw}</math></b>										
Apr-2018	-0.81	0.94 <sup>2</sup>	-0.77	-0.77	0.60	-0.71	0.84 <sup>2</sup>	-0.89 <sup>2</sup>	-0.83	0.83
May-2018	-0.81	0.94 <sup>2</sup>	-0.77	-0.77	0.60	-0.71	0.84 <sup>2</sup>	-0.89 <sup>2</sup>	-0.83	0.83
Jun-2018	-0.90 <sup>2</sup>	1.00 <sup>1</sup>	-0.89 <sup>2</sup>	-0.89 <sup>2</sup>	0.66	-0.83	0.75	-0.83	-0.71	0.94 <sup>2</sup>
Sept-2018	-0.90 <sup>2</sup>	1.00 <sup>1</sup>	-0.89 <sup>2</sup>	-0.89 <sup>2</sup>	0.66	-0.83	0.75	-0.83	-0.71	0.94 <sup>2</sup>
<i>Cumulative</i>	-0.83	0.93	-0.80	-0.80	0.61	-0.75	0.77	-0.83	-0.74	0.85
<b><math>Q_{ssw}</math></b>										
Apr-2018	-0.81	0.94 <sup>2</sup>	-0.77	-0.77	0.60	-0.71	0.84 <sup>2</sup>	-0.89 <sup>2</sup>	-0.83	0.83
May-2018	-0.81	0.94 <sup>2</sup>	-0.77	-0.77	0.60	-0.71	0.84 <sup>2</sup>	-0.89 <sup>2</sup>	-0.83	0.83
Jun-2018	-0.58	0.77	-0.43	-0.43	0.43	-0.49	0.81	-0.83	-0.71	0.54
Sept-2018	-0.58	0.77	-0.43	-0.43	0.43	-0.49	0.81	-0.83	-0.71	0.54
<i>Cumulative</i>	-0.45	0.55	-0.37	-0.37	0.35	-0.40	0.50	-0.52	-0.47	0.43
<b><math>Q_{gw}</math></b>										
Apr-2018	0.40	-0.15	0.38	0.38	-0.41	0.49	-0.04	0.09	-0.09	-0.23
May-2018	-0.49	0.71	-0.31	-0.31	0.37	-0.43	0.64	-0.66	-0.54	0.49
Jun-2018	-0.12	0.31	0.14	0.14	0.14	-0.09	0.41	-0.37	-0.31	0.03
Sept-2018	-0.12	0.31	0.14	0.14	0.14	-0.09	0.41	-0.37	-0.31	0.03
<i>Cumulative</i>	-0.02	0.12	0.06	0.06	0.02	-0.01	0.12	-0.11	-0.12	0.02

<sup>1</sup>Significance of p<0.01

<sup>2</sup>Significance of p<0.05

## Supplemental Index



**Figure S1.** Bivariate solute-solute plots of stream water geochemistry.

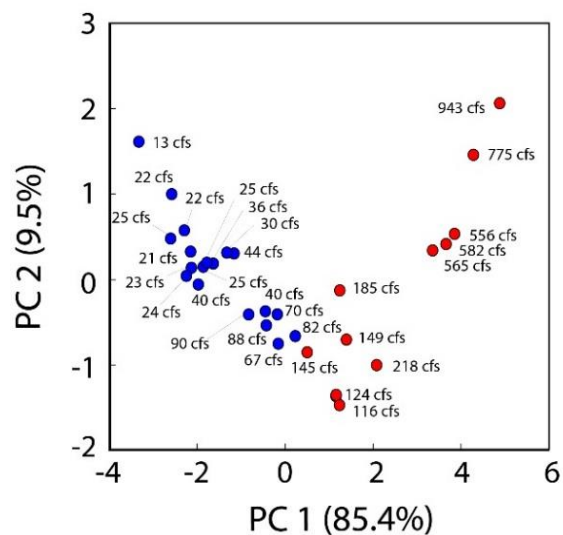


**Figure S2.** PCA of mainstem San Lorenzo River water quality data separated using k-means clustering: red markers show samples that separated out into high flow samples, and blue markers show samples that separated out into low flow samples. Corresponding flow is shown next to each sample.

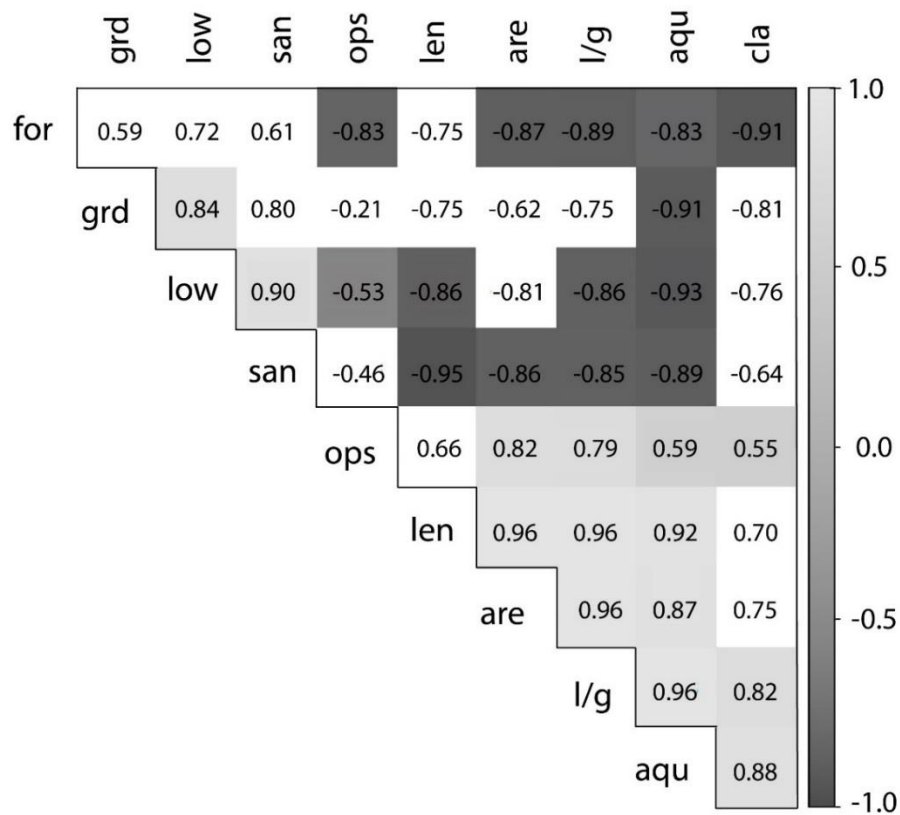


**Figure S3.** Correlogram of catchment characteristics. Shaded cells show  $R^2$  values and indicate  $p < 0.05$ . FOR, %forest; low, %low permeability bedrock; san, %sand in soil; grd, mean stream gradient; ops, %open space; cla, %clay in soil; aqu, %aquifer; l/g, stream length/mean gradient; are, watershed area; len, stream length. Table S5 for the actual values.

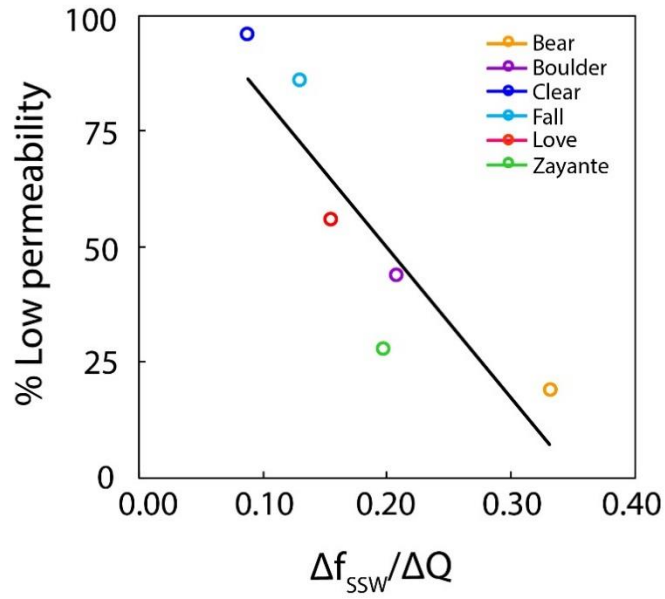


**Figure S4.** Percent of subwatershed with low permeability bedrock versus the change in the fraction of stream water baseflow from SSW ( $f_{SSW}$ ) over the change in specific discharge ( $Q$ ) ( $r_s = -0.94$ ).

**Table S1.** Analytical precision and accuracy for all analytes used in this study.

	Sp. Cond.	NO <sub>3</sub> <sup>-</sup>	PO <sub>4</sub> <sup>3-</sup>	Mg <sup>2+</sup>	Na <sup>+</sup>	Ca <sup>2+</sup>	Cl <sup>-</sup>	SO <sub>4</sub> <sup>2-</sup>	DIC	DOC	SUVA <sub>254</sub>
<b>Analytical accuracy (%)</b>	2.5	5.2	1.8	0.6	0.3	1.7	8.3	8.0	3.4	3.3	3.3
<b>Analytical precision (%)</b>	2.5	0.9	1.0	1.4	1.2	1.1	5.6	3.1	3.1	2.5	3.5
<b>Cumulative error (%)</b>	3.5	5.2	2.0	1.5	1.3	2.1	9.9	8.6	4.6	4.2	4.8

**Table S2.** EMMA residuals. The selected model explained 92.2% of the cumulative variance in stream water geochemistry.

	Sp. Cond. (μS cm <sup>-1</sup> )	NO <sub>3</sub> <sup>-</sup> (μM)	PO <sub>4</sub> <sup>3-</sup> (μM)	Mg <sup>2+</sup> (μM)	Na <sup>+</sup> (μM)	Ca <sup>2+</sup> (μM)	Cl <sup>-</sup> (μM)	SO <sub>4</sub> <sup>2-</sup> (μM)	Mean
<b>Residual structure (R<sup>2</sup>)</b>	0.0034	0.10	0.14	0.055	0.069	0.062	0.065	0.11	0.07 ± 0.04
<b>Mean absolute residual</b>	8.8	4.5	0.9	25	104	84	49	88	na
<b>Absolute analytical error</b>	12.7	1.1	0.1	5	11	21	52	39	na

**Table S3.** Surface cover of primary aquifers in each subwatershed.

<b>Primary aquifer</b>	<b>Bear</b>	<b>Boulder</b>	<b>Clear</b>	<b>Fall</b>	<b>Love</b>	<b>Zayante</b>
% Butano	24	21	0	0	12.5	14.1
% Lompico	0.5	3.5	2.6	11.9	3.7	1.4
% Santa Margarita	0	0.8	0	0	2.8	17.4

**Table S4.** SSW and GW endmember geochemistry used in EMMA.

Primary Aquifer	Sp. Cond. ( $\mu\text{S cm}^{-1}$ )	$\text{NO}_3^-$ ( $\mu\text{M}$ )	$\text{PO}_4^{3-}$ ( $\mu\text{M}$ )	$\text{Mg}^{2+}$ ( $\mu\text{M}$ )	$\text{Na}^+$ ( $\mu\text{M}$ )	$\text{Ca}^{2+}$ ( $\mu\text{M}$ )	$\text{Cl}^-$ ( $\mu\text{M}$ )	$\text{SO}_4^{2-}$ ( $\mu\text{M}$ )
SSW <sub>LOWER</sub>	39	3	0	1	10	1	11	2
SSW <sub>UPPER</sub>	175	0	0	210	400	412	207	51
Butano GW	933	0	1	1355	3734	1568	1443	1054
Lompico I GW	194	10	19	84	683	424	263	404
Lompico II GW	422	0	2	226	1539	888	768	915
Santa Margarita GW	146	192	28	42	451	390	340	107

**Table S5.** Subwatershed spatial characteristics. See Figure 3 for a graphic depiction of the characteristics.

Classification	Indices	Bear	Boulder	Clear	Fall	Love	Zayante
Topography	Area ( $\text{km}^2$ )	42.7	29.9	3.7	12.9	7.9	69.5
	Stream length (km)	13.5	12.4	3.6	8.2	6.2	16.5
	Stream gradient (%)	2.9	2.5	13.2	6.4	2.9	2.1
Geology	%Low Permeability	21	44	96	86	56	33
	%Aquifer	25	25	3	12	19	33
Land use	%Forest	84	85	88	89	84	75
	%Open Space	16	14	11	10	15	21
Soil	%Sand	58	60	66	62	63	59
	%Clay	17	17	15	16	18	20

**Table S6.** Soil organic matter percentages (%SOM) for each subwatershed taken as weighted averages by depth from SSURGO.

Indices	Bear	Boulder	Clear	Fall	Love	Zayante
%SOM (0-200 cm)	2.3	1.3	1.3	1.2	2.3	1.9
%SOM (0-10 cm)	6.1	3.6	3.7	4.2	4.7	3.6

## Chapter 2

# **LATERAL CARBON EXPORTS FROM DRAINED PEATLANDS: AN UNDERSTUDIED CARBON PATHWAY IN THE SACRAMENTO-SAN JOAQUIN DELTA, CALIFORNIA**

Submitted to Journal of Geophysical Research Biogeochemistry: Richardson, C., J. K. Fackrell, T. E.C. Kraus, M. Young, and A. Paytan. Lateral carbon exports from drained peatlands: an understudied carbon pathway in the Sacramento-San Joaquin Delta, California.

## **Abstract**

Degradation of peatlands via drainage is increasing globally and destabilizing peat carbon (C) stores. The effects of drainage on the timing and magnitude of lateral C losses from degraded peatlands remains understudied. We measured spatial and temporal variability in lateral C exports from three drained peat islands in the Sacramento-San Joaquin Delta in California across the 2017 and 2018 water years using measurements of DIC, DOC, and POC concentration combined with discharge. These measurements were supplemented with stable isotope data ( $\delta^{13}\text{C-DIC}$ ,  $\delta^{13}\text{C-POC}$ ,  $\delta^{15}\text{N-PON}$ , and  $\delta^2\text{H-H}_2\text{O}$  values) to provide insight into hydrological and biogeochemical controls on lateral C exports from drained peatlands. Drainage C concentrations were seasonally variable with the highest values in the winter rainy season, when discharge, as well as DOC and DIC concentrations, were elevated. This seasonal difference in the mobilization of dissolved C appeared to be a response to changing water sources and water table levels. Peat island drainage C contributions to surrounding waterways were also greatest during the winter. Although temporal variability in C cycling processes and trends were generally similar across islands, baseline drainage DIC, DOC, and POC concentrations were spatially variable, likely a result of sub-island scale differences in soil organic matter content and hydrology. This spatial variability complicates system-wide assessments of C budgets. Net lateral C exports were water year dependent and comparable to previously published vertical C emission rates for this system. This work highlights the importance of including

lateral C exports from drained peatlands in local and regional C budgets.

## **2.1 Introduction**

Peatlands are an important land based carbon (C) sink, storing almost 1/3 of the world's soil C (Gorham, 1991; Jenkinson et al., 1991). Human disturbances to peatlands are increasing globally, destabilizing peat C stores and compromising their capacity to serve as C sinks (Leifeld & Menichetti, 2018; Sanderman et al., 2017). Over 10 percent of the planet's peatlands have been drained or mined (Joosten, 2009). Drainage of peatlands can alter prevailing biogeochemical processes, with effects on dissolved/particulate (lateral) and gaseous (vertical) C exports. Greenhouse gas (GHG) emissions have been the focus of many studies in degraded peatlands as these systems can emit large amounts of CO<sub>2</sub>, CH<sub>4</sub>, and N<sub>2</sub>O to the atmosphere (Leifeld & Menichetti, 2018). Lateral C exports, as dissolved inorganic C (DIC), dissolved organic C (DOC), and suspended particulate organic carbon (POC), remain an understudied component of peatland C budgets (Worrall et al., 2005). Past work suggests that lateral C losses from peatlands can be significant components of local C budgets, and not accounting for lateral C terms can lead to mischaracterizations of gaseous C sequestration. DOC exports are 10 percent of C losses in some systems (Limpens et al., 2008), and water flowing through peatlands is typically supersaturated with respect to CO<sub>2</sub> (Billett & Moore, 2008; Dawson et al., 2002; Dawson et al., 2004), indicating that DIC exports may be important as well. Lateral C exports can impact downstream ecosystems through the delivery of organic and

inorganic C with effects on water quality, primary productivity, calcification, bacterial production, metal mobilization, and light availability (Carpenter & Pace, 1997; Schindler et al., 1997; Wetzel, 2003; Williamson et al., 1999; Wit et al., 2018). Many questions still exist regarding the nature of and controls on the magnitude of lateral C exports from peatlands, especially in altered and drained systems.

Drainage changes fundamental hydrologic properties of peatlands (e.g., water storage, recharge, and release). Water table declines induced by drainage have been documented in a number of altered peatlands (Deverel et al., 2007; Deverel & Rojstaczer, 1996; Holden et al., 2011; Price, 2003; Strack et al., 2008). Drainage has also been shown to shift flow pathways through peat; Holden et al. (2006) found drainage reduces overland flow and increases throughflow. These changes in peat hydrology can affect subsurface properties (e.g., macropore density, bulk density, soil water content, oxygen availability, and temperature). Water table draw down is commonly associated with an ingress of O<sub>2</sub>, and this ingress can shift historically anaerobic peat systems to aerobic environments (Limpens et al., 2008). These physicochemical properties control biotic and abiotic C storage and release mechanisms. For example, Chow et al. (2006) found that C mineralization rates and CO<sub>2</sub> production respond to changes in soil water content and temperature in peat soils.

In this study, we leverage the artificial infrastructure of drained peatlands in the

Sacramento-San Joaquin Delta (the Delta) in central California, a system that provides freshwater to over 27 million people and generates 1.6 billion in economic output from agriculture (DPC, 2012), to better understand variability and controls on peat drainage C geochemistry and exports (DPC, 2012). The Delta is a ~2800 km<sup>2</sup> inverse delta that consists of approximately fifty-seven peat islands that are drained into surrounding river channels; all drainage occurs via managed outlets, allowing for relatively robust estimates of discharge. Peat oxidation from continuous drainage of Delta islands for farming over the past century has led to land subsidence of up to 15 meters in some locations (Deverel & Leighton, 2010). While gaseous C exchange has been extensively studied on Delta islands (Anderson et al., 2016; Baldocchi et al., 2012; Hatala et al., 2012; Hemes et al., 2019; Knox et al., 2015; Teh et al., 2011; Windham-Myers et al., 2018), little quantitative work exists documenting the magnitude and timing of lateral C exports. A better understanding of lateral C losses from Delta islands is needed to address current knowledge gaps on local C budgets and C accounting and, more broadly, degraded peatland C balances. This is especially relevant in the Delta as stakeholders and agencies are pursuing new initiatives to reduce GHG emissions in the Delta using GHG accounting to incentivize low emissions land use management practices. Lateral C exports from Delta islands may also create water quality issues in surrounding waterways and in water conveyed to other areas of California (Fleck et al., 2007; Fujii et al., 1998). Previous work has shown that dissolved organic matter (DOM) inputs from drained Delta islands are associated with seasonal changes in downstream river DOM quality (Kraus et al.,

2008), suggesting that lateral C exports from these islands are measurable and important sources of C to Delta waters seasonally. In this study, we present hydrological and biogeochemical data from three artificially drained peat islands in the Delta over the course of two water years to: (1) quantify lateral C exports from drained Delta peat islands and assess whether they vary in time and space, (2) examine the timing and magnitude of lateral C exports to better understand physical and biogeochemical controls on C geochemistry, and (3) compare lateral C fluxes to vertical C fluxes to assess the importance of this term in peat C budgets. This work will improve our conceptual understanding of similarly drained and cultivated peatlands elsewhere, which are growing in number worldwide due to human alteration.

## **2.2 Methods**

### **2.2.1 Study location**

The Sacramento-San Joaquin Delta (Delta), which makes up the landward region of the San Francisco Estuary (Fig. 1), has a Mediterranean climate that is generally defined by cool, wet winters and hot, dry summers. The Sacramento and San Joaquin rivers provide the majority of freshwater inflow and allochthonous organic C to Delta waters as they drain ~40% of California's land area (Jassby & Cloern, 2000; Roy et al., 2006). Wastewater treatment plants are major anthropogenic sources of allochthonous C to the Delta as well, with the Sacramento Regional County Wastewater Treatment Plant contributing the greatest mass fluxes of DOC (~350 to

550 Mg C per month) (Sickman et al., 2007).

The Central Delta is comprised of surficial peat deposits, up to 15 m thick, and mineral soils at depth (Atwater & Belknap, 1980). The peat soils of the Delta contain 5 to 52% organic matter (Deverel et al., 2016). This region was drained beginning in the mid-1880's, and by the 1930's was transformed into a patchwork of leveed tracts of lands surrounded by fixed channels, commonly referred to as "islands". The elevation of Delta islands is typically below the water level of surrounding river channels. To prevent island inundation and flooding, water levels on Delta islands are artificially managed by a system of ditches which route excess water for discharge at pump stations on each island. Peat island drainage waters are a combination of seepage waters, irrigation waters (e.g., water deliberately suctioned onto the island from surrounding river channels), and precipitation. The proportion of these sources varies by season, land use, and management practices.

For this study, drainage water from pump stations on three Delta islands – Sherman, Staten, and Twitchell (Fig. 1) – were sampled monthly from June 2017 to September 2018 for a suite of geochemical parameters (concentrations and stable isotope composition of dissolved and particulate C as well as more ancillary water quality parameters). Sherman Island is dominated by pastureland (>55%), with cropland secondary in spatial coverage (~30%) (Table S1). Twitchell Island has a more mixed land use with several experimental wetlands (~30%), pastureland (20%), and

cropland (48%) (Table S1). Staten Island is predominantly cropland (>95%). Crops on Staten Island include alfalfa, corn, potatoes, and wheat. In addition to the drainage samples, samples were collected from surrounding river channels at seven locations (Fig. 1). A multi-parameter water quality meter (YSI ProPlus) was used to measure ancillary water parameters (pH, dissolved oxygen, conductivity, and temperature) at the time of sample collection. This study focuses on the peat drainage C geochemistry data and only limited river geochemistry data are presented. Additionally, we excluded geochemistry data for any sites where monthly discharge was zero (e.g., May 2018 to September 2018 at SH-P4 and all of SH-P1).

### 2.2.2 Geochemistry sample collection and analysis

Drainage samples were collected monthly from water in ditches within ~5 feet of pump stations, and river samples were collected from island shores. Water samples were collected in 1 to 4 L bottles for subsampling. Samples for DIC were immediately poured off into 125 mL borosilicate bottles with Si-free greased glass stoppers and poisoned with  $\text{HgCl}_2$  to inhibit biological activity. DIC concentrations were measured using a UIC Carbon Coulometer Analyzer. DOC samples were vacuum filtered to 0.2  $\mu\text{m}$  in the lab (generally within 24 hours) into 22 mL glass vials and frozen for storage until analysis (typically within a week of collection). DOC concentrations were measured as non-purgeable organic carbon (NPOC) on a Shimadzu TOC-VCPH TOC/TN Analyzer. The NPOC method was used instead of the total organic carbon (TOC) method due to the effect of high DIC concentrations

on TOC measurements in fresh waters (Findlay et al., 2010).  $\text{SiO}_4^{4-}$  concentrations were measured using a Lachat AutoAnalyzer AA3, and  $\text{Cl}^-$  concentrations were determined using a Dionex ICS-2000 ion chromatography analyzer. Absorbance of light at 254 nm was measured for all samples on a Thermo Genesys 10S UV-Visible Spectrophotometer. These values were normalized to DOC concentration to obtain mass-specific UV absorbance ( $\text{SUVA}_{254}$ ). Errors on precision and accuracy for all of the above analyses were generally below 5%. Total suspended sediment (TSS) concentrations were determined by weight after passing known volumes of unfiltered sample water through combusted, pre-weighed GF/F filters (0.7  $\mu\text{m}$ ). Particulate organic matter (POM) concentrations were estimated from TSS concentrations. POM was assumed to comprise the majority of TSS (75%) since carbonates make up  $\ll 1\%$  of Delta soils (Drexler et al., 2009), and 50% of POM was assumed to be C by mass (Deverel & Rojstaczer, 1996). For river TSS samples, we used previously published relationships for TSS and POC for the Delta from Murrell and Hollibaugh (2000) to calculate POC concentrations. Temperature, DIC, and pH data were used to calculate  $\text{pCO}_2$  using CO2calc (Robbins et al., 2010). Mean values, as averages of all drainage or river sites, are denoted herein as " $\bar{x}$ " and typically presented with their 1-sigma standard deviation. All seasonal means and fluxes presented in this study are from WY 2018 only and grouped monthly as follows: fall (September through November), winter (December through February), spring (March through May), and summer (June through August).

### 2.2.3 Stable isotope sample collection and analysis

$\delta^{13}\text{C}$ -DIC samples were collected in 20 mL glass vials with minimal headspace and poisoned with  $\text{HgCl}_2$  immediately upon collection to inhibit biological activity.  $\delta^{13}\text{C}$ -DIC values were determined on a ThermoQuest Finnigan Delta PlusXL at the University of Arizona Stable Isotope Facility. Analytical precision for  $\delta^{13}\text{C}$ -DIC values was 0.2‰.  $\delta^{13}\text{C}$ -POC and  $\delta^{15}\text{N}$ -PON samples were collected quarterly, and all samples were processed and analyzed at the USGS-Menlo Park Stable Isotope Facility using a Carlo Erba NC 1500 elemental analyzer coupled to an Isoprime mass spectrometer. POM ratios of C to N are presented herein as molar fractions as  $(\text{C/N})_m$ . Analytical precision for  $\delta^{13}\text{C}$ -POC and PON values was 0.3‰ and 0.4‰, respectively, and 0.1 for  $(\text{C/N})_m$  of POM.  $\delta^2\text{H}$ - $\text{H}_2\text{O}$  samples were collected monthly and run at the University of Hawaii's Biogeochemical Stable Isotope Facility on a Picarro L2130-i. Analytical precision for  $\delta^2\text{H}$ - $\text{H}_2\text{O}$  values was 0.5‰.

### 2.2.4 Discharge measurements, mass flux estimates, and net flux estimates

Discharge for each pump site,  $D$  (ac-ft), was calculated using an empirical equation based on the unit-power consumption method, which relies on electrical usage,  $P$  (kW-hr), and measured pump efficiency,  $U$  (kW-hr ac-ft<sup>-1</sup>), to generate discharge estimates where  $D=P/U$  (Diamond & Williamson, 1983; Ogilbee, 1966; Ogilbee & Mitten, 1979). Electrical records were obtained from the electrical utility for each pump station (e.g., peat island drainage outlet) from October 2016 to October 2018, and each pump was assessed for pump efficiency (defined as the unit-use coefficient

which is a measure of the amount of electrical energy it takes to pump a known volume of water) within two months of the start of sampling except for TW-P1, which had a recent active test in October 2016 (Table S2). Discharge estimates were cross-checked with 1.5 years of daily flow meter data (AgriFlo XCi ultrasonic sensor) available from TW-P1 on Twitchell Island. This cross-comparison indicated that the unit-power consumption method is a relatively robust approximation of discharge ( $m=0.87$ ,  $R^2=0.75$ ) (Fig. S1). Importantly, this cross-comparison suggested that the unit-power consumption method consistently underestimates actual discharge. As such, our export and flux calculations herein are considered conservative estimates of actual total lateral C losses (as the sum of DIC, DOC, and POC) from drained Delta islands.

Discharge and mass flux data are presented in the context of water years (WY). WY 2017 (10/01/2016 to 09/30/2017) was classified as above normal (referred to herein as “wet”), with cumulative annual precipitation at California Irrigation Management Information System (CIMIS) Station 242 (located on Staten Island) totaling 95.4 cm (<https://cimis.water.ca.gov/>). WY 2018 (10/01/2017 to 09/30/2018) was below normal (referred to herein as “dry”), with cumulative annual precipitation at CIMIS Station 242 totaling 27.9 cm.

Peat drainage DOC and DIC fluxes were calculated from monthly concentration and discharge data for each island. On islands with more than one drainage outlet (Staten

and Sherman), we summed C fluxes for each outlet. POC fluxes were generated quarterly, at the same interval as POC sample collection. We report export rates as mass flux divided by area. Drainage areas for each site were subdivided based on topographical divides within islands (see Fig. S2). Export rates for WY 2017 were extrapolated from WY 2018 concentration-water yield (discharge normalized to area) relationships to fill in missing concentration data for WY 2017 (Table S3). Specifically, regressions developed from WY 2018 for each station were applied to associated WY 2017 data and sites; 19 of 25 regressions were statistically significant ( $p < 0.05$ ) (Table S3).

DOC fluxes from other regionally important allochthonous sources were calculated for comparison to peat island drainage DOC contributions to Delta waters. DOC flux from the Sacramento River at Freeport was calculated at 15-minute resolution using fluorescent dissolved organic matter (fDOM) data corrected to DOC concentrations ( $R^2 = 0.63$ ,  $n = 26$  between 10/19/2016 to 08/20/2019) and discharge data from the United States Geological Survey (USGS) monitoring station 11447650. San Joaquin River at Vernalis DOC flux was calculated using the average concentration of sub-monthly grab samples collected by the USGS and discharge data from USGS monitoring station 11303500. Sacramento Regional Wastewater Treatment Plant (WWTP) DOC flux was calculated using monthly DOC concentrations and discharge data downloaded via the California Integrated Water Quality System (<https://www.waterboards.ca.gov/ciwqs/>).

Island water budgets were developed for WY 2017 and WY 2018 to generate baseline estimates of lateral C imports to Delta islands via river inflow for use in net lateral C calculations. Annual water inflow, including both seepage through levees and water diverted onto the island for irrigation, were calculated for each island studied (ST, SH, and TW) as follows:

$$I = O + ET - P$$

where I is river inflow (ac-ft), O is island drainage outflow (ac-ft), ET is evapotranspiration (ac-ft), and P is precipitation (ac-ft). Water budget data are shown in Table S4. Outflow was determined by the unit-use power consumption method discussed above. P was based on measured data from Station 247 for Sherman Island, Station 242 for Staten Island, and Station 140 for Twitchell Island via CIMIS (<https://cimis.water.ca.gov/>). ET was calculated at a monthly scale and summed to annual by correcting monthly reference evapotranspiration rates using crop coefficients for land use cover on each island for both a wet WY (2017) and dry WY (2018) (<http://www.itrc.org/etdata/index.html>). Land use cover on each island was determined using a statewide crop mapping geodatabase available online (<https://data.cnra.ca.gov/dataset/statewide-crop-mapping>) (see Table S1). Change in storage was assumed to be negligible on an annual scale. Inflow C import rates were calculated using C species concentration data for waterways surrounding each island averaged across WY 2018 (Table 1). Net C fluxes from each island were calculated

by subtracting inflow C flux (or import) from drainage C flux (or export).

## **2.3 Results**

### 2.3.1 Discharge trends from peat drainage outlets

Peat drainage discharge was highly variable across islands and water years, though seasonal trends were apparent. Across all three islands, discharge was generally greatest in the winter (December to February), with 49% and 32% of annual discharge occurring in winter of WY 2017 and WY 2018, respectively (Fig. 2).

Additional pulses of high discharge occurred in the summer on Twitchell and Staten islands, both of which contain greater proportions of irrigated cropland relative to Sherman Island (Table S1).

Cumulative discharge from all islands was substantially higher in wet WY 2017 than in dry WY 2018. On Sherman Island, discharge decreased 17%, from 12,700 ac-ft to 10,600 ac-ft, between WY 2017 and WY 2018. On Staten Island, discharge decreased 55% from 30,400 ac-ft to 13,800 ac-ft; this decrease was mainly driven by much lower discharge (up to 87%) during winter months in WY 2018. On Twitchell Island, annual discharge decreased 19% from 17,500 ac-ft in WY 2017 to 14,200 ac-ft in WY 2018.

### 2.3.2 Peat drainage geochemistry

$\delta^2\text{H-H}_2\text{O}$  values as well as concentrations of  $\text{Cl}^-$  and  $\text{SiO}_4^{4-}$  were used as semi-conservative tracers of water source. Peat drainage samples generally had an inverse relationship between (1)  $\text{Cl}^-$  and  $\delta^2\text{H-H}_2\text{O}$ , and (2)  $\text{Cl}^-$  and  $\text{SiO}_4^{4-}$  (Fig. 3). The two most southern drainage sites on Sherman Island, SH-P2 and SH-P3, generally had higher  $\text{Cl}^-$  concentrations compared to all other sites (Fig. 2). These sites also had higher  $\delta^2\text{H-H}_2\text{O}$  values, but a wide range of  $\text{SiO}_4^{4-}$  concentrations (120 to 590  $\mu\text{M}$ ). The two other Sherman Island drain sites, SH-P4 and SH-P5, had slightly lower  $\text{Cl}^-$  concentrations and  $\delta^2\text{H-H}_2\text{O}$  values, but higher  $\text{SiO}_4^{4-}$  values than the sites to the south.

Seasonal and annual mean DOC and DIC concentrations in peat island drainage waters were much higher than surrounding rivers and typically peaked in winter and early spring (Tables 1 and 2, Fig. 4a,b). On islands with multiple pump sites, DIC and DOC concentrations in drainage waters were highly variable between sites. On Sherman Island, mean annual DIC concentrations in drainage waters for all four sites (SH-P2, SH-P3, SH-P4, and SH-P5) ranged from  $2380 \pm 690$  to  $5580 \pm 2120$   $\mu\text{M}$ , and mean DOC concentrations ranged from  $1120 \pm 410$  to  $3540 \pm 1280$   $\mu\text{M}$ . Peat drainage on Staten Island (ST-P1 and ST-P2) had mean DIC and DOC concentrations of  $3160 \pm 1230$  to  $3800 \pm 1460$   $\mu\text{M}$  and  $1320 \pm 630$  to  $2670 \pm 1400$   $\mu\text{M}$ , respectively. Mean DIC and DOC concentrations in drainage from TW-P1 on Twitchell Island were less variable at  $1460 \pm 600$   $\mu\text{M}$  and  $2400 \pm 260$   $\mu\text{M}$ , respectively. Mean peat

island drainage water POC concentrations across all sites ranged from  $640 \pm 380$  to  $2180 \pm 720 \mu\text{M}$ , with no clear spatial or temporal trends (Table 1, Fig.4c).  $(\text{C/N})_m$  ratios of drainage POM were seasonally variable and generally fluctuated between 7.3 to 10.5 ( $\bar{x} = 9.0 \pm 1.8$ ) in the summer and 9.9 to 13.4 ( $\bar{x} = 11.5 \pm 1.2$ ) in the winter/spring (Table 2, Fig. 4d). Nearly all drainage sites were supersaturated with  $\text{CO}_2$  each month, and the highest  $\text{pCO}_2$  values occurred in winter and spring (Table 2). Multiple sites on Sherman Island had  $\text{pCO}_2$  values over 20,000  $\mu\text{atm}$ .

Peat drainage  $\text{SUVA}_{254}$  values ranged between 3.8 to 4.7  $\text{L mg C}^{-1} \text{m}^{-1}$ , with no notable patterns by site or date (Table 1).  $\delta^{13}\text{C-DIC}$  values were highly variable both spatially and temporally (Fig. 5a, Tables 1 and 2). Similar to variability in dissolved C concentrations, significant differences in  $\delta^{13}\text{C-DIC}$  values were recorded even for samples collected on the same island; for example, mean  $\delta^{13}\text{C-DIC}$  values for ST-P1 and ST-P2 were  $-7.3 \pm 3.0$  and  $-12.3 \pm 1.4$ , respectively.  $\delta^{13}\text{C-POC}$  and  $\delta^{15}\text{N-PON}$  values changed seasonally as well, alternating between: (1) lower  $\delta^{13}\text{C-POC}$  values and higher  $\delta^{15}\text{N-PON}$  values in the summer, and (2) higher  $\delta^{13}\text{C-POC}$  values and variable, but low  $\delta^{15}\text{N-PON}$  values in the winter and spring (Fig. 5b, c, Fig. S3).

### 2.3.3. Lateral C exports from drained peatlands

Mean annual DOC and DIC exports for each drainage site in WY 2018 ranged between 4.3 to 19.8  $\text{g C m}^{-2} \text{yr}^{-1}$  and 6.9 to 30.7  $\text{g C m}^{-2} \text{yr}^{-1}$ , respectively (Fig. 6, Table 3). Mean annual POC exports ranged from 2.1 to 18.3  $\text{g C m}^{-2} \text{yr}^{-1}$ . DIC and

DOC exports positively correlated with water yield at all sites, though islands with substantial cropland (e.g., Staten Island) showed two distinct relationships between water yield and C exports that were dependent on season (Fig. 6a-f). POC exports also correlated linearly with water yield, but regression strength was generally lower than those for DIC and DOC trends as sample numbers were limited due to quarterly collection frequency (Fig. 6g-i, Table S3). For 2017, because not all months were sampled, we used the 2018 relationship between water yield and C export to fill in missing C concentration data where discharge data was available (Oct-16 to May-17) (Table 3). Extrapolated lateral C export rates for WY 2017 were 1.5 to 2.8 times greater than WY 2018. Mean annual DIC, DOC, and POC exports for WY 2017 ranged from 15.5 to 48.3 g C m<sup>-2</sup> yr<sup>-1</sup>, 8.8 to 30.6 g C m<sup>-2</sup> yr<sup>-1</sup>, and 3.9 to 19.6 g C m<sup>-2</sup> yr<sup>-1</sup>, respectively. Inflow C import rates ranged in magnitude depending on water year, with WY 2017 rates generally lower than WY 2018 (Table 3). Total inflow C import rates ranged between 15.4 to 43.7 g C m<sup>-2</sup> yr<sup>-1</sup> for WY 2017 and 17.5 to 40.5 g C m<sup>-2</sup> yr<sup>-1</sup> for WY 2018. Net lateral C exports, after accounting for inflow C, ranged between 42.0 to 64.9 g C m<sup>-2</sup> yr<sup>-1</sup> for WY 2017 and 11.7 to 21.5 g C m<sup>-2</sup> yr<sup>-1</sup> for WY 2018.

## 2.4 Discussion

### 2.4.1 Hydrological and biogeochemical controls on peat drainage C geochemistry

The spatial and temporal trends in peat drainage water particulate and dissolved C concentrations and associated stable isotope values show that the biogeochemical controls on peat C geochemistry are complex. Previous work in peatlands have documented the dominant effect of hydrology on subsurface biogeochemistry, and many studies exist showing the key hydrologic role that water table elevation plays in peat C storage and release mechanisms (Aguilar & Thibodeaux, 2005; Chow et al., 2006; Limpens et al., 2008). While not measured directly in this study, work by Deverel et al. (2007) shows that Delta island water tables rise and fall seasonally. These seasonal trends in water table elevation and their connection to C biogeochemistry are corroborated by several years of historical data from Delta islands, available from Deverel et al. (2015) and online through the California Integrated Water Quality System (<https://www.waterboards.ca.gov/ciwqs/>), which show similar winter peaks and summer lows in not only water table elevation, but also peat drainage DOC concentrations (Fig. 7a, b). In fact, peat drainage DOC concentrations were strongly positively correlated to normalized changes in groundwater levels (Fig. 7c). Past work by Chow et al. (2006) shows that these increases in DOC concentrations during water table rises or “re-wetting periods” arise from changes in biogeochemistry, and this wet-dry cycling is often described as the “tea-bag effect” (Thibodeaux & Aguilar, 2005). The re-wetting phase induces DOC concentration increases through: (1) abiotic generation of a “quick-release” DOC

fraction from simple hydrolysis, and (2) biotic generation of a slow-release fraction from ongoing microbial C cycling (Aguilar & Thibodeaux, 2005).

This “tea-bag effect” also likely impacts related C parameters measured in this study, such as DIC and pCO<sub>2</sub>, due to the close connection between higher rates of organic matter decomposition and CO<sub>2</sub> production. Other geochemical variables, such as pH and dissolved oxygen content, are also closely connected to C cycling processes and can induce shifts in carbonate chemistry and oxygen availability. High pCO<sub>2</sub> values in peat drainage, an indication of heterotrophic utilization of organic matter, were generally associated with: (1) low pH and dissolved oxygen content, (2) high DOC, DIC, and SiO<sub>4</sub><sup>4-</sup> concentrations, and (3) low δ<sup>13</sup>C-DIC values (Fig. 8). These trends indicate differences in biogeochemical process and water source that are best explained by changes in groundwater elevation.

In the wet winter typical of Mediterranean climates, water tables rise and saturate the upper section of soils on Delta islands, which are rich in organic matter replenished during and after the summer growing season (Fig. 9a). Discharge of this shallow groundwater to drainage ditches constitutes a seasonal source of C with distinct geochemistry (Deverel et al., 2007). Respired soil CO<sub>2</sub> from upper soil layers dissolves in the water, which is subsequently transported to drainage ditches through hydraulic gradients induced by pumping. High pCO<sub>2</sub> values in this water were associated with high SiO<sub>4</sub><sup>4-</sup> concentrations, which is consistent with increased

groundwater contributions (Uhlenbrook et al., 2000). The high pCO<sub>2</sub> drainage waters in the winter were also associated with: (1) low dissolved oxygen concentrations, which indicates oxygen utilization for aerobic respiration (without sufficient replenishment from photosynthetic production of O<sub>2</sub>), (2) low pH from increases in dissolved CO<sub>2</sub> from respiration, and (3) low δ<sup>13</sup>C-DIC values, which represent seasonally increased contributions from mineralization of soil organic matter in the winter. While high pCO<sub>2</sub> values in peat drainage were associated with low δ<sup>13</sup>C-DIC values at most of our sampling sites, ST-P2 showed increases in δ<sup>13</sup>C-DIC values with elevated pCO<sub>2</sub> under anoxic conditions (Fig. 8c, S4). This site drains seasonally flooded agricultural fields that are hotspots of CH<sub>4</sub> emission (Pellerin et al., 2013). The winter enrichment in δ<sup>13</sup>C-DIC values at ST-P2 is likely a consequence of acetoclastic methanogenesis, a biogeochemical process that occurs under anaerobic conditions and produces DIC enriched in <sup>13</sup>C (Campeau et al., 2017). Carbonate mineral dissolution could also potentially increase DIC concentrations and δ<sup>13</sup>C-DIC values, but sediment cores from Delta islands indicate carbonates comprise <<1% of sediment (Drexler et al., 2009), making this mechanism unlikely. Drainage POM in the winter/spring was generally dominated by soil organic matter, as indicated by higher (C/N)<sub>m</sub> ratios of the POM (9.9 to 13.4,  $\bar{x} = 11.5 \pm 1.2$ ), elevated δ<sup>13</sup>C-POC values that best reflect degradation of terrestrial POM sources, and variable, but low δ<sup>15</sup>N-PON values that support N sources originating from recycling of fixed atmospheric N or residual fertilized crop biomass (Fig. S3) (Kendall et al., 2001).

During the summer, groundwater levels on Delta islands decrease due to diminished surface recharge (Fig. 9b). Summer also marks the start of the growing season, and islands with crops maintain water tables below the rooting zone via managed pumping. These water table declines, whether they result from natural weather patterns or crop management, allow for seasonal windows of peat oxygenation during times when soil temperatures are also elevated. Peat aeration increases aerobic C respiration in the unsaturated zone. Previous work on vertical C fluxes on Delta islands generally show increases in the magnitude of CO<sub>2</sub> fixed and produced by ecosystem photosynthesis and respiration during this time frame. At the same time as these increases in C emission and fixation, two seasonal differences in island hydrology drive changes in peat drainage C concentrations and isotopic composition in the summer: (1) drainage receives less groundwater and the groundwater that does drain is from deeper soil layers, which contribute less DOC (as carbon found at depth on Delta islands is generally more humified, under reducing conditions, and not replenished as frequently as surface soils (Deverel et al., 2007)), and (2) drainage receives more surface water runoff in the form of excess irrigation water diverted from surrounding channels, which dilutes groundwater C inputs and shifts peat drainage C composition towards river C geochemistry (Tables 1 and 2). Soils at depth on Delta islands generally have lower organic matter content (Drexler et al., 2009), and past work by Deverel et al. (2007) shows that deep groundwater on Delta islands has low DOC concentrations (~1570 μM) relative to shallow groundwater (~6870 μM), though the exact magnitude of each likely varies island-to-island from

differences in soil organic matter content and C cycling. Deverel et al. (2007) also found seasonal differences in SUVA<sub>254</sub> values in peat drainage. In this study, drainage SUVA<sub>254</sub> values were generally consistent across sites and through time, suggesting that drainage DOC remained compositionally similar year-round. This consistency in DOC aromaticity is possible since groundwater sources (shallow or deep) maintain DOC concentrations that are generally an order of magnitude greater than surrounding river DOC concentrations. As a result, groundwater DOC contributions dominate the DOC pool regardless of the season, and irrigation runoff contributions to drainage mainly act to dilute deep groundwater DOC inputs in the summer. This could account for the observed overall reductions in drainage DOC concentrations in peat drainage during the summer, while allowing drainage DOC to remain compositionally similar year-round.

These lower peat drainage DOC concentrations translate to lower DIC concentrations and pCO<sub>2</sub> values in peat drainage during the summer as organic matter availability for mineralization (and thus, CO<sub>2</sub> production) in the saturated zone is diminished relative to shallow winter C pools (Table 2). Summer enrichment of  $\delta^{13}\text{C}$ -DIC values under oxic conditions also suggest increases in photosynthesis by algae and/or aquatic vegetation growing within the ditches; photosynthesis preferentially uses <sup>12</sup>C which leaves remaining C enriched in <sup>13</sup>C. Summer algal blooms are further evidenced by the generally low (C/N)<sub>m</sub> ratios of POM (7.3 to 10.5,  $\bar{x} = 9.0 \pm 1.8$ ), low  $\delta^{13}\text{C}$ -POC values, and high  $\delta^{15}\text{N}$ -PON values observed in peat island drainage during the

summer (Kendall et al., 2001) (Fig. S3). These blooms would help explain several other summer trends in peat island drainage geochemistry. Specifically, photosynthetic CO<sub>2</sub> fixation should decrease pCO<sub>2</sub> values and increase pH and dissolved oxygen concentrations, similar to trends observed for most drainage sites in the summer (Fig. 8). Unsurprisingly, the algal POM signal was strongest in summer and fall, when physical conditions (e.g., increased sunlight availability and lower rates of discharge which increase residence time) can best support photosynthetic activity.

The suite of geochemical tracers we analyzed provide new information on the dominant sources of and processes affecting peat island drainage C delivered to Delta waters, and the quality of organic matter delivered to the greater Delta ecosystem from peat drainage. In the summer, drainage POM is likely more bioavailable (N-rich), while indicators of DOC quality (e.g., SUVA<sub>254</sub>) suggest DOC remains compositionally similar year-round. δ<sup>13</sup>C-DIC values revealed that DIC is mostly affected by autotrophic/heterotrophic utilization of C, though methanogenesis was evident in some locations. While these general seasonal trends in C biogeochemistry (evidenced by C concentrations and stable isotope composition) were discernable, peat drainage C concentrations and stable isotope compositions show significant spatial variability when observed at higher temporal resolution. Moreover, some sites were inconsistent with overall seasonal trends (e.g., SH-P2 and SH-P3), and this variability suggests that controls on metabolic processes affecting C biogeochemistry

are probably spatially heterogeneous at the sub-island level.

#### 2.4.2 Transport driven lateral C losses from drained peatlands

In line with Gibson et al. (2009), which found that DOC exports in UK peatlands are transport driven, a majority of peat drainage DIC, DOC, and POC exports in the Delta were strongly positively correlated to water yield (e.g., discharge/area). This suggests that seasonal changes in water yield are a major driver of C flux. Interestingly, islands with substantial cropland cover, like Staten Island, showed two distinct trends in export-yield relationships, which likely arose from the seasonality in the hydrological regime on Delta islands as discussed previously: (1) summer when precipitation is negligible and surface irrigation increases, and (2) winter when inflow is high (from increased levee seepage and rainfall contributions) and subsurface flow dominates. DOC and DIC exports on Staten Island, when divided based on these two seasons which represent distinct hydrological regimes, correlated well with water yield (Fig. 6). The winter hydrologic regime is ubiquitous across all Delta islands as increased discharge is a regional response to higher water tables from increases in river water levels and direct precipitation in the winter rainy season. Exports during this period are driven by (1) high rates of pumping to remove excess water from the islands, and (2) elevated dissolved C concentrations as water interacts with re-wetted soils via subsurface flow pathways. In the summer, irrigation-driven discharge is a localized response to dominant land use and crop type, which varies between and across islands. Dissolved C concentrations during this time are lower, and exports are less

consequential to overall island C budgets. These export trends highlight the importance of discharge in C loss, and future efforts aimed at minimizing winter discharge could help curb lateral C losses from Delta islands (Deverel et al., 2017). Reductions in winter discharge may also affect CO<sub>2</sub> and CH<sub>4</sub> emissions, and the potential tradeoff in lowering lateral C fluxes at the expense of increased GHG emissions needs to be carefully considered in future work.

#### 2.4.3 Importance of lateral C exports in C budgets of drained peatlands

Previous work on lateral C exports in the Delta has been limited in scope; no estimates consider DIC exports, and no studies have comprehensively evaluated all lateral C constituents at regular time intervals with complete discharge data. We found that peat island drainage lateral C exports were similar in magnitude to previously published vertical C fluxes for various land use types in the Delta and often greater than past estimates of C losses via DOC export in drainage waters (Table 4). Previously unconsidered DIC exports comprised almost 50% of C lost laterally. After accounting for river C imports (0.04 to 0.12 g C m<sup>-2</sup> d<sup>-1</sup>), the three studied Delta islands were sources of lateral C to the Delta environment, with net contributions from WY 2017 (0.12 to 0.18 g C m<sup>-2</sup> d<sup>-1</sup>, 690 to 2410 Mg C yr<sup>-1</sup>) much larger than WY 2018 (0.03 to 0.06 g C m<sup>-2</sup> d<sup>-1</sup>, 310 to 680 Mg C yr<sup>-1</sup>) (Table 4). Net lateral C export rates for WY 2017 were comparable in magnitude to current estimates of net per area gaseous C emissions from a range of land use types. However, carbon inflow from rivers does not exclusively cycle through Delta islands

in dissolved and particulate form. Inflow C was predominantly comprised of DIC (~75%), while DIC comprised about 50% of drainage C. This study showed that dissolved and particulate organic C pools in drainage are often sourced from terrestrial OM, which suggests that inflow C is cycled and processed on island. Interplay between lateral and vertical C cycling complicates assessments that consider gaseous and dissolved/particulate C pathways separately, and these assessments would benefit from more refined budgeting of carbon imports. This study's lateral C export estimates also do not account for the fate of C in drainage waters, which could result in direct increases in CO<sub>2</sub> emissions via evasion (as drainage waters are super-saturated) and longer-term increases in CO<sub>2</sub> emissions from C cycling of drainage-sourced organics in Delta waterways. Müller et al. (2015) found that CO<sub>2</sub> outgassing from water can account for over 30% of C lost laterally in a peat-draining river, and future work in the Delta should explicitly account for near-term and long-term C emissions from drainage waters.

We also found that lateral C exports were spatially and temporally variable due to differences in dissolved C concentrations and water budget terms (both water inflow and discharge). Studies on gaseous C have found similar spatial variability. Even across uniform land use sites in the Delta, CH<sub>4</sub> flux and C fixation rates can vary substantially (Anderson et al., 2016; Hemes et al., 2018). Variability in both hydrology and soil organic matter content between sites may account for the spatial discrepancies observed in this study and previous studies on gaseous C fluxes in the

Delta. Soil organic matter content varies considerably both within islands and across the entire legal Delta boundary, from ~5 to 52% (Deverel et al., 2016; Drexler et al., 2009), and we found that soil organic matter content at our study sites on Sherman Island could explain 93% the observed variability in total dissolved C concentrations for each drainage catchment (Fig. S5). Similarly, water table levels can vary at the sub-island scale from differences in water management and land use. Past work by Aguilar and Thibodeaux (2005) and this study show that water table levels can drive seasonal trends in C geochemistry in the Delta's drained peatlands. These spatial differences in aqueous and gaseous C dynamics can easily be missed when sampling is sporadic or not spatially rigorous in biogeochemically complex systems, like the Delta, and this study's results raise new and important questions about the uniformity of not only vertical but also lateral C exchange rates across and within Delta islands as well as across differing water years.

#### 2.4.4 Annual variability in peat drainage C loads delivered to the Delta ecosystem

To examine annual variability in the magnitude and timing of dissolved and particulate C fluxes from peat drainage, we back calculated DIC, DOC, and POC fluxes for each island using the established C export relationships with water yield for the period for which discharge information is available but no geochemistry data exists (June 2016 to May 2017). While the timing of annual discharge peaks remained relatively consistent across water years, the magnitude of dissolved and particulate C fluxes changed substantially. Large differences between wet WY 2017 (95.4 cm) and

dry WY 2018 (27.9 cm) precipitation had a measurable effect on annual discharge from each island and, subsequently, the magnitude of peat drainage C inputs to surrounding Delta waters (Fig. S6). In general, C fluxes from peat drainage to Delta channels were greatest in the winter of both water years, and cumulative C fluxes (the sum of DOC, DIC, and POC) from each island were 1.7 to 5.4 times larger in winters of wet years (220 to 600 Mg C month<sup>-1</sup>) than winters in dry years (110 to 220 Mg C month<sup>-1</sup>). Islands where summer irrigation takes place also showed secondary summer peaks in C fluxes (Fig. S6).

To get an estimate of the overall C contribution to Delta waterways from all of the Delta's island drains, monthly DIC, DOC, and POC fluxes were upscaled to obtain Delta-wide C fluxes using previous discharge estimates (431,179 ac-ft) for peat island drainage for the entirety of the Delta from Templin and Cherry (1997) and C concentration data from this study. This allows for: (1) a broader understanding of the overall magnitude of total peat drainage C flux to Delta waters, and (2) comparison to other recognized significant contributors of DOC to the Delta (as POC and DIC concentration data for other sources is limited in this system). We scaled annual peat drainage discharge to monthly resolution using flow percentiles calculated from this study; flow percentiles were generated separately for islands dominated by pastureland (Sherman, SH) versus cropland (Staten, ST), and fluxes presented herein are the mean of these values (Fig. S7). These estimates suggested drainage from subsided peat islands contributed 76 and 73 Mg C d<sup>-1</sup> of DIC to surrounding

waterways in WY 2017 and WY 2018, respectively (Table 5). Mean annual POC contributions from peat drainage were 35 to 39 Mg C d<sup>-1</sup>. On a seasonal basis, WY 2017 and WY 2018 total Delta peat drainage DOC estimates ranged between 11 and 97 Mg C d<sup>-1</sup>, which is similar in magnitude to estimates from Jassby and Cloern (2000) (Table 5). Mean annual DOC contributions during WY 2017 and WY 2018 ranged between 38 to 43 Mg C d<sup>-1</sup> and were similar to recent estimates of 37 Mg C d<sup>-1</sup> (Roy et al., 2006). These water year comparisons of C mass flux show how drainage C exports can change seasonally and annually in a region with increasing hydroclimatic variability (Swain et al., 2018) and suggest that more extensive monitoring of interannual variability in lateral C fluxes is needed to better assess the contribution of this flux to the whole Delta C pool.

Relative to other regional contributors of DOC, including the San Joaquin River, Sacramento River, and Sacramento Regional WWTP, data from this study suggests peat drainage accounted for up to ~24 to 26% and ~24 to 40% of DOC contributions to Delta waters during winter months of wet WY 2017 and dry WY 2018, respectively (Fig. 10). DOC contributions from drained peat islands were sustained over the course of several months in the winter of WY 2018, while drainage DOC inputs in WY 2017 quickly subsided as other inputs dominated local C mass fluxes (Fig. 10a). This mass flux comparison suggests that DOC inputs from drained peat islands in the Delta comprise a slightly larger fraction of the total flux during winter of dry water years, even though wet water years see greater mass fluxes of DOC from

peat drainage. Our work as well as that reported by Kraus et al. (2008) shows that over 1/4 of DOC in Delta waters in the winter may be attributable to peat drainage. The delivery of DOC (and POC) from peat drainage to surrounding waterways has consequences for in-Delta water quality and water exported to other areas of California (Fleck et al., 2007), for example, high DOC concentrations in water exports to other regions can lead to the formation of harmful disinfection by-products upon chlorination (Bachand et al., 2019; Fleck et al., 2007; Hansen et al., 2018). Taken together, these results suggest that: (1) peat drainage DOC inputs can, during some seasons, outpace other contributors of DOC in this system, (2) the fractional contribution of drainage DOC is dependent on prior precipitation, and (3) drainage C inputs are consequential for downstream water quality.

## **2.5 Conclusion**

This study is the first to measure DIC, DOC, and POC exports from multiple drained peat islands in the Sacramento-San Joaquin Delta in central California. Alongside measurements of particulate and dissolved C concentration and discharge, we used supplemental stable isotope data to better understand biogeochemical controls on drainage C geochemistry. We found that biogeochemical and hydrological controls on drainage C concentrations and stable isotope composition were complex, varying in both space and time. Seasonal changes in water table elevation shifted dominant water sources contributing to drainage. Groundwater contributions to peat drainage increased in the winter and spring, when C concentrations and discharge were high.

In the summer, peat drainage C concentrations were lower (though still higher than surrounding rivers) due to reductions in shallow groundwater contributions and increases in surface water inputs as irrigation runoff. Seasonal shifts in water sources affected biogeochemical processing of C. C stable isotope values and concentrations were primarily influenced by C mineralization in the winter and autotrophic production in the ditches in the summer. While C cycling processes were generally similar across drainage sites, baseline particulate and dissolved C concentrations were site specific, likely from differences in soil organic matter content and prevailing hydrology. This spatial and temporal variability highlights that the Delta's peat islands are not static and homogenous systems; each function as separate catchments with similar biogeochemical processes, but distinct propensities to cycle C. Spatial heterogeneity in C concentrations and stable isotope composition was substantial even across individual islands, and this internal variability in C concentration, speciation, and stable isotope values is likely to also affect gaseous fluxes. Previous work on GHG emissions from many of the same islands also show substantial variability in CO<sub>2</sub> and CH<sub>4</sub> flux across uniform land use types, and more work is needed to better understand higher-order spatial controls on both lateral C losses and gaseous C dynamics from drained peatlands.

This study also highlights the potential importance of accounting for DIC, DOC, and POC exports in C budgets of drained peatlands. The magnitude of C exported from peat drainage to Delta channels varied based on water year, with wet WY 2017 (0.12

to  $0.18 \text{ g C m}^{-2} \text{ d}^{-1}$ ) exporting more net C than dry WY 2018 ( $0.03$  to  $0.06 \text{ g C m}^{-2} \text{ d}^{-1}$ ). Peat island drainage C fluxes were also able to account for over 1/4 of DOC fluxes in the Delta during winters of both dry and wet water years. New studies that integrate measurements of both lateral and vertical C exports will improve our understanding of C dynamics in drained peatlands, allow for more accurate C and GHG accounting, and can be used to better understand temporal controls as they relate to the increasing hydroclimatic variability projected for California and beyond.

### **Acknowledgements**

The authors thank the California Department of Water Resources, including Juan Mercado and David Mraz, for graciously helping arrange access to sampling locations. We thank Rick Carter, Joel McElroy, and the Nature Conservancy for their assistance in accessing sampling locations. We thank Kaylee Glenney, Carolyn Brady, and Rob Franks for their endless help in the Marine Analytical Lab. The authors thank Carol Kendall for her early support of this work. This research was supported by grants from National Geographic, the International Association of Geochemistry, the Robert Wiegel Scholarship for Coastal Studies, and the J. Casey Moore Award. Additional support for C. Richardson was provided by the National Science Foundation Graduate Research Fellowship Program (DGE-1329626), and J. Fackrell received support from the California Sea Grant Delta Fellowship (Grant #R/SF-84). Data will be made available through the Consortium of Universities for the Advancement of Hydrologic Science, Inc. (CUAHSI).

## References

- Aguilar, L., & Thibodeaux, L. (2005). Kinetics of peat soil dissolved organic carbon release from bed sediment to water. Part 1. Laboratory simulation. *Chemosphere*, 58(10), 1309-1318.
- Anderson, F. E., Bergamaschi, B., Sturtevant, C., Knox, S., Hastings, L., Windham-Myers, L., et al. (2016). Variation of energy and carbon fluxes from a restored temperate freshwater wetland and implications for carbon market verification protocols. *121*(3), 777-795.
- Atwater, B. F., & Belknap, D. F. (1980). Tidal-wetland deposits of the Sacramento-San Joaquin Delta, California.
- Bachand, P. A., Bachand, S. M., Kraus, T. E., Stern, D., Liang, Y. L., & Horwath, W. R. (2019). Sequestration and Transformation in Chemically Enhanced Treatment Wetlands: DOC, DBPPs, and Nutrients. *Journal of Environmental Engineering*, 145(8), 04019044.
- Baldocchi, D., Detto, M., Sonnentag, O., Verfaillie, J., Teh, Y. A., Silver, W., & Kelly, N. M. (2012). The challenges of measuring methane fluxes and concentrations over a peatland pasture. *Agricultural Forest Meteorology*, 153, 177-187.
- Billett, M., & Moore, T. (2008). Supersaturation and evasion of CO<sub>2</sub> and CH<sub>4</sub> in surface waters at Mer Bleue peatland, Canada. *Hydrological Processes: An International Journal*, 22(12), 2044-2054.
- Campeau, A., Wallin, M. B., Giesler, R., Löfgren, S., Mörth, C.-M., Schiff, S., et al. (2017). Multiple sources and sinks of dissolved inorganic carbon across Swedish streams, refocusing the lens of stable C isotopes. 7(1), 1-14.
- Carpenter, S. R., & Pace, M. L. (1997). Dystrophy and eutrophy in lake ecosystems: implications of fluctuating inputs. *Oikos*, 3-14.
- CDWR. (1995). California Department of Water Resources. Sacramento-San Joaquin Delta Atlas: State of California, 121 p.
- Chow, A., Tanji, K., Gao, S., & Dahlgren, R. (2006). Temperature, water content and wet-dry cycle effects on DOC production and carbon mineralization in agricultural peat soils. *Soil Biology and Biochemistry*, 38(3), 477-488.
- Dawson, J. J., Billett, M., Neal, C., & Hill, S. (2002). A comparison of particulate, dissolved and gaseous carbon in two contrasting upland streams in the UK. *Journal of Hydrology*, 257(1-4), 226-246.

- Dawson, J. J., Billett, M. F., Hope, D., Palmer, S. M., & Deacon, C. M. (2004). Sources and sinks of aquatic carbon in a peatland stream continuum. *Biogeochemistry*, 70(1), 71-92.
- Deverel, S. J., Ingram, T., & Leighton, D. (2016). Present-day oxidative subsidence of organic soils and mitigation in the Sacramento-San Joaquin Delta, California, USA. *Hydrogeology*, 24(3), 569-586.
- Deverel, S. J., & Leighton, D. A. (2010). Historic, recent, and future subsidence, Sacramento-San Joaquin Delta, California, USA. *San Francisco Estuary and Watershed Science*, 8(2).
- Deverel, S. J., Leighton, D. A., & Finlay, M. R. (2007). Processes affecting agricultural drainwater quality and organic carbon loads in California's Sacramento–San Joaquin Delta. *San Francisco Estuary and Watershed Science*, 5(2).
- Deverel, S. J., Leighton, D. A., Lucero, C., & Ingram, T. (2017). Simulation of subsidence mitigation effects on island drain flow, seepage, and organic carbon loads on subsided islands Sacramento–San Joaquin Delta. *San Francisco Estuary and Watershed Science*, 15(4).
- Deverel, S. J., Lucero, C. E., & Bachand, S. (2015). Evolution of Arability and Land Use, Sacramento–San Joaquin Delta, California. *San Francisco Estuary and Watershed Science*, 13(2).
- Deverel, S. J., & Rojstaczer, S. (1996). Subsidence of agricultural lands in the Sacramento-San Joaquin Delta, California: Role of aqueous and gaseous carbon fluxes. *Water Resources Research*, 32(8), 2359-2367.
- Diamond, J., & Williamson, A. (1983). A summary of ground-water pumpage in the Central Valley of California. 1961-1977: U.S. Geological Survey Water-Resources Investigations Report 83-4037, 70 p.
- DPC. (2012). Economic Sustainability Plan for the Sacramento-San Joaquin Delta. A report prepared for the Delta Protection Commission.
- Drexler, J. Z., de Fontaine, C. S., & Deverel, S. J. J. W. (2009). The legacy of wetland drainage on the remaining peat in the Sacramento—San Joaquin Delta, California, USA. 29(1), 372-386.
- Findlay, S., McDowell, W. H., Fischer, D., Pace, M. L., Caraco, N., Kaushal, S. S., et al. (2010). Total carbon analysis may overestimate organic carbon content of fresh waters in the presence of high dissolved inorganic carbon. 8(5), 196-201.

- Fleck, J. A., Fram, M. S., & Fujii, R. (2007). Organic Carbon and Disinfection Byproduct Precursor Loads from a Constructed, Non-Tidal Wetland in California's Sacramento–San Joaquin Delta. *San Francisco Estuary and Watershed Science*, 5(2).
- Fregoso, T. A., Wang, R.-F., Alteljevich, E., & Jaffe, B. E. (2017). San Francisco Bay-Delta bathymetric/topographic digital elevation model (DEM): U.S. Geological Survey data release, <https://doi.org/10.5066/F7GH9G27>.
- Fujii, R., Ranalli, A. J., Aiken, G. R., & Bergamaschi, B. A. (1998). Dissolved organic carbon concentrations and compositions, and trihalomethane formation potentials in waters from agricultural peat soils, Sacramento-San Joaquin Delta, California: Implications for drinking-water quality. *U.S. Geological Survey Water-Resources Investigations Report 98-4147*, 75 p.
- Gibson, H., Worrall, F., Burt, T., & Adamson, J. (2009). DOC budgets of drained peat catchments: implications for DOC production in peat soils. *Hydrological Processes*, 23(13), 1901-1911.
- Gorham, E. (1991). Northern peatlands: role in the carbon cycle and probable responses to climatic warming. *Ecological applications*, 1(2), 182-195.
- Hansen, A. M., Kraus, T. E., Bachand, S. M., Horwath, W. R., & Bachand, P. A. (2018). Wetlands receiving water treated with coagulants improve water quality by removing dissolved organic carbon and disinfection byproduct precursors. *Science of the Total Environment*, 622, 603-613.
- Hatala, J., Detto, M., Sonnentag, O., Deverel, S., Verfaillie, J., & Baldocchi, D. (2012). Greenhouse gas (CO<sub>2</sub>, CH<sub>4</sub>, H<sub>2</sub>O) fluxes from drained and flooded agricultural peatlands in the Sacramento-San Joaquin Delta. *Agriculture, Ecosystems & Environment*.
- Hemes, K. S., Chamberlain, S. D., Eichelmann, E., Anthony, T., Valach, A., Kasak, K., et al. (2019). Assessing the carbon and climate benefit of restoring degraded agricultural peat soils to managed wetlands. *Agricultural Forest Meteorology*, 268, 202-214.
- Hemes, K. S., Chamberlain, S. D., Eichelmann, E., Knox, S. H., & Baldocchi, D. D. (2018). A biogeochemical compromise: The high methane cost of sequestering carbon in restored wetlands. *Geophysical Research Letters*, 45(12), 6081-6091.
- Holden, J., Evans, M., Burt, T., & Horton, M. J. J. o. E. Q. (2006). Impact of land drainage on peatland hydrology. 35(5), 1764-1778.

- Holden, J., Wallage, Z., Lane, S., & McDonald, A. (2011). Water table dynamics in undisturbed, drained and restored blanket peat. *Journal of Hydrology*, 402(1-2), 103-114.
- Ingebritsen, S. E., Ikehara, M. E., Galloway, D. L., & Jones, D. R. (2000). *Delta subsidence in California: the sinking heart of the state*. US Department of the Interior, US Geological Survey.
- Jassby, A. D., & Cloern, J. E. (2000). Organic matter sources and rehabilitation of the Sacramento–San Joaquin Delta (California, USA). *Aquatic Conservation: Marine and Freshwater Ecosystems*, 10(5), 323-352.
- Jenkinson, D. S., Adams, D., & Wild, A. (1991). Model estimates of CO<sub>2</sub> emissions from soil in response to global warming. *Nature*, 351(6324), 304.
- Joosten, H. (2009). The Global Peatland CO<sub>2</sub> Picture: peatland status and drainage related emissions in all countries of the world.
- Kendall, C., Silva, S. R., & Kelly, V. J. (2001). Carbon and nitrogen isotopic compositions of particulate organic matter in four large river systems across the United States. *Hydrological Processes*, 15(7), 1301-1346.
- Knox, S. H., Sturtevant, C., Matthes, J. H., Koteen, L., Verfaillie, J., & Baldocchi, D. (2015). Agricultural peatland restoration: effects of land-use change on greenhouse gas (CO<sub>2</sub> and CH<sub>4</sub>) fluxes in the Sacramento-San Joaquin Delta. *Global Change Biology*, 21(2), 750-765.
- Kraus, T. E., Bergamaschi, B. A., Hernes, P. J., Spencer, R. G., Stepanauskas, R., Kendall, C., et al. (2008). Assessing the contribution of wetlands and subsided islands to dissolved organic matter and disinfection byproduct precursors in the Sacramento–San Joaquin River Delta: a geochemical approach. 39(9), 1302-1318.
- Leifeld, J., & Menichetti, L. (2018). The underappreciated potential of peatlands in global climate change mitigation strategies. *Nature Communications*, 9(1), 1071.
- Limpens, J., Berendse, F., Blodau, C., Canadell, J., Freeman, C., Holden, J., et al. (2008). Peatlands and the carbon cycle: from local processes to global implications—a synthesis. *Biogeosciences*, 5(5), 1475-1491.
- Müller, D., Warneke, T., Rixen, T., Müller, M., Jamahari, S., Denis, N., et al. (2015). Lateral carbon fluxes and CO<sub>2</sub> outgassing from a tropical peat-draining river. *Biogeosciences*, 12(20), 5967-5979.

- Murrell, M., & Hollibaugh, J. (2000). Distribution and composition of dissolved and particulate organic carbon in northern San Francisco Bay during low flow conditions. *Estuarine, Coastal Shelf Science*, 51(1), 75-90.
- Ogilbee, W. (1966). Progress report Methods for estimating ground-water withdrawals in Madera County, California: U.S. Geological Survey open-file report, 42. p.
- Ogilbee, W., & Mitten, H. (1979). A continuing program for estimating ground-water pumpage in California--Methods: U.S. Geological Survey open-file report, 22 p.
- Pellerin, B., Anderson, F., & Bergamaschi, B. (2013). Assessing the role of winter flooding on baseline greenhouse gas fluxes from corn fields in the Sacramento-San Joaquin Bay Delta. *Energy Research and Development Division, Final Project Report. A report prepared for the California Energy Commission.*
- Price, J. S. (2003). Role and character of seasonal peat soil deformation on the hydrology of undisturbed and cutover peatlands. *Water Resources Research*, 39(9).
- Robbins, L. L., Hansen, M. E., Kleypas, J. A., & Meylan, S. C. (2010). CO2calc—A user-friendly seawater carbon calculator for Windows, Max OS X, and iOS (iPhone): U.S. Geological Survey Open-File Report 2010–1280, 17 p.
- Roy, S., Heidel, K., Creager, C., Chung, C., & Grieb, T. (2006). Conceptual model for organic carbon in the Central Valley and Sacramento-San Joaquin Delta. Final Report. Prepared for US EPA and Central Valley Drinking Water Policy Workgroup.
- Sanderman, J., Hengl, T., & Fiske, G. J. (2017). Soil carbon debt of 12,000 years of human land use. *Proceedings of the National Academy of Sciences*, 114(36), 9575-9580.
- Schindler, D. W., Curtis, P. J., Bayley, S. E., Parker, B. R., Beaty, K. G., & Stainton, M. P. (1997). Climate-induced changes in the dissolved organic carbon budgets of boreal lakes. *Biogeochemistry*, 36(1), 9-28.
- Sickman, J. O., Zanolli, M., & Mann, H. (2007). Effects of urbanization on organic carbon loads in the Sacramento River, California. *Water Resources Research*, 43(11).
- Strack, M., Waddington, J., Bourbonniere, R., Buckton, E., Shaw, K., Whittington, P., & Price, J. (2008). Effect of water table drawdown on peatland dissolved

- organic carbon export and dynamics. *Hydrological Processes*, 22(17), 3373-3385.
- Swain, D. L., Langenbrunner, B., Neelin, J. D., & Hall, A. (2018). Increasing precipitation volatility in twenty-first-century California. *Nature Climate Change*, 8(5), 427-+. <Go to ISI>://WOS:000431139900027
- Teh, Y. A., Silver, W. L., Sonnentag, O., Detto, M., Kelly, M., & Baldocchi, D. (2011). Large greenhouse gas emissions from a temperate peatland pasture. *Ecosystems*, 14(2), 311-325.
- Templin, W. E., & Cherry, D. E. (1997). Drainage-return, surface-water withdrawal, and land-use data for the Sacramento-San Joaquin Delta, with emphasis on Twitchell Island, California; U.S. Geological Survey Open-file Report 97-350, 31 p.
- Thibodeaux, L., & Aguilar, L. (2005). Kinetics of peat soil dissolved organic carbon release to surface water. Part 2. A chemodynamic process model. *Chemosphere*, 60(9), 1190-1196.
- Uhlenbrook, S., Leibundgut, C., & Maloszewski, P. (2000). Natural tracers for investigating residence times, runoff components and validation of a rainfall-runoff model. *IAHS Publication*(262), 465-471.
- Wetzel, R. G. (2003). Dissolved organic carbon: detrital energetics, metabolic regulators, and drivers of ecosystem stability of aquatic ecosystems. In *Aquatic Ecosystems* (pp. 455-477): Elsevier.
- Williamson, C. E., Morris, D. P., Pace, M. L., & Olson, O. G. (1999). Dissolved organic carbon and nutrients as regulators of lake ecosystems: resurrection of a more integrated paradigm. *Limnology and Oceanography*, 44(3part2), 795-803.
- Windham-Myers, L., Bergamaschi, B., Anderson, F., Knox, S., Miller, R., & Fujii, R. (2018). Potential for negative emissions of greenhouse gases (CO<sub>2</sub>, CH<sub>4</sub> and N<sub>2</sub>O) through coastal peatland re-establishment: Novel insights from high frequency flux data at meter and kilometer scales. *Environmental Research Letters*, 13(4), 045005.
- Wit, F., Rixen, T., Baum, A., Pranowo, W. S., & Hutahaean, A. A. (2018). The Invisible Carbon Footprint as a hidden impact of peatland degradation inducing marine carbonate dissolution in Sumatra, Indonesia. *Nature Scientific Reports*, 8(1), 1-10.

Worrall, F., Burt, T., & Adamson, J. (2005). Fluxes of dissolved carbon dioxide and inorganic carbon from an upland peat catchment: implications for soil respiration. *Biogeochemistry*, 73(3), 515-539.

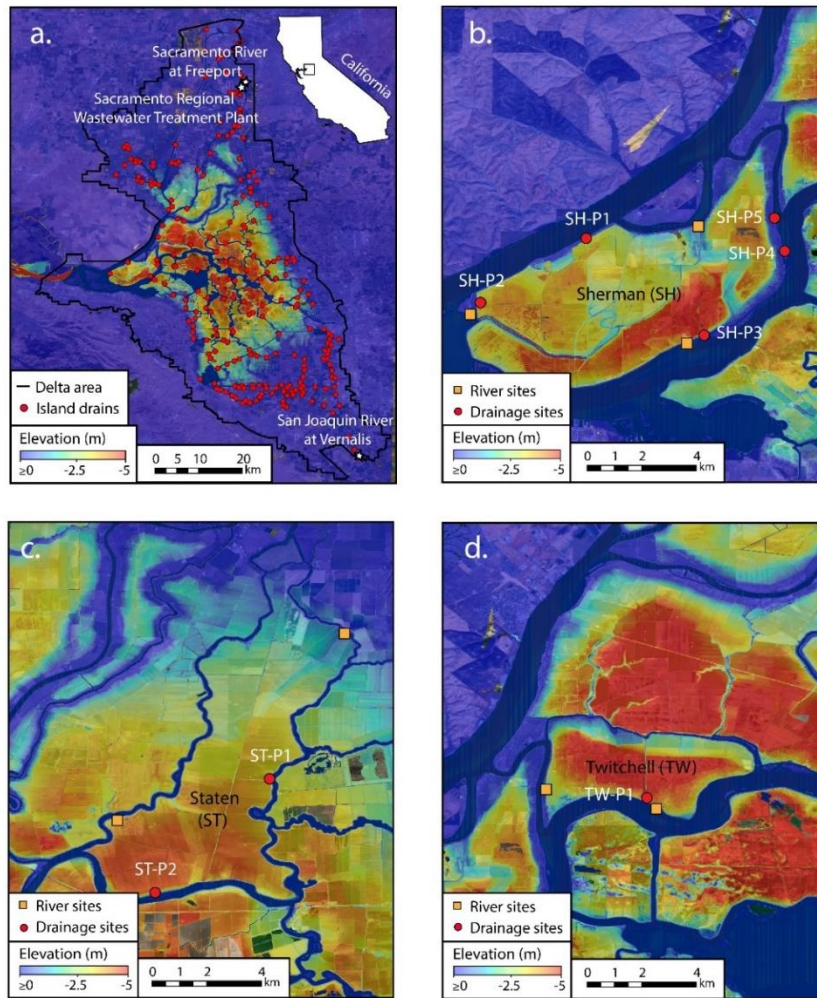


**Figure 2-1. Overview of the study area in the Delta.**

(a) Map of the study area, the Sacramento-San Joaquin Delta (shown as a black box on subfigure), in central California with a high-resolution (10-meter per pixel) digital elevation model (DEM) showing drain locations (red circles) from a digitized version of CDWR (1995). (b-d) overviews of islands sampled, Sherman (SH), Staten (ST), and Twitchell (TW), showing where drainage samples (red circles) and river samples (orange squares) were collected between June 2017 and September 2018. The DEM depicts land elevations between 0 and -5 meters below sea level. DEM is available from Fregoso et al. (2017).

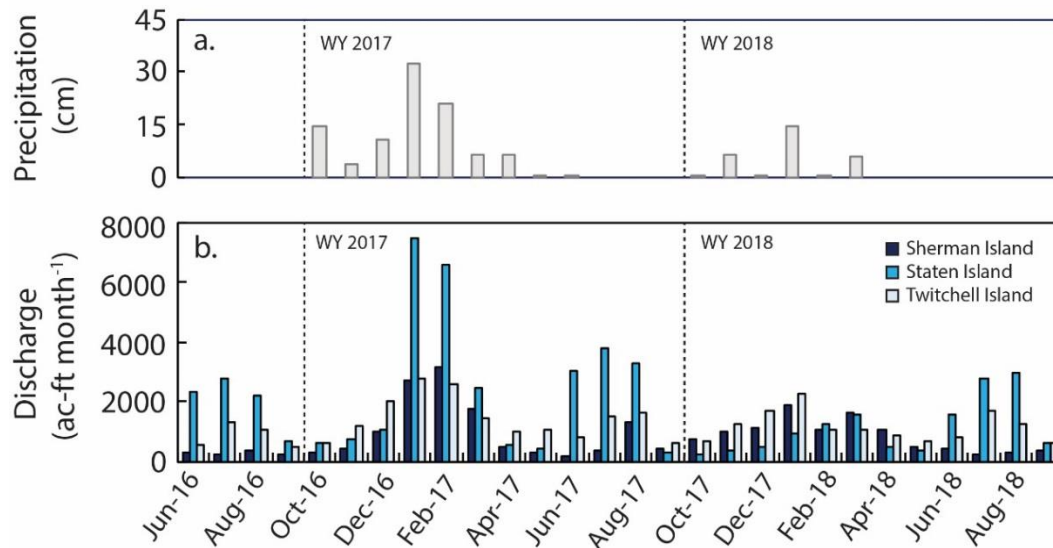


**Figure 2-2. Monthly precipitation and discharge data from Delta islands.**

(a) Monthly precipitation and (b) discharge from Sherman, Staten, and Twitchell islands. Precipitation data was acquired from Station 242 via the California Irrigation Management Information System (CIMIS). Discharge data was determined using the unit-power consumption method and cross-checked with measured flow meter estimates.

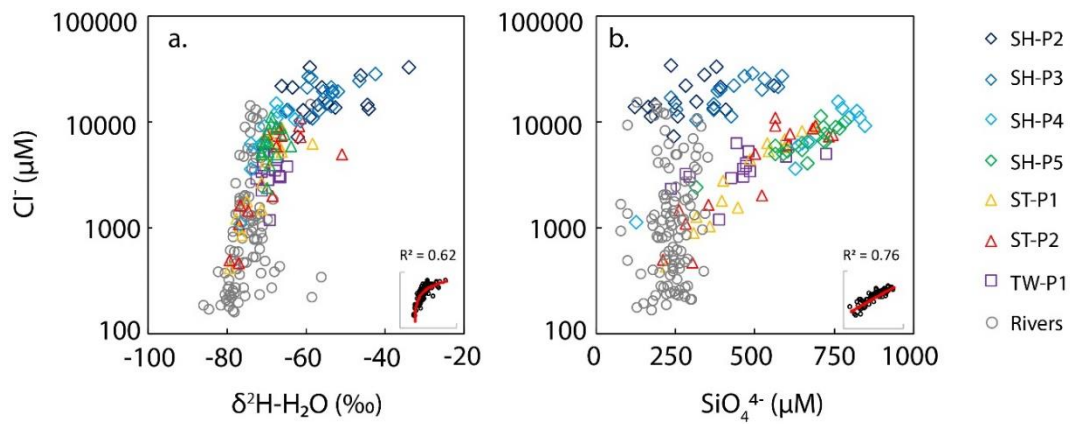


**Figure 2-3.  $\text{Cl}^-$  and  $\text{SiO}_4^{4-}$  concentrations versus water stable isotope values in peat drainage.**

Peat drainage  $\text{Cl}^-$  concentration versus (a)  $\delta^2\text{H-H}_2\text{O}$  values and (b)  $\text{SiO}_4^{4-}$  concentrations. Inset figures show cumulative  $R^2$  between (a) all sites (b) and all sites except SH-P2 and SH-P3. See Figure 1 for site locations (SH: Sherman Island sites, ST: Staten Island sites; TW, Twitchell Island sites).

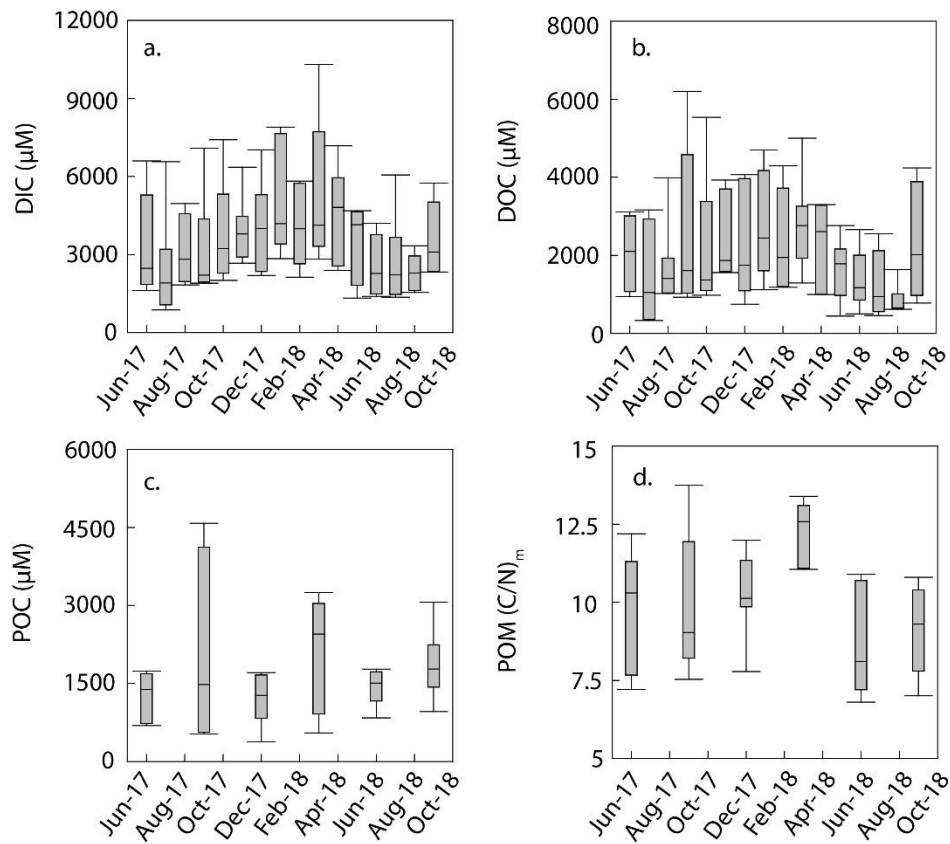


**Figure 2-4. Box plots of monthly peat drainage dissolved carbon geochemistry.**

Box plot time series for (a) monthly DIC concentrations (b) monthly DOC concentrations, (c) quarterly POC concentrations, and (d) quarterly POM ( $\text{C/N}_m$ ) in peat island drainage waters from all active drainage pump sites sampled across WY 2017 and WY 2018.

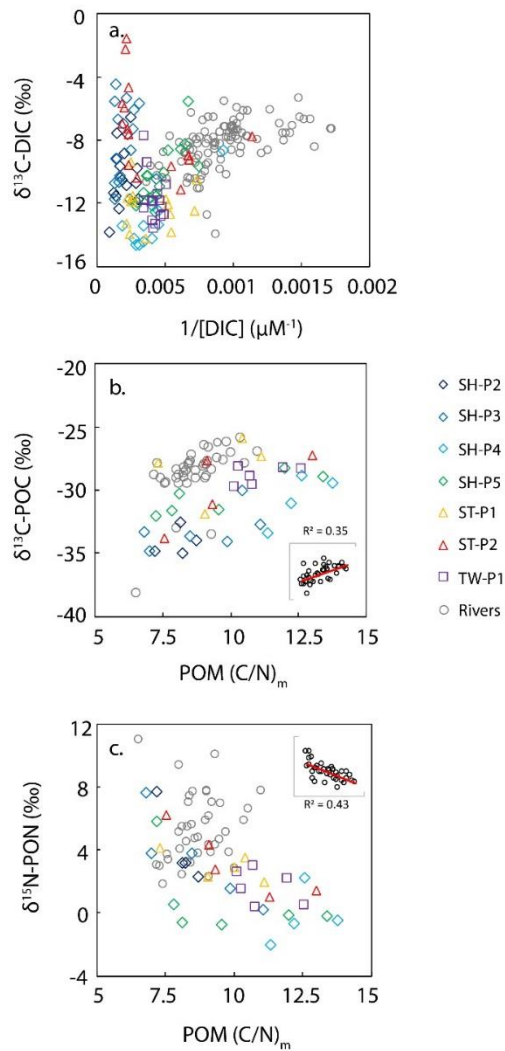


**Figure 2-5. Carbon stable isotope data for peat drainage.**

(a) Monthly  $\delta^{13}\text{C-DIC}$  values (‰) versus  $1/[\text{DIC}]$ . (b) Quarterly  $\delta^{13}\text{C-POC}$  values versus  $\text{POM (C/N)}_m$ . (c) Quarterly  $\delta^{15}\text{N-PON}$  values versus  $\text{POM (C/N)}_m$ . Inset figures in (b) and (c) show cumulative trends and associated  $R^2$  values. Sites shown include river water (grey circles), Sherman Island drainage sites (diamonds), Staten Island sites (triangles), and Twitchell Island drainage sites (squares). See Figure 1 for site locations (SH: Sherman Island sites, ST: Staten Island sites; TW, Twitchell Island sites).

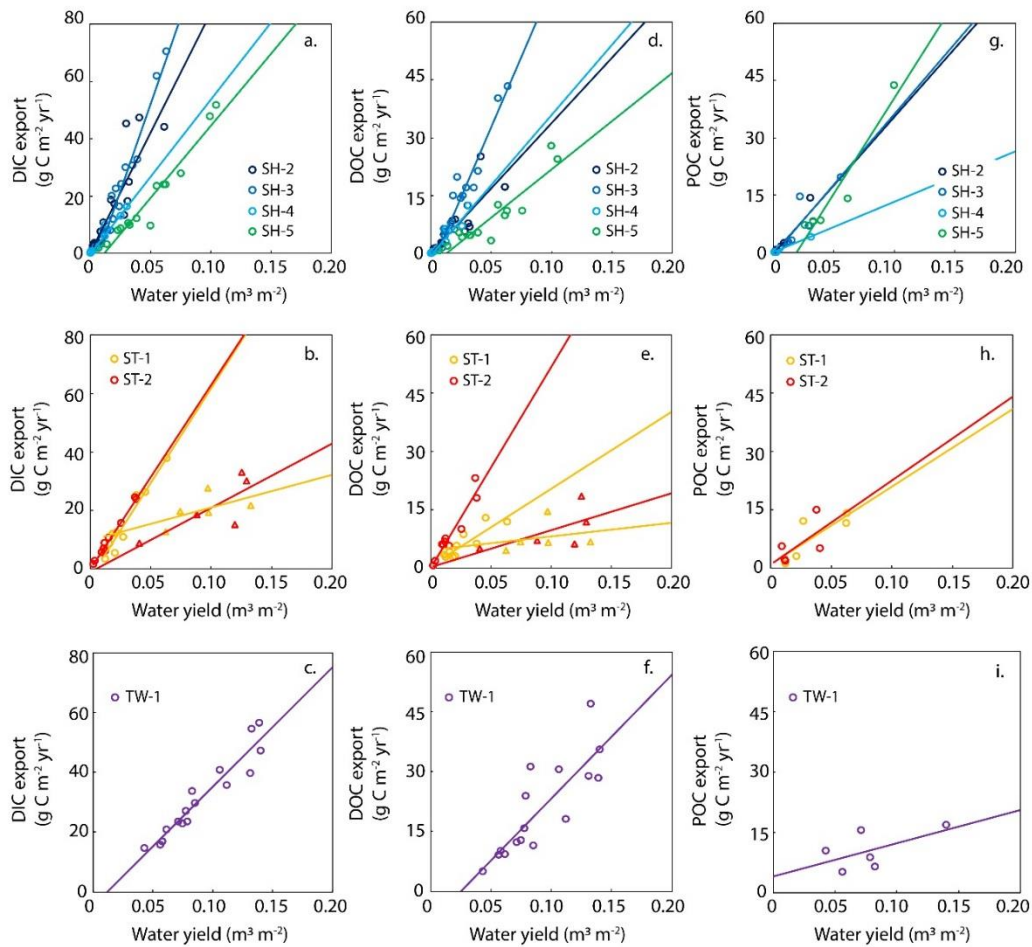


**Figure 2-6. Lateral carbon export relationships for each island.**

Peat island drainage DIC, DOC, and POC annual exports versus water yield for (a, d, g) Sherman Island (SH), (b, e, h) Staten Island (ST), and (c, f, i) Twitchell island (TW). Summer month (June, July, and August) DIC and DOC exports on Staten Island are shown as triangles whereas summer month POC exports on Staten Island (ST) were not seasonally separated due to sample number limitations. Regression equations, sample numbers, and  $R^2$  values are presented in Table S3.

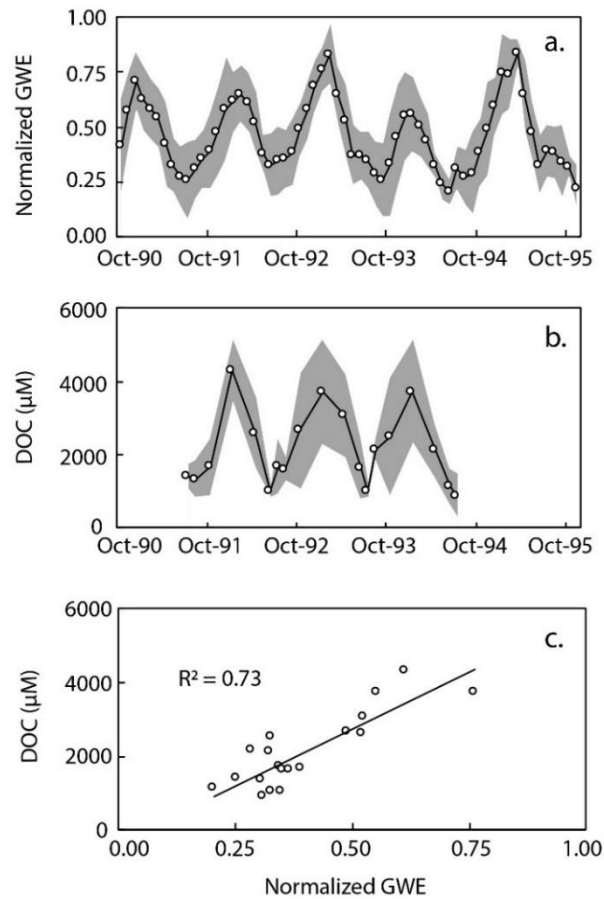


**Figure 2-7. Historical peat drainage carbon and groundwater elevation data.**

(a) Historical time series mean normalized groundwater elevation (GWE) from seven Delta islands (Bouldin, Empire, Mandeville, Palm, Staten, Twitchell, and Webb), (b) historical time series DOC concentrations from seven drainage outlets in the Delta (Bacon, Bouldin, Holland, Mandeville, Palm, Staten, and Webb), and (c) drainage DOC concentrations versus mean normalized GWE. Gray areas show the standard deviation around the mean of each sample date. Groundwater elevation data is from Deverel et al. (2015) and was aggregated first using a 3-point moving average and then min-max normalized individually for each site. Peat drainage DOC concentration data is available online from the California Integrated Water Quality System (<https://www.waterboards.ca.gov/ciwqs/>).

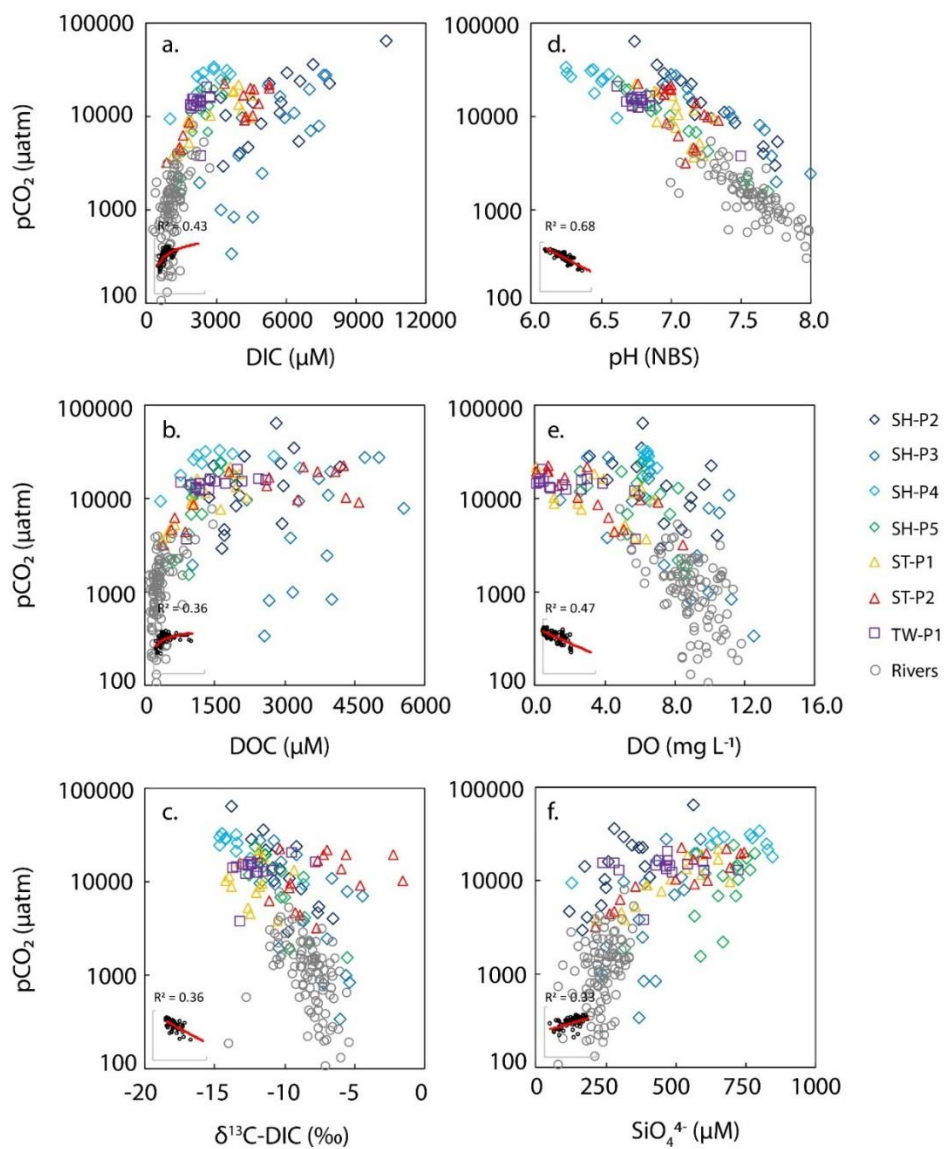


**Figure 2-8. Peat drainage carbon geochemistry.**

Peat island drainage and river pCO<sub>2</sub> values versus (a) DIC concentrations, (b) DOC concentrations, (c) δ<sup>13</sup>C-DIC values, (d) pH, (e) DO, and (f) SiO<sub>4</sub><sup>4-</sup>. Inset figures show cumulative R<sup>2</sup> between all sites except SH-P2 and SH-P3 for all figures, while (c) also excludes ST-P2.

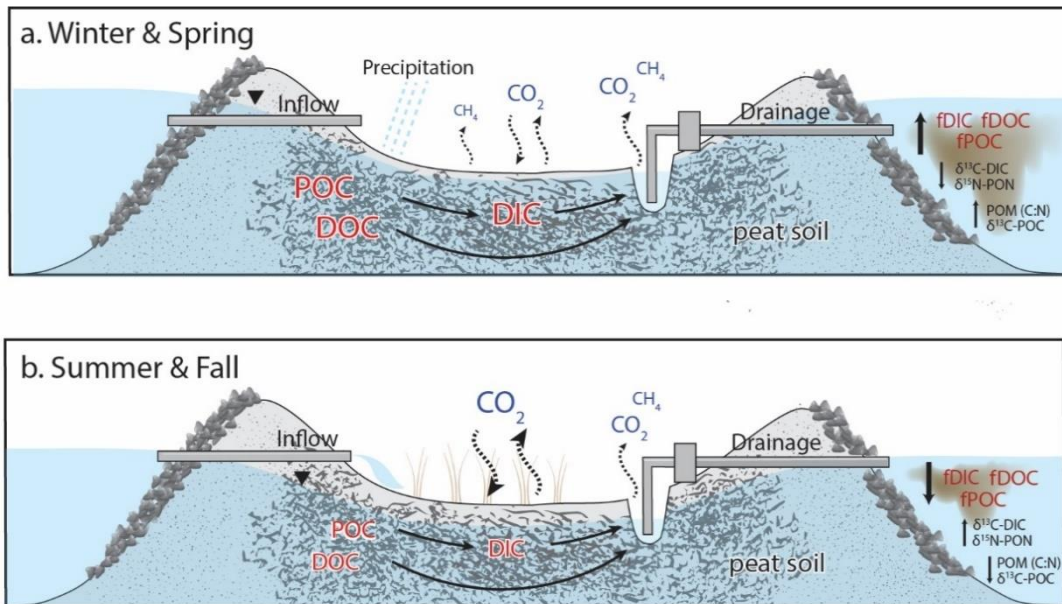


**Figure 2-9. Conceptual diagram of seasonal changes in island hydrology and biogeochemistry.**

Generalization of seasonal changes in hydrology and C geochemistry on Delta islands in (a) winter/spring and (b) summer/fall; “fPOC” denotes flux of POC. Figure modified from Ingebritsen et al. (2000) and not to scale. Figure modified from Ingebritsen et al. (2000).

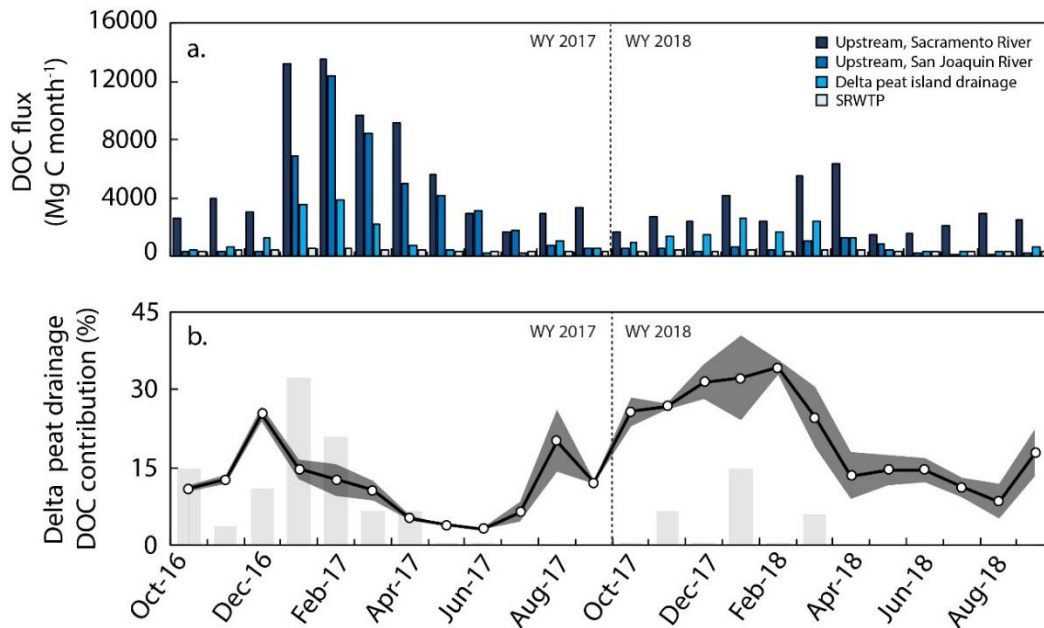


**Figure 2-10. Regional comparison of carbon fluxes.**

(a) Monthly estimates of DOC flux for the Sacramento River at Freeport (black), San Joaquin River at Vernalis (dark grey), total Delta peat island drainage (light grey), and Sacramento Regional Wastewater Treatment Plant, WWTP (white). (b) Delta peat drainage DOC contributions as a percentage of total DOC flux from the sources considered in (a), with monthly precipitation (cm) totals shown by the transparent grey bars. The shaded region around the monthly peat drainage DOC flux estimates shows the standard deviation of the drainage DOC flux generated for cropland (ST) and pastureland-dominated systems (SH).

**Table 2-1. Mean annual river and peat drainage geochemistry.**

WY 2018 mean and standard deviation of river and drainage C geochemistry and related parameters. WY 2017 data are not included so as not to bias the annual mean. For explanation of site abbreviations and locations see Figure 1. \*SH-P4 water year data is incomplete as data collected during net zero discharge months was not included.

Site		Rivers	SH-P2	SH-P3	SH-P4*	SH-P5	ST-P1	ST-P2	TW-P1
POC ( $\mu\text{M}$ )	mean	70	2180	1810	640	2060	1700	1440	1140
	stdev	65	720	440	380	660	940	860	530
DOC ( $\mu\text{M}$ )	mean	290	2230	3540	1690	1120	1320	2670	1460
	stdev	150	880	1280	900	410	630	1400	600
DIC ( $\mu\text{M}$ )	mean	1180	5580	5560	3430	2380	3160	3800	2400
	stdev	360	2120	1790	880	690	1230	1460	260
pCO <sub>2</sub> ( $\mu\text{atm}$ )	mean	1270	20480	11280	25800	10830	11940	14150	13500
	stdev	920	16700	9800	4250	7250	6000	6800	3800
SUVA <sub>254</sub> ( $\text{L mg}^{-1} \text{m}^{-1}$ )	mean	2.6	4.3	4.1	4.5	4.0	3.8	4.1	4.7
	stdev	1.1	0.3	0.3	0.8	0.7	0.6	1.1	1.6
$\delta^{13}\text{C-DIC}$ (‰)	mean	-8.4	-10.8	-9.0	-12.3	-10.5	-12.3	-7.3	-12.2
	stdev	1.5	1.8	2.3	2.4	2.0	1.4	3.0	1.1
POM ( $\text{C/N}$ ) <sub>m</sub>	mean	8.7	8.0	8.6	12.6	10.2	9.8	10.0	11.1
	stdev	0.9	0.6	1.8	1.2	2.4	1.5	2.1	1.0
$\delta^{13}\text{C-POC}$ (‰)	mean	-28.3	-34.4	-33.7	-32.2	-29.7	-25.7	-26.9	-29.1
	stdev	1.3	3.0	0.9	2.3	1.5	2.7	3.9	0.6
$\delta^{15}\text{N-PON}$ (‰)	mean	4.9	3.0	3.3	-1.5	-0.1	3.2	2.4	1.6
	stdev	2.1	3.4	3.2	2.6	0.5	0.9	1.5	1.4
pH (NBS)	mean	7.6	7.2	7.6	6.6	7.1	7.0	7.1	6.8
	stdev	0.4	0.3	0.5	0.2	0.4	0.2	0.1	0.2
DO ( $\text{mg L}^{-1}$ )	mean	9.4	7.1	7.2	0.8	6.6	3.8	2.6	2.5
	stdev	1.4	2.3	3.3	1.0	1.8	2.3	2.0	1.9
$\delta^2\text{H-H}_2\text{O}$ (‰)	mean	-73.7	-59.5	-56.5	-67.1	-68.7	-69.7	-67.3	-68.9
	stdev	4.5	4.1	4.9	3.5	1.7	5.4	7.3	1.9
SiO <sub>4</sub> <sup>4-</sup> ( $\mu\text{M}$ )	mean	240	310	440	900	670	510	540	500
	stdev	60	120	100	180	130	140	170	110

**Table 2-2. Seasonal means of peat drainage carbon geochemistry.**

Seasonal means of peat island drainage C geochemistry and ancillary water quality parameters in peat drainage from Sherman Island (SH), Staten Island (ST) and Twitchell Island (TW) for data across WY 2017 and WY 2018.

Site	Season	POC ( $\mu\text{M}$ )	DOC ( $\mu\text{M}$ )	DIC ( $\mu\text{M}$ )	pCO <sub>2</sub> ( $\mu\text{atm}$ )	SUVA <sub>254</sub> ( $\text{L mg}^{-1} \text{m}^{-1}$ )	$\delta^{13}\text{C}$ - DIC (‰)	POM (C/N) <sub>m</sub>	$\delta^{13}\text{C}$ - POC (‰)	$\delta^{15}\text{N}$ - PON (‰)	pH (NBS)	DO ( $\text{mg L}^{-1}$ )	$\delta^2\text{H}$ - H <sub>2</sub> O (‰)	SiO <sub>4</sub> <sup>4-</sup> ( $\mu\text{M}$ )
<b>SH-P2</b>	Fall	2030	1690	4340	8920	4.4	-9.0	8.5	-34.5	2.8	7.41	7.2	-55.1	240
	Winter	1710	2860	6340	19590	4.2	-10.8	n.a.	-38.0	2.3	7.10	7.8	-62.4	380
	Spring	3250	2650	7360	37900	4.3	-12.1	n.a.	-30.7	-0.3	6.93	7.4	-60.3	340
	Summer	1760	2150	5160	13380	3.9	-9.8	7.7	-33.6	5.5	7.36	6.7	-49.0	260
<b>SH-P3</b>	Fall	3080	4890	6470	7120	4.0	-6.0	7.7	-34.2	3.8	7.68	10.2	-48.9	480
	Winter	1670	4130	6810	21300	4.0	-10.1	9.9	-34.0	1.6	7.08	5.4	-57.4	490
	Spring	2450	3480	5940	15640	4.0	-11.4	11.1	-32.7	0.3	7.25	3.8	-58.7	430
	Summer	1580	2750	3580	1470	4.2	-7.3	8.6	-31.7	7.7	8.20	9.0	-56.8	340
<b>SH-P4</b>	Fall	530	1240	2530	29800	3.9	-14.1	13.8	-29.4	-0.5	6.35	0.7	-70.8	860
	Winter	380	1410	2970	24500	4.2	-14.0	11.3	-33.4	-2.0	6.46	2.0	-68.4	810
	Spring	910	3040	4460	24890	4.9	-13.9	12.6	-28.8	2.2	6.79	0.3	-63.5	820
	Summer	1380	940	2160	21800	4.0	-11.5	12.2	-31.0	-0.6	6.58	1.2	-74.1	750
<b>SH-P5</b>	Fall	1690	1140	2420	15010	4.1	-11.7	8.7	-31.6	-0.1	6.77	4.1	-70.3	710
	Winter	1600	1300	2920	14530	4.5	-10.9	12.0	-28.2	-0.1	6.87	7.4	-68.5	730
	Spring	3040	1120	2400	9870	4.1	-11.1	13.4	-28.9	-0.2	7.11	7.1	-67.2	600
	Summer	1200	1020	1820	7600	4.5	-8.8	7.7	-31.1	2.6	7.19	6.2	-68.3	620
<b>ST-P1</b>	Fall	1810	1920	3050	13800	3.7	-12.5	9.7	-28.9	2.9	6.97	1.8	-68.5	520
	Winter	940	1630	4180	17330	4.3	-11.5	10.0	n.a.	2.9	6.93	3.4	-65.5	620
	Spring	1530	1090	3470	10090	3.5	-13.2	11.1	-27.3	2.0	7.12	5.0	-68.9	560
	Summer	1280	600	1540	5240	3.7	-11.9	7.3	-27.8	4.1	7.15	4.6	-76.9	320
<b>ST-P2</b>	Fall	2540	3980	4350	18290	3.5	-7.4	8.4	-32.5	4.5	7.01	2.9	-65.9	600
	Winter	1270	3680	4690	15760	3.5	-5.0	11.3	n.a.	1.0	7.06	1.4	-61.5	600
	Spring	2700	2550	4590	14390	3.7	-6.0	13.0	-27.2	1.5	7.15	2.7	-64.2	680
	Summer	840	690	1460	5430	5.0	-9.4	9.1	-27.6	4.4	7.09	5.2	-76.7	280
<b>TW-P1</b>	Fall	1150	1270	2240	14970	3.2	-11.5	11.4	-28.9	1.3	6.73	1.9	-71.4	500
	Winter	830	1790	2440	14170	5.2	-12.1	10.1	-29.7	2.6	6.73	3.3	-69.3	550
	Spring	550	1670	2530	13890	4.8	-12.5	12.6	-28.3	0.5	6.82	2.1	-67.3	560
	Summer	1130	1370	2320	12790	5.1	-11.9	10.5	-28.5	2.3	6.91	1.4	-67.6	360

**Table 2-3. Peat drainage carbon exports across two contrasting water years.**

Comparison of annual WY 2017 and WY 2018 C exports from available drainage sites and C imports from rivers. WY 2017 estimates for SH-P5 are not included as this site was missing discharge data for WY 2017. Exports for SH-P4 when discharge was zero were not included in its water year mean (May through September of 2018). WY 2017 inflow C imports are based on mean annual river concentration data from WY 2018.

Site	WY 2017 (g C m <sup>-2</sup> yr <sup>-1</sup> )				WY 2018 (g C m <sup>-2</sup> yr <sup>-1</sup> )			
	DIC	DOC	POC	Total	DIC	DOC	POC	Total
<b>Exports</b>								
Export TW-P1	44.6	30.6	14.2	89.4	30.7	19.8	12.3	62.8
Export ST-P1	45.3	15.5	19.6	80.4	16.3	6.3	10.1	32.7
Export ST-P2	34.9	26.5	16.8	78.2	13.1	8.6	5.9	27.6
Export SH-P2	21.8	8.8	8.9	39.5	17.3	7.0	6.7	31.0
Export SH-P3	48.3	30.5	16.7	95.6	25.6	16.0	8.2	49.8
Export SH-P4	15.5	10.2	3.9	29.6	6.9	4.3	2.1	13.3
Export SH-P5	n.a.	n.a.	n.a.	n.a.	20.2	9.6	18.3	48.1
<b>Imports</b>								
Import-SH	12.6	3.1	0.7	16.4	15.8	3.9	0.9	20.6
Import-ST	11.8	2.9	0.7	15.4	13.5	3.3	0.8	17.5
Import-TW	33.5	8.2	2.0	43.7	31.1	7.6	1.9	40.5

**Table 2-4. Comparison of lateral carbon exports to vertical carbon exports.**

Comparison of lateral (aqueous) C export rates to published vertical (gaseous) C export rates for the Delta. NEE and NECB represent net ecosystem exchange and net ecosystem carbon balance (e.g.,  $NEE + CH_4$ ), respectively. Cumulative drainage exports from this study are taken as area-weighted averages based on catchments associated with each site (Fig. S2). WY 2018 export rates for SH-P5 were used in the weighted average for Sherman Island during WY 2017 as SH-P5 was missing discharge data for that year. C imported via inflow water estimated for WY 2017 was generated using mean river geochemistry from WY 2018.

Site description	Island	Study area details	Phase	Date	<sup>1</sup> Export (g C m <sup>-2</sup> d <sup>-1</sup> )	Study
<b>Lateral Fluxes (Aqueous)</b>						
Cumulative drainage	Sherman	weighted average of exports from all outlets on each island; dry WY	<sup>2</sup> Aqueous	Oct-17 – Sep-18	0.10	This study
Cumulative drainage	Staten		<sup>2</sup> Aqueous	Oct-17 – Sep-18	0.08	This study
Cumulative drainage	Twitchell		<sup>2</sup> Aqueous	Oct-17 – Sep-18	0.17	This study
Cumulative drainage	Sherman	weighted average of exports from all outlets on each island; wet WY	<sup>2</sup> Aqueous	Oct-16 – Sep-17	0.16	This study
Cumulative drainage	Staten		<sup>2</sup> Aqueous	Oct-16 – Sep-17	0.22	This study
Cumulative drainage	Twitchell		<sup>2</sup> Aqueous	Oct-16 – Sep-17	0.25	This study
Drainage ditch	Jersey	single ditch	Aqueous (DOC)	May-90 – Jul-90	0.30	Deverel and Rojstaczer (1996)
Drainage ditch	Orwood		Aqueous (DOC)	May-90 – May-91	0.02	Deverel and Rojstaczer (1996)
Drainage ditch	Sherman		Aqueous (DOC)	May-90 – Nov-90	0.002	Deverel and Rojstaczer (1996)
Cumulative drainage	Twitchell	multi-year average including approximated loads	Aqueous (DOC)	Aug-00 – Aug-03	0.45	Deverel et al. (2007)
Managed wetlands		average of three managed flow-through wetland cells	Aqueous (DOC)	Jul-12 – Oct 13	0.14	Bachand et al. (2019)
Inflow waters	Sherman	annual inflow volume estimated via water budget with mean annual river geochemistry; dry WY	<sup>2</sup> Aqueous	Oct-17 – Sep-18	-0.06	This study
Inflow waters	Staten		<sup>2</sup> Aqueous	Oct-17 – Sep-18	-0.05	This study
Inflow waters	Twitchell		<sup>2</sup> Aqueous	Oct-17 – Sep-18	-0.11	This study
Inflow waters	Sherman	annual inflow volume estimated via water budget with mean annual river geochemistry; wet WY	<sup>2</sup> Aqueous	Oct-16 – Sep-17	-0.04	This study
Inflow waters	Staten		<sup>2</sup> Aqueous	Oct-16 – Sep-17	-0.04	This study
Inflow waters	Twitchell		<sup>2</sup> Aqueous	Oct-16 – Sep-17	-0.12	This study
<b>Vertical Fluxes (Gaseous)</b>						

Grazed land	Sherman	pastureland, disconnected from main island	Gaseous, NEE	Apr-09 – Apr-10	0.82	Hatala et al. (2012)
Grazed land	Sherman		Gaseous, NEE	Apr-10 – Apr-11	0.48	Hatala et al. (2012)
Rice paddy	Twitchell	central part of island	Gaseous, NEE	Apr-09 – Apr-10	-0.23	Hatala et al. (2012)
Rice paddy	Twitchell		Gaseous, NEE	Apr-10 – Apr-11	-0.78	Hatala et al. (2012)
Managed wetland	Twitchell	central part of island, impounded wetland	Gaseous, NEE	Apr-02- Apr-03	-2.20	Anderson et al. (2016)
Managed wetland	Twitchell		Gaseous, NEE	Apr-10 – Apr-11	-0.06	Anderson et al. (2016)
Grazed land	Sherman	footprint includes drainage ditches	Gaseous, NEE	Mar-12 – Mar-13	0.93	Knox et al. (2015)
Farmland (corn)	Twitchell		Gaseous, NEE	May-12 – May-13	0.76	Knox et al. (2015)
Farmland (rice)	Twitchell		Gaseous, NEE	Mar-12 – Mar-13	-0.14	Knox et al. (2015)
Managed wetland	Sherman	young, partially disconnected from main island	Gaseous, NEE	Mar-12 – Mar-13	-1.01	Knox et al. (2015)
Managed wetland	Twitchell	old, central part of island	Gaseous, NEE	Aug-12 – Aug-13	-1.09	Knox et al. (2015)
Farmland (corn)	Twitchell		Gaseous, NECB	May-12 – May-13	1.60	Hemes et al. (2019)
Farmland (corn)	Bouldin		Gaseous, NECB	Apr-17 – Apr-18	4.22	Hemes et al. (2019)
Farmland (rice)	Twitchell		Gaseous, NECB	2010 – 2016	0.99	Hemes et al. (2019)
Grazed land	Sherman		Gaseous, NECB	2010 – 2014	0.86	Hemes et al. (2019)
Farmland (alfalfa)	Twitchell		Gaseous, NECB	2014 – 2017	1.28	Hemes et al. (2019)
Farmland (alfalfa)	Bouldin		Gaseous, NECB	2017	0.55	Hemes et al. (2019)
Restored wetland	n.a.	integrated flux	Gaseous, NECB	n.a.	-0.65	Hemes et al. (2019)

<sup>1</sup>Positive values indicate export from the system, either to receiving waters (lateral/aqueous) or to the atmosphere (vertical/gaseous)

<sup>2</sup>Aqueous includes DIC, DOC, and POC unless noted otherwise

**Table 2-5. Delta wide island drainage C fluxes for WY 2017 and WY 2018.**

Total Delta wide peat island drainage annual and seasonal C fluxes for WY 2017 and WY 2018.

	DIC (Mg C d <sup>-1</sup> )	DOC (Mg C d <sup>-1</sup> )	POC (Mg C d <sup>-1</sup> )
<b>WY 2017</b>	76	43	39
Summer	32	17	29
Fall	32	18	16
Winter	179	97	75
Spring	65	38	37
<b>WY 2018</b>	73	38	35
Summer	27	11	21
Fall	64	38	32
Winter	118	64	47
Spring	93	46	45

## Supplemental Index

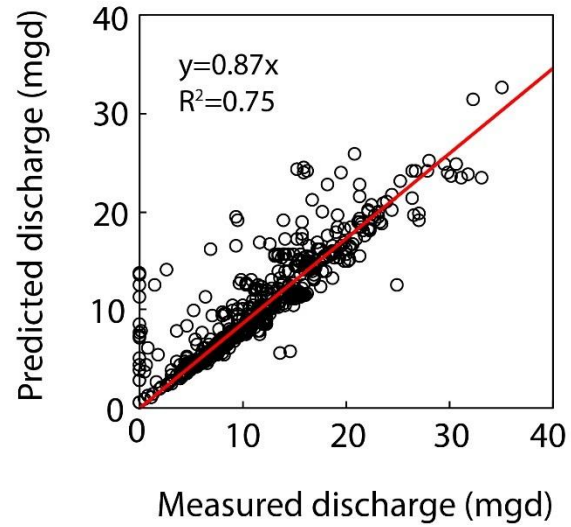


**Figure S1.** Scatter plot showing measured discharge using an in situ ultrasonic flow meter versus discharge predicted using the unit-power consumption method. Data from TW-P1 on Twitchell Island for 06/01/2017 to 12/31/2018. Each dot represents a cross-referenced daily flow value.

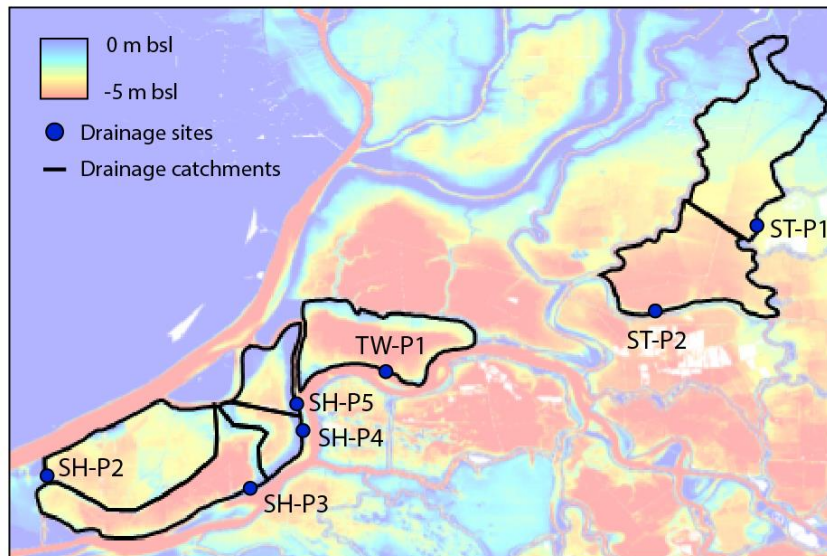


**Figure S2.** Approximated drainage catchments for Sherman (SH), Staten (ST), and Twitchell (TW) islands. Drainage areas were estimated using approximated elevational boundaries within islands.

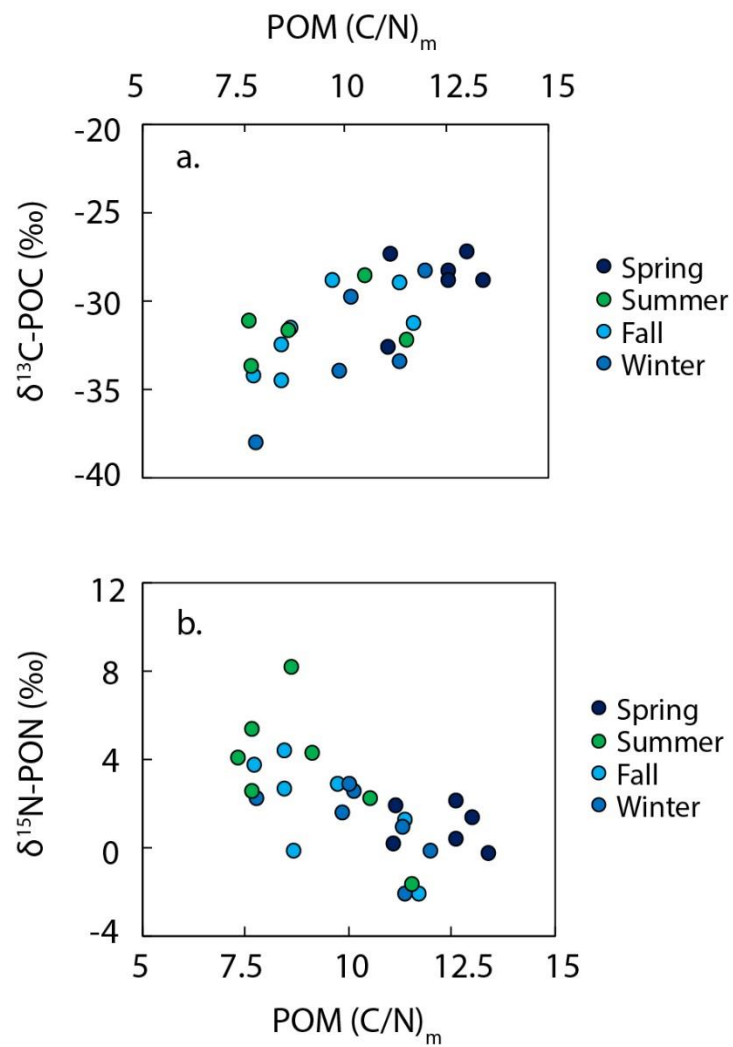


**Figure S3.** (a) Seasonal peat drainage  $\delta^{13}\text{C-POM}$  values versus POM (C/N)<sub>m</sub>, and (b) seasonal peat drainage  $\delta^{15}\text{N-POM}$  values versus POM (C/N)<sub>m</sub>.

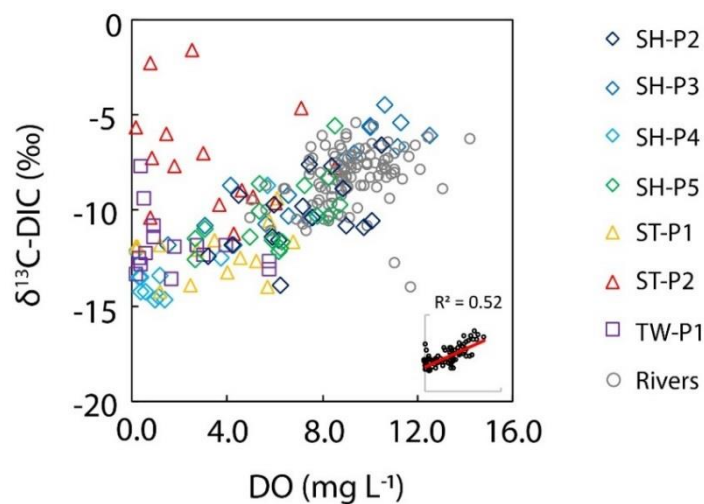


**Figure S4.**  $\delta^{13}\text{C-DIC}$  values versus dissolved oxygen (DO) concentration in peat drainage and river water (grey circles). Inset figure shows cumulative  $R^2$  across all drainage sites except ST-P2 outliers.

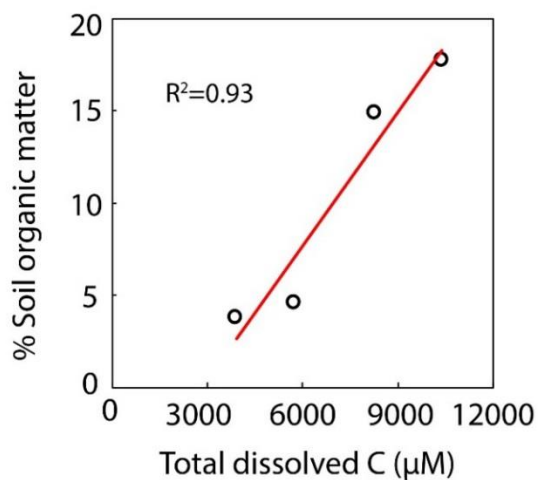


**Figure S5.** Soil organic matter content versus discharge-weighted total dissolved C. Soil organic matter content was calculated for each drainage basin on Sherman Island (see Figure S2) as a weighted average between 0 to 200 cm depth using the Soil Survey Geographic Database (SSURGO) available online (<https://data.nal.usda.gov/dataset/soil-survey-geographic-database-ssurgo>).

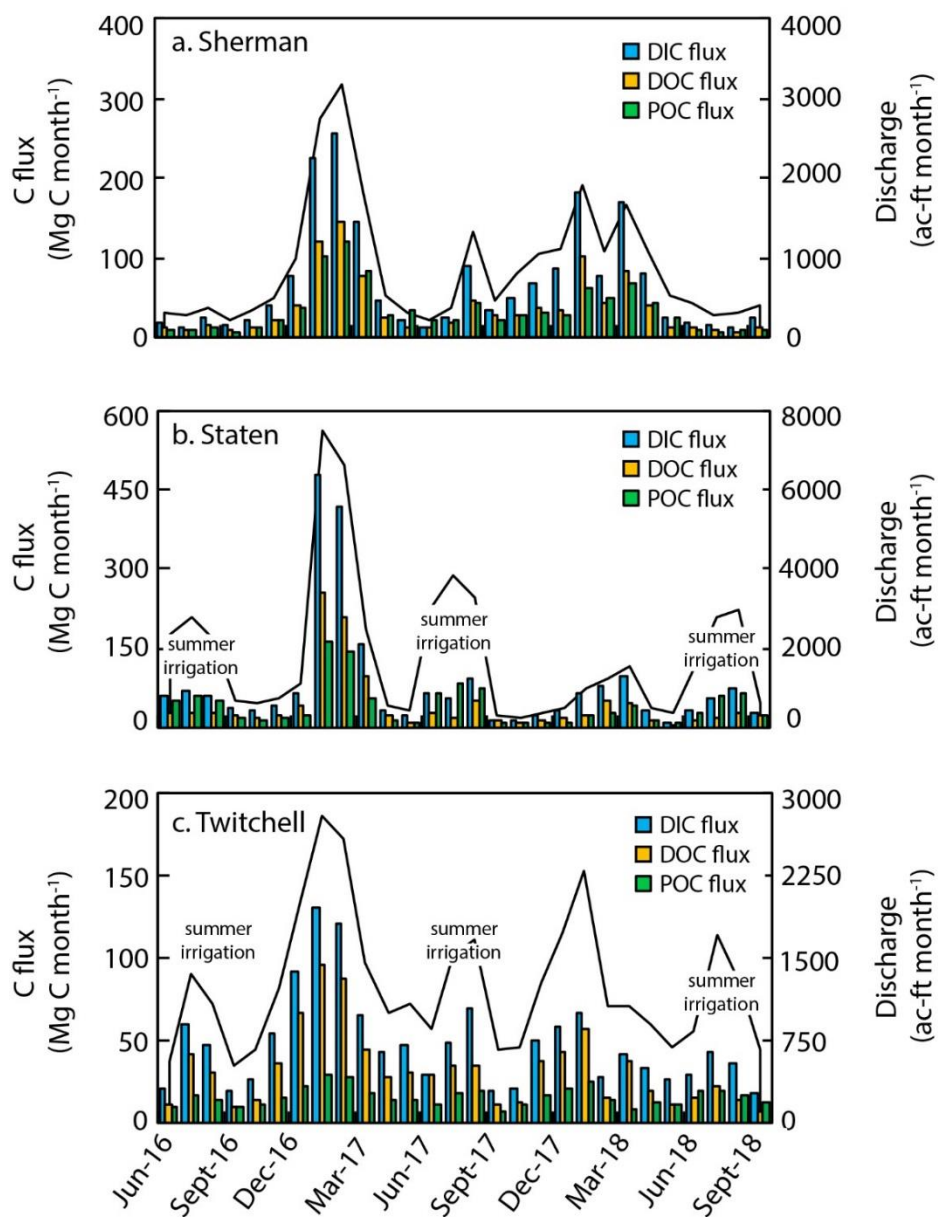


**Figure S6.** Monthly DIC (blue), DOC (yellow), and POC (green) fluxes and discharge (black line) for (a) Sherman, (b) Staten, and (c) Twitchell islands.

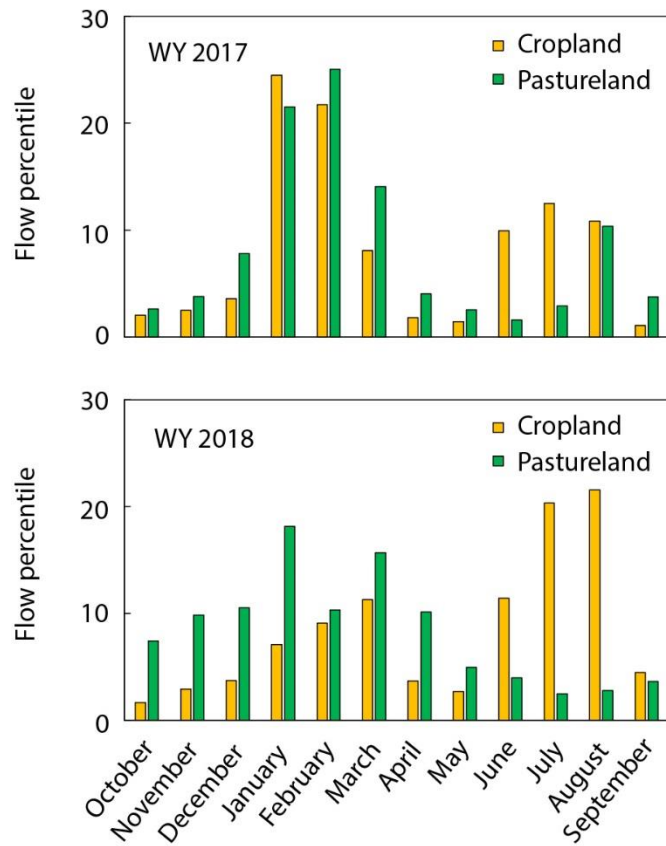


**Figure S7.** Flow percentiles for pastureland and cropland dominated islands for (a) WY 2017 and (b) WY 2018. Sherman Island was used to represent pastureland dominated islands, and Staten Island was used to represent cropland dominated islands.

**Table S1.** Land use or crop cover for each island studied based on spatial data from the California Crop Mapping database (<https://data.cnra.ca.gov/dataset/statewide-crop-mapping>).

<b>Land use (%)</b>	<b>Sherman</b>	<b>Staten</b>	<b>Twitchell</b>
Alfalfa and Alfalfa Mixtures	5.6	2.4	22.1
Corn, Sorghum and Sudan	16.8	72.2	
Idle	2.8		2.0
Managed Wetland	3.3		29.6
Miscellaneous Grasses	6.9		
Miscellaneous Deciduous			0.5
Mixed Pasture	57.3	6.5	19.8
Potatoes and Sweet Potatoes		9.6	
Rice			18.2
Wheat	7.3	9.1	

**Table S2.** Measured pump efficiencies for each outlet.

<b>Site</b>	<b>Date of test</b>	<b>Pump power coefficient (kWh ac-ft<sup>-1</sup>)</b>
SH-P1	9/6/2017	71.5
SH-P2	9/6/2017	49.3
SH-P3	9/6/2017	43.9
SH-P4	9/6/2017	41.6
SH-P5	9/6/2017	43.2
ST-P1	9/7/2017	33.3
ST-P2	9/7/2017	64.1
TW-P1	10/13/2016	41.5

**Table S3.** Equations for linear regressions and associated  $R^2$  values between water yield and DIC, DOC, and POC exports (as shown in Figure 4). Due to the limited number of POC samples collected (quarterly), POC regressions were not seasonally separated for ST-P1 and ST-P2.

Site	DIC	DOC	POC
TW-P1	$y = 399.8x - 4.81$ $R^2 = 0.91, n=16,$ $p < 0.01$	$y = 311.1x - 7.79$ $R^2 = 0.69, n=16,$ $p < 0.01$	$y = 82.6x + 3.99$ $R^2 = 0.34, n=6$
ST-P1 (Summer)	$y = 111.9x + 9.73$ $R^2 = 0.31, n=5$	$y = 35.1x + 4.54$ $R^2 = 0.06, n=5$	
ST-P1	$y = 646.3x - 2.97$ $R^2 = 0.94, n=10$ $p < 0.01$	$y = 197.9x + 0.66$ $R^2 = 0.77, n=10$ $p < 0.01$	$y = 200.3x + 0.78$ $R^2 = 0.66, n=5,$ $p < 0.10$
ST-P2 (Summer)	$y = 219.3x - 0.91$ $R^2 = 0.63, n=5$	$y = 95.0x + 0.21$ $R^2 = 0.41, n=5$	
ST-P2	$y = 630.1x + 0.13$ $R^2 = 0.99, n=10,$ $p < 0.01$	$y = 518.1x - 0.09$ $R^2 = 0.91, n=10,$ $p < 0.01$	$y = 216.4x + 0.96$ $R^2 = 0.40, n=5$
SH-P2	$y = 839.0x + 0.05$ $R^2 = 0.78, n=16,$ $p < 0.01$	$y = 339.0x - 0.01$ $R^2 = 0.72, n=16,$ $p < 0.01$	$y = 358.4x - 0.35$ $R^2 = 0.83, n=6,$ $p < 0.05$
SH-P3	$y = 1209.8x - 8.68$ $R^2 = 0.96, n=16,$ $p < 0.05$	$y = 729.5x - 3.86$ $R^2 = 0.92, n=16,$ $p < 0.05$	$y = 368.6x - 0.61$ $R^2 = 0.75, n=6,$ $p < 0.05$
SH-P4	$y = 538.8x - 0.23$ $R^2 = 0.97, n=11,$ $p < 0.01$	$y = 364.0x - 0.45$ $R^2 = 0.92, n=11,$ $p < 0.01$	$y = 131.9x + 0.02$ $R^2 = 0.98, n=4,$ $p < 0.01$
SH-P5	$y = 503.8x - 5.99$ $R^2 = 0.94, n=14,$ $p < 0.01$	$y = 250.4x - 3.30$ $R^2 = 0.85, n=14,$ $p < 0.01$	$y = 500.3x - 9.68$ $R^2 = 0.92, n=5,$ $p < 0.01$

**Table S4.** WY 2017 and WY 2018 water budget estimates.

	Inflow (ac-ft yr <sup>-1</sup> )	Outflow (ac-ft yr <sup>-1</sup> )	ET (ac-ft yr <sup>-1</sup> )	Precipitation (ac-ft yr <sup>-1</sup> )
<b>WY 2017</b>				
Sherman	30700	12700	34500	16410
Staten	25100	30420	23400	28700
Twitchell	28000	17500	15200	4700
<b>WY 2018</b>				
Sherman	38600	10600	37300	9200
Staten	28600	13800	23700	8900
Twitchell	25900	14200	15400	3600

## **Chapter 3**

### **NUTRIENT AND TRACE METAL CONTRIBUTIONS FROM DRAINED ISLANDS IN THE SACRAMENTO-SAN JOAQUIN DELTA, CALIFORNIA**

In preparation for submission to San Francisco Estuary and Watershed Science:

Richardson, C., J. K. Fackrell, , T. E. C. Kraus, M. B. Young, C. Kendall, and A.

Paytan. Nutrient and trace metal contributions drained islands in the Sacramento-San

Joaquin Delta, California.

## Abstract

Inventorying nutrient sources in the Sacramento-San Joaquin Delta (the Delta) is critical in the face of the forthcoming upgrade to the Sacramento Regional Wastewater Treatment Plant (SRWTP), which is expected to alter the Delta's nutrient regime. While island drains are a ubiquitous feature of the Delta, limited data exists to evaluate island drainage nutrient and trace metal fluxes in this system. To better constrain inputs from this understudied source, we calculated nutrient ( $\text{NH}_4^+$ ,  $\text{NO}_3^-$ ,  $\text{NO}_2^-$ ,  $\text{PO}_4^{3-}$ , DON, PON,  $\text{SiO}_4^{4-}$ ) and trace metal (total dissolved Fe, Mn, As) contributions from three Delta islands at monthly resolution from June 2017 to September 2018 and upscaled island-specific fluxes to Delta-wide contributions. This study provides new baseline estimates of gross and net nutrient and trace metal fluxes from island drains that can be used to ground-truth existing box models along with concomitant N stable isotope data that improves our understanding of N sources and cycling on Delta islands. Upscaled gross annual total N (TN) loads from island drainage were  $2.7 \times 10^6$  kg, with organic N contributing ~76% and dissolved inorganic N contributing ~24%. Over 59% of all nutrient and trace metal loads from island drainage, except for  $\text{PO}_4^{3-}$ , occurred in winter and spring. Gross and net annual island drainage  $\text{PO}_4^{3-}$  loads were negligible in the context of other major inflows, while gross and net annual TN loads were high and comprised an estimated 13 to 17% and 9% of annual TN inputs to this system, respectively. Using forecasted changes in total dissolved N (TDN) and ammonium ( $\text{NH}_4^+$ ) concentrations from SRWTP, we calculated changes in pre- and post-upgrade contributions relative to

other major freshwater inflow sources (San Joaquin River and Sacramento River) based on the 2018 water year (a dry water year). Pre-upgrade, net annual island drainage TDN and  $\text{NH}_4^+$  contributions were about 5% and 4%, respectively. Under a post-upgrade scenario, net annual island drainage TDN contributions increased to 8% and  $\text{NH}_4^+$  contributions increased to 46% as the SRWTP  $\text{NH}_4^+$  load diminished. Most of the net annual dissolved N load from island drains was delivered seasonally, with 11% of TDN and 60% of  $\text{NH}_4^+$  sourced from island drainage during the winter. While the SRWTP upgrade will result in net reductions in N delivered to the Delta, this study's results suggest that island drainage is a measurable anthropogenic N source that will become increasingly important in the face of the SRWTP upgrade, with the majority of N (along with other nutrients and trace metals) discharged during winter and spring.

### **3.1 Introduction**

Over the last four decades, the San Francisco Bay and Sacramento-San Joaquin Delta (the Delta) have experienced a number of drastic ecological changes. From the 1970s to the 1990s, primary production and phytoplankton biomass decreased by 40% and 60%, respectively (Jassby, 2008). More recent work shows that chlorophyll-*a* concentrations have declined by over 70% since 1975 (Cloern, 2019). The introduction of a number of invasive species, including two clams, *Corbula amurensis* and *Corbicula fluminea*, are commonly thought of as important catalysts of structural ecological change in this system, and many studies suggest that their

introductions have led to at least some of the observed declines in phytoplankton biomass due to high grazing rates (Jassby, 2008; Jassby et al., 2002). Winder and Jassby (2011) showed zooplankton community shifts over a 37-year period and also associated this with the *Corbula* invasion. Other invasive species, including a number of aquatic macrophytes (ex., *Eichhornia crassipes*, water hyacinth, and *Ludwigia hexapetala*, water primrose), persist in the Delta today, and are affecting both habitat and water quality (Dahm et al., 2016; Ta et al., 2017).

Higher trophic level species have experienced similar widespread declines. Decreases over the past two decades in pelagic fish abundance, often referred to as Pelagic Organism Decline, have prompted a number of food web studies (Sommer et al., 2007). However, master controls on biomass and production trends remain elusive, likely owing to the hydrologic and biogeochemical complexity of the estuary. While no one variable has been able to fully account for the previously discussed changes, water quality, and especially nutrient availability, remains an important control on ecosystem function in estuaries worldwide (Howarth et al., 2011; Paerl et al., 1998; Paerl et al., 2006; Seitzinger & Sanders, 1997).

A number of studies have attempted to assess the effects of nutrient forms and ratios on primary productivity in the Delta environment (see reviews by Senn and Novick (2014), Dahm et al. (2016), Ward and Paerl (2016)). Most research on nutrients in the Delta has focused on nitrogen (N) biogeochemistry due to both its ubiquitous

presence in human-impacted watersheds and because of the widely debated importance of N speciation for primary production in the Delta. Cloern (2019) shows that ammonium ( $\text{NH}_4^+$ ) and nitrate plus nitrite ( $\text{NO}_3^- + \text{NO}_2^-$ ) concentrations in the SF Bay-Delta have changed significantly since the mid-1970s, with mean annual concentrations increasing over 50%. While previous work had suggested that nutrients were at saturation levels for phytoplankton in the Delta (Jassby et al., 2002), more recent work has found that N forms and concentrations as well as N ratios to other nutrients play an important role in phytoplankton ecology and uptake kinetics (Dugdale et al., 2015; Kraus et al., 2017; Stumpner et al., 2020). These complex relationships between nutrients and Delta ecology highlight the importance of adequately characterizing and accounting for all internal and external nutrient sources in this system.

Dominant N sources to the Delta at present include upstream rivers and wastewater treatment plants. The Sacramento River and San Joaquin River generally represent about 84% and 13% of water inflow to the Delta, respectively (Jassby & Cloern, 2000). Together, they deliver over 17 million kg of total N (TN, as particulate and dissolved inorganic and organic N) annually (Jassby & Cloern, 2000; Saleh & Domagalski, 2015). Diffuse (non-point source) agricultural sources account for the majority of TN in these rivers upstream of the Delta (Saleh & Domagalski, 2015). The largest anthropogenic point source of TN to the Delta is currently the Sacramento Regional Wastewater Treatment Facility (SRWTP), which annually discharges

around 4 million kg of TN, predominantly as  $\text{NH}_4^+$ , into the Sacramento River in the northern portion of the Delta. The SRWTP TN input comprises roughly 32% of the Sacramento River annual TN load, though the importance of the SRWTP TN load is amplified during low flow months (Saleh & Domagalski, 2015). Upgrades to SRWTP are slated to come online in the summer of 2020. Once complete, these upgrades are expected to reduce  $\text{NH}_4^+$  concentrations in the discharged effluent by up to 99%, and TDN by over 65% (Cooke et al., 2018; Kraus et al., 2017). This decrease in  $\text{NH}_4^+$  will substantially lower total dissolved N and  $\text{NH}_4^+$  inputs from the SRWTP, which are thought to account for over 90% of  $\text{NH}_4^+$  input into the Delta (Jassby, 2008). With this reduction,  $\text{NH}_4^+$  and TDN contributions from other sources, such as drainage from subsided islands in the central Delta, may increase in relative importance as sources of N to the Delta.

While nutrient budgets for the Delta account for upstream river and wastewater inputs, Delta island drainage inputs remain widely understudied. For example, most existing N budgets in the Delta can generally only ground-truth inputs entering the area into account as data on internal sources of N such as island drainage is sporadic and incomplete. The Delta contains over fifty drained peat islands, many of which are commercially farmed. Long-term drainage of Delta islands for farming has resulted in extensive land subsidence from soil oxidation, with many islands now residing over 3 m below sea level (Deverel & Leighton, 2010). As a result, most Delta islands must artificially maintain water tables below the sediment surface via managed pumping.

Water exported from Delta islands is commonly referred to as agricultural drainage, return flow, and/or island drainage, and here we use ‘island drainage’ to refer to this flow. While previous estimates of water discharge from island drainage (~320 mgd), are comparable in magnitude to those from major wastewater treatment plants, like SRWTP (~120 mgd) (Templin & Cherry, 1997), little work has been done to characterize island drainage geochemistry and inputs to the Delta. As a result, major macronutrient (N, P, Si) and trace element (Mn, Fe, As) inputs from island drainage to the Delta remain unconstrained. There may be over two hundred active island drainage outfalls in the Delta, however, even our understanding of drain locations is outdated (Siegfried et al., 2014). The delivery of macronutrients and trace elements to nearby waterways can have profound effects on habitat quality, primary productivity, and aquatic biota (Bricker et al., 1999; Luoma & Rainbow, 2008; Seitzinger & Sanders, 1997).

Recent companion work by Richardson et al. (in review) suggests that island drainage is an important seasonal source of dissolved and particulate carbon to the Delta, and also found that seasonal increases in dissolved carbon concentrations in island drainage were best explained by water table rises that help mobilize carbon in island soils. This seasonality in carbon cycling and transport raises important questions regarding concomitant changes in N species and other macronutrient and trace metal concentrations in drainage waters. Fluctuations in water table elevation and flow likely shift the oxic-anoxic boundary in the subsurface of Delta islands, with

subsequent effects on biogeochemical processes that ultimately control observed island drainage geochemistry and water quality. In the saturated zone, microbial processing of carbon is largely controlled by the influx of oxygenated waters, water residence times, and availability of carbon for respiration (Limpens et al., 2008). When O<sub>2</sub> demand is greater than O<sub>2</sub> influx, anoxic conditions can develop given sufficient carbon substrate. Naturally reduced zones (NRZs) exist in these saturated areas where organic matter is abundant and oxidant-consuming reactions are continuous (Yabusaki et al., 2017). As a result, NRZs can affect concentrations of dissolved organic carbon (DOC), dissolved inorganic N (DIN), dissolved organic N (DON), and reduced metal species (Du Laing et al., 2009; Yabusaki et al., 2017). Past work has shown that both trace elements and organo-metal complexes, like methylmercury, are mobilized in managed Delta wetlands and that methylmercury concentrations correlate with DOC, Fe, and Mn concentrations (Alpers et al., 2014; Bachand et al., 2019; Stumpner et al., 2015). As such, island drainage in the Delta may contribute seasonally important fluxes of N species as well as other major macronutrients and trace elements. To address this gap in knowledge, we characterized monthly island drainage inputs from Sherman, Staten, and Twitchell islands in the Delta from June 2017 to September 2018 to establish a baseline understanding of the geochemistry of this poorly characterized anthropogenic input to the larger Delta environment (Fig. 1). We then upscaled the island-drainage fluxes we measured to the entire Delta to constrain the total magnitude of island drainage inputs

of N species, other macronutrients ( $\text{PO}_4^{3-}$  and  $\text{SiO}_4^{4-}$ ), and trace metals (Mn, Fe, and As) with respect to other inputs under both pre- and post-SRWTP upgrade conditions.

## **3.2 Methods**

### 3.2.1 Site description

Drainage from three Delta islands was sampled in this study: Sherman (SH), Staten (ST), and Twitchell (TW) (Fig. 1). Sherman Island has five pump stations, Staten Island has two pump stations, and Twitchell Island has one pump station. Sherman Island is dominated by pastureland (55%), while cropland accounts for about 30% of land use (based on spatial data available online from the California Crop Mapping database <https://data.cnra.ca.gov/dataset/statewide-crop-mapping>). Staten Island is predominantly farmed (95%) for alfalfa, corn, potatoes, and wheat. Twitchell Island is mixed land use, with several experimental wetlands (30%), pastureland (20%), and cropland (~48%).

A multi-parameter water quality meter (YSI ProPlus) was used to measure ancillary water parameters (pH, dissolved oxygen, conductivity, and temperature) at the time of sample collection. This study focuses on the island drainage geochemistry data and only limited river geochemistry data are presented. Additionally, we excluded geochemistry data for any sites where monthly discharge was zero (e.g., May 2018 to

September 2018 at SH-P4 and all of SH-P1).” In addition to the drainage samples, we collected samples from surrounding river channels at seven locations.

### 3.2.2 Water analyses

Water samples were collected monthly from all drains on the three islands as well as from surrounding rivers from June 2017 through September 2018 for nutrients ( $\text{NH}_4^+$ ,  $\text{NO}_3^-$ ,  $\text{NO}_2^-$ , DON,  $\text{PO}_4^{3-}$ ,  $\text{SiO}_4^{4-}$ ), stable isotopes of nitrate ( $\delta^{15}\text{N}-\text{NO}_3^-$  and  $\delta^{18}\text{O}-\text{NO}_3^-$ ) and trace elements (total dissolved As, Mn, Fe) (Fig. 1). Samples for total suspended solids (TSS),  $\delta^{15}\text{N}-\text{NH}_4^+$ ,  $\delta^{15}\text{N}$  of particulate organic N (PON), and  $\delta^{15}\text{N}-\text{DON}$  were collected quarterly during the same time period. Water samples for all analyses except for trace metals were vacuum filtered in the lab to 0.2  $\mu\text{m}$ , while samples for trace metals were filtered on site to 0.45  $\mu\text{m}$  using trace-clean certified capsule filters and immediately acidified to  $\text{pH} < 2$  with triple-distilled trace clean HCl. Samples were kept on ice until filtered and subsequently frozen or refrigerated, as dictated by their storage requirements.

All nutrient and trace metal analyses were run at the Marine Analytical Laboratory at the University of California at Santa Cruz. Nutrients were measured on a Lachat QuikChem 8000 Flow Injection Analyzer. DON was determined indirectly by conversion to inorganic N using Kjeldahl digestions and run on a Lachat QuikChem 8000 Flow Injection Analyzer. Dissolved trace element concentrations were determined on a Thermo ElementXR High Resolution Inductively Coupled Plasma

Mass Spectrometer and run together with certified reference materials (NIST Standard Reference Material 1643f). DOC samples were vacuum filtered to 0.2  $\mu\text{m}$  in the lab (generally within 24 hours) into 22 mL glass vials and frozen for storage until analysis (typically within a week of collection). DOC concentrations were measured as non-purgeable organic carbon (NPOC) on a Shimadzu TOC-VCPH TOC/TN Analyzer. Island drainage particulate organic matter (POM) concentrations were estimated from TSS concentrations as described in Richardson et al. (in review), and POM molar ratios of C to N  $(\text{C/N})_m$  of POM values were used to estimate PON concentrations. For river samples, we used the previously published relationship between TSS and POC for the Delta from Murrell and Hollibaugh (2000) to calculate PON concentrations. Sample precision and accuracy were generally below 5% for all analyses. Means and standard deviation of geochemical data are presented in the context of water year 2018 (October 2017 to September 2018), a below normal water year which we refer to herein as “dry”. We excluded data for sites where monthly discharge was zero (e.g., May 2018 to September 2018 at SH-P4 and all of SH-P1).

Stable isotope samples ( $\delta^{15}\text{N-NH}_4^+$ ,  $\delta^{15}\text{N-NO}_3^-$ ,  $\delta^{18}\text{O-NO}_3^-$ ,  $\delta^{15}\text{N-PON}$ , and  $\delta^{15}\text{N-DON}$ ) were run at USGS Menlo Park Stable Isotope Facility using the methods described in Kendall et al. (2015). All values are presented in permil notation (‰) relative to Vienna Air (VAIR) for  $\delta^{15}\text{N}$  and Vienna Standard Mean Oceanic Water (VSMOW) for  $\delta^{18}\text{O}$ . Analytical precision for  $\delta^{15}\text{N-NH}_4^+$ ,  $\delta^{15}\text{N-NO}_3^-$ , and  $\delta^{18}\text{O-NO}_3^-$  was 1.1‰, 0.3‰, and 0.7‰, respectively. Analytical precision for  $\delta^{15}\text{N-DON}$  and

PON was 0.4‰.

Statistical analysis of geochemistry data presented in this study was performed using (1) a Kruskal-Wallis One Way Analysis of Variance on Ranks to determine if seasonal values were statistically significantly different, and (2) a coupled pairwise multiple comparisons procedure using Dunn's Method to determine which seasonal values were different from one another.

### 3.2.3 Discharge, mass flux estimates, and net flux estimates

Water discharge from islands was measured or calculated as discussed by Richardson et al. (in review). Briefly, records documenting electrical usage,  $P$  (kW-hr), from each pump station were used together with pump efficiency,  $U$  (kW-hr ac-ft<sup>-1</sup>), to calculate discharge,  $D$  (ac-ft), using the unit-power consumption method where  $D=P/U$  (Diamond & Williamson, 1983; Ogilbee, 1966; Ogilbee & Mitten, 1979). Discharge estimates from TW-P1 on Twitchell Island were cross-checked with 1.5 years of daily flow meter data (AgriFlo XCi ultrasonic sensor). This cross-comparison indicated that the unit-power consumption method is a relatively robust approximation of discharge ( $m=0.87$ ,  $R^2=0.75$ ) that underestimates actual discharge. As such, mass fluxes generated using these discharge estimates herein are considered conservative estimates.

Island drainage mass fluxes off island to Delta waterways are referred to herein as

effluxes or gross fluxes. Island drainage gross fluxes were calculated from monthly concentration and discharge data for each drainage site and summed for islands with more than one drain (Sherman and Staten). All fluxes reported in this study are reported as elemental mass per unit of time. PON fluxes were calculated quarterly, at the same frequency as sample collection. Island drainage mass fluxes were upscaled to Delta-wide contributions based on annual volumetric estimates of drainage discharge from Templin and Cherry (1997). Annual discharge was subsequently broken down into monthly time-steps using monthly flow percentiles calculated from discharge data in this study, where discharge for each month was calculated as a percentage of total annual discharge. Flow percentiles were generated for Sherman Island, a pastureland dominated land use, and Staten Island, a cropland dominated land use, and used to scale the annual discharge to monthly discharge values for these two land-uses in the Delta for subsequent gross flux calculations. Gross mass flux calculations resulted in two estimates: upscaled mass fluxes based on Staten Island (cropland) flow percentiles and geochemistry, and upscaled mass fluxes based on Sherman Island (pastureland) flow percentiles and geochemistry. A spatial analysis of land-use for the Delta indicated that around 82.4% of the region within the legal boundary of the Delta is cropland and 17.6% is pastureland, idle, or grassland. These spatial coverage percentages were used to weight the upscaled fluxes relative to dominant land use in the Delta, and the data presented herein are the weighted average of these two estimates. Up-scaled quarterly PON fluxes from rivers and island drainage were calculated at monthly resolution using the relationship between

TDN and PON flux, which was correlated for both rivers and island drainage (Table S1).

To calculate net fluxes for island drainage, we used a water budget approach to calculate annual water inflow to each island as follows:

$$I = O + ET - P$$

where I is total inflow (or import), including groundwater infiltration and diversions that bring river water onto the island (ac-ft), O is outflow (or export) from island drainage pumps (ac-ft), ET is evapotranspiration (ac-ft), and P is precipitation (ac-ft). Water budget data are provided in Table S2. P was based on measured data from Station 247 for Sherman Island, Station 242 for Staten Island, and Station 140 for Twitchell Island via CIMIS (<https://cimis.water.ca.gov/>). ET was calculated at a monthly scale and summed to annual by correcting monthly reference evapotranspiration rates using crop coefficients for land use cover on each island for both a wet WY (2017) and dry WY (2018) (<http://www.itrc.org/etdata/index.html>). Land use cover on each island was determined using a statewide crop mapping geodatabase available online (<https://data.cnra.ca.gov/dataset/statewide-crop-mapping>). Change in storage was assumed to be negligible on an annual scale. Inflow nutrient and trace metal concentrations were calculated from monthly river geochemistry from all river sites. Inflows for each island were upscaled to Delta-wide

inflow, which was used to calculate Delta-wide river inflow fluxes or “influx”, using inflow to outflow ratios for pastureland dominated islands (Sherman) versus cropland dominated islands (Staten). WY 2017 (Oct-2016 to Sept-2017) and WY 2018 (Oct-2017 to Sept-2018) water inflow to outflow ratios for Staten Island were 0.8 and 2.1, respectively. WY 2017 (Oct-2016 to Sept-2017) and WY 2018 (Oct-2017 to Sept-2018) inflow to outflow ratios for Sherman Island were 2.4 and 3.6, respectively. These net flux estimates are used for comparison to existing box models. All seasonal means and seasonal gross and net fluxes presented in this study are from WY 2018 only and grouped monthly as follows: fall (September through November), winter (December through February), spring (March through May), and summer (June through August).

Monthly dissolved N and P concentrations and monthly-averaged discharge from the Sacramento River at Freeport (USGS 11447650), which is located just upstream of the SRWTP discharge point, San Joaquin River at Vernalis (USGS 11303500), and SRWTP were used for mass flux comparisons to total Delta-wide island drainage fluxes (<https://waterdata.usgs.gov/nwis>). Concentration and flow data for SRWTP fluxes were downloaded via the California Integrated Water Quality System (<https://www.waterboards.ca.gov/ciwqs/>).

### 3.3 Results

#### 3.3.1 Island drainage discharge and geochemistry

Island drainage discharge was highly variable across sites and water years, though seasonal trends were apparent. Discharge was greatest in the winter across all three islands, with 49% and 32% of annual discharge occurring in winter of WY 2017 and WY 2018, respectively (Fig. S2). Cumulative discharge was also greater in wet WY 2017 than dry WY 2018.

Monthly averaged island drainage constituent concentrations showed seasonal trends for many, though not all, constituents as well (Fig. 2). TDN, DON,  $\text{NH}_4^+$ ,  $\text{SiO}_4^{4-}$ , and total dissolved Mn were significantly higher in the winter and spring across all sites compared to the summer ( $p < 0.05$ ), while  $\text{NO}_3^-$  and  $\text{NO}_2^-$  concentrations were more variable, but generally higher in the winter and spring. Island drainage TDN concentrations averaged  $201 \pm 104 \mu\text{M}$  in fall,  $240 \pm 109 \mu\text{M}$  in winter,  $199 \pm 60 \mu\text{M}$  in spring, and  $93 \pm 22 \mu\text{M}$  in summer. A majority of TDN was comprised of DON, and DON concentrations were statistically significantly different across seasons at  $161 \pm 99 \mu\text{M}$ ,  $132 \pm 56 \mu\text{M}$ ,  $115 \pm 42 \mu\text{M}$ , and  $79 \pm 39 \mu\text{M}$ , in fall, winter, spring, and summer, respectively ( $p < 0.05$ ). Relative proportions of DIN and DON shifted seasonally as well, with DIN generally increasing in relative proportion during winter and spring compared to summer and fall.  $\text{NH}_4^+$  concentrations were typically higher than  $\text{NO}_3^-$  and thus a larger proportion of DIN in island drainage, except for some dates on Staten Island where  $\text{NO}_3^-$  concentrations were elevated (Fig. 4). Specifically,

$\text{NH}_4^+$  concentrations averaged  $26 \pm 17 \mu\text{M}$  across all sites in summer months and were notably higher at  $26 \pm 17 \mu\text{M}$  in fall,  $61 \pm 35 \mu\text{M}$  in winter, and  $60 \pm 44 \mu\text{M}$  in spring, respectively ( $p < 0.05$ ).  $\text{NO}_3^-$  concentrations in island drainage averaged  $10 \pm 10 \mu\text{M}$  across all sites in summer months and were significantly higher in winter  $34 \pm 58 \mu\text{M}$  in winter ( $p < 0.05$ ), though other seasons did change measurably with mean concentrations of  $15 \pm 34 \mu\text{M}$  in fall and  $23 \pm 35 \mu\text{M}$  in spring. Island drainage PON concentrations did not show a consistent seasonal pattern and averaged  $210 \pm 70 \mu\text{M}$  in fall,  $120 \pm 61 \mu\text{M}$  in winter,  $156 \pm 74 \mu\text{M}$  spring, and  $180 \pm 58 \mu\text{M}$  in summer.  $\text{PO}_4^{3-}$  concentrations in drainage were variable across sites and through time as well, with concentrations only slightly higher in summer months ( $2.7 \pm 1.2 \mu\text{M}$ ) relative to winter ( $1.6 \pm 0.8 \mu\text{M}$ ).  $\text{SiO}_4^{4-}$  concentrations in island drainage were significantly lower in the summer ( $380 \pm 130 \mu\text{M}$ ) relative to fall, winter, and spring, when means ranged between  $540 \pm 160 \mu\text{M}$  to  $600 \pm 140 \mu\text{M}$  ( $p < 0.05$ ). Total dissolved Mn concentrations were significantly higher during fall ( $670 \pm 210 \mu\text{g L}^{-1}$ ), winter ( $760 \pm 370 \mu\text{g L}^{-1}$ ), and spring ( $1100 \pm 740 \mu\text{g L}^{-1}$ ) compared to summer ( $310 \pm 300 \mu\text{g L}^{-1}$ ) as well ( $p < 0.05$ ). Total dissolved Fe and As concentrations showed no significant seasonal trends with means ranging between  $820 \pm 970 \mu\text{g L}^{-1}$  to  $1550 \pm 1450 \mu\text{g L}^{-1}$  for Fe and  $5.5 \pm 5.0 \mu\text{g L}^{-1}$  to  $6.9 \pm 5.0 \mu\text{g L}^{-1}$  for As across all seasons.

At an annual scale, mean island drainage TDN,  $\text{NH}_4^+$ ,  $\text{NO}_2^-$ , DON, PON, and  $\text{SiO}_4^{4-}$  concentrations for WY 2018 were always greater than surrounding rivers, while  $\text{NO}_3^-$  and  $\text{PO}_4^{3-}$  concentrations were more variable with monthly concentrations both higher

and lower than nearby rivers (Table 1). Mean annual dissolved Mn, Fe, and As concentrations were generally higher in island drainage, by up to two orders of magnitude, relative to river water (Table 1).

$\delta^{15}\text{N}$  values of PON, DON,  $\text{NH}_4^+$ , and  $\text{NO}_3^-$ , and  $\delta^{18}\text{O}$  values of  $\text{NO}_3^-$  indicated clear differences in stable isotope composition amongst N pools that were common to all island drainage sites (Fig. 3). DON and PON pools overlapped in concentration range and N stable isotope composition, ranging from 120 to 150  $\mu\text{M}$  and  $1.2 \pm 0.5\text{‰}$  to  $2.2 \pm 1.6\text{‰}$ , on average, respectively.  $\text{NH}_4^+$  concentrations were similar or lower than organic N pools and had generally higher  $\delta^{15}\text{N}$  values compared to PON and DON that averaged around  $10.3 \pm 1.1\text{‰}$ .  $\text{NO}_3^-$  concentrations and  $\delta^{15}\text{N}\text{-NO}_3^-$  values were generally lower and more variable than the  $\text{NH}_4^+$  pool, with mean values of  $6.7 \pm 3.2\text{‰}$ .

### 3.3.2 Island drainage nutrient and trace metal fluxes

Island specific gross TN and TDN fluxes, which were calculated from monthly concentration and discharge data, ranged between 70 to 230  $\text{kg d}^{-1}$  and 20 to 100  $\text{kg d}^{-1}$  in the summer and between 170 to 320  $\text{kg d}^{-1}$  and 120 to 200  $\text{kg d}^{-1}$  in the winter, respectively (Table 2, Fig. 4). Organic N dominated gross annual island level TN fluxes across all sites and seasons (~77 to 81% of the gross TN flux), while DIN accounted for the remaining ~19 to 23%. Island specific gross total dissolved Mn and Fe fluxes ranged between 10 and 70  $\text{kg d}^{-1}$  and 10 to 110  $\text{kg d}^{-1}$ , respectively (Table 2). Gross total dissolved As fluxes ranged between 0.1 to 0.5  $\text{kg d}^{-1}$  across all sites

and seasons. While many nutrient and trace metal gross fluxes peaked in the winter across all islands, Staten and Twitchell islands also experienced secondary peaks during summer. Island level net drainage fluxes were highest in the winter and spring for TN, TDN,  $\text{NH}_4^+$ , DON, PON, total dissolved As, Mn, and Fe (Table 2). All islands were sinks for TDN in the summer, and Sherman Island was a temporary sink for all dissolved N species in the summer.

Upscaled to annual Delta-wide contributions, we calculated that island drainage contributed a total annual gross TN load of  $2.7 \times 10^6$  kg to Delta waterways in WY 2018. Similar to island specific estimates, this annual TN load was compositionally dominated by organic N (76%), with dissolved inorganic N comprising the remaining ~24% (Fig. 5). The annual total island drainage gross  $\text{SiO}_4^{4-}$  load was estimated to be about  $7.6 \times 10^6$  kg, while the  $\text{PO}_4^{3-}$  load was about  $2.8 \times 10^4$  kg (Table 3). Calculated annual total gross dissolved Mn and Fe loads from all islands were similar in magnitude,  $3.7 \times 10^5$  to  $5.9 \times 10^5$  kg, while total dissolved As contributions were the smallest of all loads and averaged around  $4.4 \times 10^3$  kg annually. Delta-wide net island drainage fluxes (fluxes off the islands corrected for river fluxes onto islands) also resulted in net positive contributions for TN,  $\text{NH}_4^+$ , DON, PON, total dissolved Mn, and total dissolved Fe, while islands acted as sinks for TDN,  $\text{NO}_3^- + \text{NO}_2^-$ ,  $\text{SiO}_4^{4-}$ , and  $\text{PO}_4^{3-}$  and metals during WY 2018 (Table 3).

### 3.4 Discussion

#### 3.4.1 Controls on island drainage nutrient and trace metal composition

##### *Nitrogen*

The multi-species stable isotope data we collected provides new insight into the dominant biogeochemical processes controlling N species concentrations and stable isotope composition in island drainage. The clear distinctions in  $\delta^{15}\text{N}$  values of inorganic and organic N pools in drainage from all islands suggests that N is cycled in a relatively consistent biogeochemical manner across Delta islands (Fig. 3, 5).

Similarity between  $\delta^{15}\text{N}$  values of PON and DON indicates that DON is mainly derived from breakdown of PON. These particulate and organic matter pools mostly originate from soil organic matter as discussed by Richardson et al. (in review), which showed that DOC aromaticity, inferred using  $\text{SUVA}_{254}$  values, is relatively similar in island drainage year-round and that POC is predominantly from soil organic matter based on annual mean molar C:N ratios of POM generally above 10 at these same sites. The enrichment in nearly all  $\delta^{15}\text{N-NH}_4^+$  values relative to  $\delta^{15}\text{N-PON}$  and  $\delta^{15}\text{N-DON}$  values suggests that the stable isotope signature of mineralization of organic N, which would lead to lower  $\delta^{15}\text{N-NH}_4^+$  values relative to its organic source, is overprinted by other biogeochemical processes common to all sites (Nadelhoffer & Fry, 1994). This unexpected increase in  $\delta^{15}\text{N-NH}_4^+$  values relative to organic N pools is best explained by a combination of nitrification, uptake, and volatilization of  $\text{NH}_4^+$ , all of which would lead to losses of  $^{14}\text{NH}_3$  that leave remaining  $\text{NH}_4^+$  enriched in  $^{15}\text{N}$  (Clark, 2015; Ostrom et al., 1998). The  $\text{NH}_4^+$  pool is likely subject to uptake and

volatilization in the unsaturated zone, and the seasonality in  $\text{NH}_4^+$  concentrations across all sites suggests increases in  $\text{NH}_4^+$  concentrations coincide with known winter and spring periods of water table rises. As such, drainage outlets likely receive mineralized  $\text{NH}_4^+$  that is mobilized and transported from shallow stores during winter and spring that was previously subjected to uptake and volatilization during the summer and fall. Under oxic conditions, a portion of  $\text{NH}_4^+$  can also be converted to  $\text{NO}_3^-$  via nitrification. The spatial and temporal variability in  $\text{NO}_3^-$  and  $\text{NO}_2^-$  concentrations along with  $\delta^{15}\text{N-NO}_3^-$  values across all sites suggests that thresholds for this process change irregularly and are not spatially or temporally consistent.

$\delta^{15}\text{N-NO}_3^-$  values were generally low with lower  $\text{NO}_3^-$  concentration relative to the  $\text{NH}_4^+$  pool, which is consistent with partial nitrification of  $\text{NH}_4^+$ . Some of the  $\text{NH}_4^+$  appears to be nitrified locally in the subsurface and/or in the drainage waters under suboxic to oxic conditions, possibly from hot spots and hot moments of  $\text{NO}_3^-$  and  $\text{NO}_2^-$  production (McClain et al., 2003). Additional inorganic N sources external to the system, such as fertilizer, were also evidenced by high  $\delta^{15}\text{N-NO}_3^-$  values in several samples on Staten Island that overlapped or were higher than  $\delta^{15}\text{N-NH}_4^+$  values. The elevated  $\text{NO}_3^-$  concentrations and  $\delta^{15}\text{N-NO}_3^-$  values of these samples show the influence of a N input that is most consistent with a high concentration, partially denitrified fertilizer source (Clark, 2015; Kendall & McDonnell, 2012).

At the individual site level, N species stable isotope values were highly variable, both

spatially and temporally (Table 1). Such variability in individual N species stable isotope values, without context to other N pools, shows that biogeochemical controls and sources are complex at small spatial and temporal scales. However, the clear distinctions among the N pools and stable isotope composition in island drainage as a whole show that there are indeed broad, common links in N cycling across Delta islands.

#### *Silicon and phosphorous*

$\text{SiO}_4^{4-}$  concentrations were seasonally elevated in the fall and winter in island drainage (Fig. 2f) and suggestive of increased groundwater contributions in line with expected water table fluctuations (Richardson et al., in review). This finding is not surprising as  $\text{SiO}_4^{4-}$  concentrations in groundwater are commonly high relative to those in river water due to water-mineral interactions in the subsurface. In contrast, controls on drainage  $\text{PO}_4^{3-}$  concentrations (Fig. 2g) were not clear, although some sites showed increases in the summer which may indicate that most  $\text{PO}_4^{3-}$  is sourced from fertilizer application during the growing season. Phosphorous is subject to complex sorption reactions in the subsurface that can significantly limit mobility, which may account for the generally low drainage  $\text{PO}_4^{3-}$  concentrations year-round (Schoumans, 2013). Studies on fertilizer applications of soluble phosphorous show that over 50% of the added  $\text{PO}_4^{3-}$  is immobilized in under three days (do Nascimento et al., 2018).

### *Trace metals*

We found increased concentrations of total dissolved Mn and Fe in island drainage during winter and spring months (Fig. 2h and i). Mobilization of Fe and Mn in water is commonly associated with redox state, and the observed seasonal increases in total dissolved Fe and Mn concentrations suggest that drainage waters receive contributions from a reduced water source seasonally. This seasonality has been observed for other trace metals in temporarily flooded fields of the Delta, where rewetting periods are thought to mobilize mercury species previously formed in unsaturated soils during dry phases (Marvin-DiPasquale et al., 2014). Regionally, reduction of Fe- and Mn-oxides commonly leads to increases in soluble Fe and Mn species in groundwater (Bennett et al., 2006). However, we found no significant relationship between total dissolved Fe and Mn concentrations across all sites, though site-specific trends were evident at some locations. Interestingly, total dissolved Mn and DOC concentrations were more strongly positively correlated ( $R^2=0.29$ ), while total dissolved Fe and dissolved oxygen concentrations ( $R^2=0.38$ ) along with pH ( $R^2=0.37$ ) were negatively correlated when considering all sites (Fig. 6). This dynamic relationship suggests that controls on total dissolved Mn and organic matter inputs may be broadly related across all islands, which is not surprising given past studies that show organic matter has a high retention capacity for trace metals (Aiken et al., 2011). The strong negative relationship between total dissolved Fe and dissolved oxygen as well as pH, but lack of a relationship between total dissolved Fe and DOC, suggests that redox processes are more important in controlling Fe

solubility in drainage waters. Since island drainage integrates the effects of both solute source contributions and biogeochemical processes that change solubility and speciation, it is hard to assess the attribution of each of these processes without detailed porewater studies. It may be that both Mn and Fe are mobilized via similar processes but that Mn forms complexes with dissolved organic matter prior to transport, while Fe remains as free aquated ions under low oxygen, low pH conditions.

Total dissolved As concentrations in island drainage were more variable than Fe and Mn, with no clear seasonal trends across sites (Fig. 2j). Reduction of As-bearing Fe- and Mn-oxides is the primary mechanism for As contamination of groundwater in the Delta and areas nearby (e.g., Northern San Joaquin Basin) (Bennett & Belitz, 2010; Izbicki et al., 2008). In fact, some of the highest concentrations of acid-extractable As, a measure of As available for desorption from mineral surfaces, in this region are from Delta sediments (Izbicki et al., 2008). Similar to  $\text{PO}_4^{3-}$ , complex sorption reactions affect As mobilization (Herath et al., 2016), and the variability in As concentrations observed across sites in our study is likely a reflection of the complex As biogeochemistry in both the subsurface and surface water of Delta islands.

Broadly, total dissolved As concentrations in drainage were higher under low oxygen conditions aside from a subset of samples collected on Sherman Island (Fig. 6g).

While reductive dissolution reasonably explains As mobilization under low oxygen conditions, this subset of Sherman Island samples may actually represent As

mobilization from a different biogeochemical process. In high pH oxic waters, As can be mobilized via alkali desorption (Herath et al., 2016). Alternatively, it could be that biogeochemical processes overprint the original As source signature too strongly to decipher master controls. Interestingly, drainage waters on Staten Island had mean annual dissolved As concentrations that were almost double the other drainage sites and, at times, exceeded recommended thresholds of total dissolved As set by the EPA ( $>10 \mu\text{g L}^{-1}$ ) and World Health Organization ( $>30 \mu\text{g L}^{-1}$ ). We suspect that these high levels of total dissolved As, which were specific to Staten Island, are related to seasonal flooding of fields that contribute to localized anoxic conditions, as evidenced by past studies showing large  $\text{CH}_4$  fluxes during these times, that allow for release of As via reductive dissolution (Pellerin et al., 2013). Taken together, trace metal geochemistry broadly suggests that island drainage receives water from a seasonally reduced water source, and future work should explicitly sample along possible flow paths to better account for differences in source geochemistry and biogeochemical transformations during transport to drainage ditches.

#### 3.4.2 Island drainage nutrient and trace metal contributions to Delta waterways

By taking both on island and off island fluxes into account, we calculated that Delta islands were net sources of TN, TDN,  $\text{NH}_4^+$ , DON, PON, total dissolved Mn, Fe, and As, while islands acted as sinks for  $\text{NO}_3^- + \text{NO}_2^-$ ,  $\text{SiO}_4^{4-}$ , and  $\text{PO}_4^{3-}$ . This finding complicates many existing nutrient mass balance models in the Delta, which commonly assume island drainage nutrient (most commonly N) inputs are negligible

or net zero (Novick et al., 2015). Calculated mean annual WY 2018 island drainage gross TN fluxes were  $7390 \text{ kg d}^{-1}$  and net TN fluxes were  $4600 \text{ kg d}^{-1}$ , which is similar to some existing model estimates that range from net zero to around  $4500 \text{ kg d}^{-1}$  (Novick et al., 2015; TetraTech, 2006).

Upscaled to Delta-wide contributions, the annual gross and net island drainage TN loads, based on WY 2018 (a dry year), were  $2.7 \times 10^6 \text{ kg}$  and  $1.6 \times 10^6 \text{ kg}$ , respectively. The net annual island drainage TN load for WY 2018 is about 9% of previously reported annual TN loads from the Sacramento River (including SRWTP) and San Joaquin River combined ( $\sim 1.8 \times 10^7 \text{ kg}$ ) (Saleh & Domagalski, 2015). To further examine the relative importance of island drainage TN and  $\text{NH}_4^+$  inputs, we revised three existing box models (“SFEI”, “DSM2”, and “EPA”) described in Novick et al. (2015) to include our new estimates of (1) island drainage TN and  $\text{NH}_4^+$  flux, and (2) river inflow (onto Delta islands) TN and  $\text{NH}_4^+$  flux. We found that gross island drainage contributions could account for ~13% to 17% of annual TN loads into the Delta, while TN loads from river inflow onto islands could account for ~8 to 10% of TN flow out of Delta waters (Table S3). These existing models by Novick et al. (2015) also suggest that the Delta is a sink for  $\text{NH}_4^+$  and TN. We found TN losses of 32 to 34%, which is slightly higher in range than original estimates of 25 to 35% (Novick et al., 2015; TetraTech, 2006) (Table S3). Annual  $\text{NH}_4^+$  losses in the Delta ranged from 65 to 88% and were similar to past estimates of 65 to 85%. These revisions to existing box models to include island drainage, which is both a net source

of TN and  $\text{NH}_4^+$ , suggest that the Delta is an even larger sink for TN (about  $3.7 \times 10^3$  kg to  $1.6 \times 10^6$  kg more) and  $\text{NH}_4^+$  (about  $2.2 \times 10^5$  kg more) than previous studies suggest.

In contrast, Delta islands were a net sink for  $\text{PO}_4^{3-}$  during WY 2018 (Table 3). The annual gross  $\text{PO}_4^{3-}$  load in drainage waters pumped off of the islands was  $2.8 \times 10^4$  kg, which is similar to the value of about  $5.1 \times 10^4$  kg previously estimated by TetraTech (2006). This export was negated by the larger import of  $\text{PO}_4^{3-}$  onto islands through, which resulted in islands being a net sink for  $\text{PO}_4^{3-}$  to the order of  $-2.8 \times 10^4$  kg annually.

To our knowledge, no studies currently exist comprehensively documenting trace metal inputs to the Delta, but the data used in this study can be a first step towards accounting for select trace metals in larger scale inventories of exports to the Delta and downstream San Francisco Bay. We calculated that Delta islands are annually a net source of Mn ( $3.4 \times 10^5$  kg), Fe ( $5.2 \times 10^5$  kg), and As ( $2.6 \times 10^3$  kg) to the larger Delta environment (Table 3). A majority of these loads likely precipitate in the Delta's oxic river waters and are deposited in the sediments. Similar to concerns about methylmercury in the Delta, resuspension of sediments via dredging or other physicochemical processes (pH changes) could remobilize metals deposited from island drainage for downstream transport with ultimate fate depending on concentrations and speciation (Shipley et al., 2011).

A large fraction of the previously discussed nutrient and trace metal exports from Delta islands occurred in the winter and spring, due to increases in both concentration and discharge (Fig. 2, Fig. S2). Seasonality in the delivery of island drainage nutrients and trace metals to Delta waters has important implications for mass flux and net flux comparisons. For example, nearly 62% and 71% of the annual upscaled gross TN and TDN load, respectively, was delivered in winter and spring of WY 2018 (Table 4). Island drainage effluxes and river influxes of nutrient and trace metals also likely shift inter-annually due to differences in island and Delta hydrology. Inflow to outflow ratios at the island level were highly variable across islands and water years (Table S2). In fact, using river inflow ratios from WY 2017 to partition upscaled inflow fluxes decreased the amount of TN imported onto Delta islands from 2880 kg d<sup>-1</sup> in WY 2018 to 1330 kg d<sup>-1</sup> in WY 2017. These changes in inflow fluxes have consequences for net flux calculations. Even if drainage concentrations were similar to WY 2018, a below normal water year, island drainage during WY 2017 would export 1.3 times more net TN than WY 2018 from increases in discharge relative to inflow. Preliminary estimates of net TN fluxes from island drainage under the wet WY 2017 conditions (6060 kg d<sup>-1</sup>) were measurably higher than WY 2018 (4510 kg d<sup>-1</sup>). Additionally inflow geochemistry may change substantially in concentration year-to-year, and even slight changes could impact upscaled inflow fluxes onto Delta islands.

Richardson et al. (in review) showed that wet water years see greater mass fluxes of

carbon from island drainage, and these results likely scale to N. While gross nutrient and trace metal fluxes off the island, and thus net fluxes would likely be greater during a wet year, their contribution to nearby waterways may decrease in importance relative to other major inflows which have much larger contributions during wet years from increases in event flow, as seen for carbon exports from Delta islands based on Richardson et al. (in review). Future work must consider the importance of water year variability when estimating the relative contributions of different nutrient sources internal and external to the Delta.

#### 3.4.3 Importance of island drainage nutrient contributions under a pre- and post-upgrade SRWTP scenario

To better understand the potential significance of island drainage nutrient contributions in the context of the larger Delta environment under a pre-upgrade scenario, we compared island drainage dissolved N and P contributions to other major inflows (Sacramento and San Joaquin rivers) to the Delta along with contributions for SRWTP for WY 2018. Mean annual net island drainage TDN,  $\text{NH}_4^+$ ,  $\text{NO}_3^- + \text{NO}_2^-$ , and  $\text{PO}_4^{3-}$  contributions were 5, 4, 0, and -4% of total inputs pre-upgrade, respectively (Table 4). During WY 2018, SRWTP  $\text{NH}_4^+$  contributions were almost 90% of all  $\text{NH}_4^+$  inputs, and this mass flux percentage was nearly identical to past estimates by Jassby (2008). Seasonally, island drainage contributed around 7% of TDN, 8% of  $\text{NH}_4^+$ , -1% of  $\text{NO}_3^- + \text{NO}_2^-$ , and -5% of  $\text{PO}_4^{3-}$  in winter months under pre-upgrade conditions (Fig. 7a-d). In the summer and fall, island drainage net contributions

ranged between 0 to 7% of TDN, 0 to 1% of  $\text{NH}_4^+$ , -6 to 1% of  $\text{NO}_3^- + \text{NO}_2^-$ , and -3 to -2% of  $\text{PO}_4^{3-}$  under pre-upgrade conditions. While these mass balance comparisons leave out other smaller inflows, the general agreements between estimates from this baseline comparison and more comprehensive models examined above suggest that island drainage is seasonally a measurable N source, at least during dry years similar to 2018.

Predicted effluent  $\text{NO}_3^- + \text{NO}_2^-$ ,  $\text{NH}_4^+$ ,  $\text{PO}_4^{3-}$ , and TDN concentrations for SRWTP, once upgraded to tertiary treatment with biological nutrient removal (i.e., nitrification and denitrification), were used to forecast possible changes in dominant N and P sources to and within the Delta under a post-upgrade SRWTP scenario. Post-upgrade, island drainage, taken as a net annual load, comprised 46% of the  $\text{NH}_4^+$ , 0% of the  $\text{NO}_3^- + \text{NO}_2^-$ , and 8% of the TDN delivered to and within the Delta relative to inputs from major inflows and SRWTP. Because SRWTP does not anticipate changes to its  $\text{PO}_4^{3-}$  loads, net island drainage  $\text{PO}_4^{3-}$  contributions remained the same, around -4%, under pre- and post-upgrade scenarios. Seasonal percentages for winter island drainage net N contributions, from pre- to post-upgrade, shifted from 7 to 11% for TDN, and 8 to 60% for  $\text{NH}_4^+$ , while  $\text{NO}_3^- + \text{NO}_2^-$  contributions remained around -1% (Fig. 7). While overall  $\text{NH}_4^+$  inputs to the Delta will be reduced as SRWTP transitions to be a more advanced treatment plant, most  $\text{NH}_4^+$  in the Delta will likely be sourced from island drainage. Importantly, a majority of island drainage N delivery to Delta waterways will occur seasonally, in the winter and spring, when carbon and trace

metal contributions from drainage are similarly elevated (Richardson et al., in review) (Fig. 7). Though  $\text{NO}_3^-$  will likely dominate external inorganic loads to the Delta post-upgrade, the seasonal delivery of N from island drainage may be locally relevant. The spatially diffuse locations of drainage outfalls may mean that these seasonal loads are delivered to regions of the Delta with long residence times that allow for extended biogeochemical processing and incorporation into the food web.

#### 3.4.4 Future recommendations

This study is an important first step towards better constraining and evaluating the importance of island drainage nutrient contributions to the Delta, but future work needs to address issues relating to scale – both in space and time. High-frequency monitoring of drainage outlets – including discharge constituent concentrations, and related ancillary water quality parameters such as dissolved oxygen and pH – would allow for better resolution of shifting nutrient concentrations in island drainage. Similar recent work, enabled by deployment of high-frequency sensor networks, shows nutrient dynamics change at timescales of hours, days, and weeks in the Delta (Downing et al., 2017; Kraus et al., 2017), and we suspect a similar high-frequency dataset for multiple island drainage sites would help resolve some of the variability seen in this study and companion work by Richardson et al. (in review). Such monitoring would also generate more refined and accurate load estimates both within and across water years. Coupled physicochemical instrumentation (e.g., water level, chemical sensors) of island groundwater and drainage waters would allow for more

explicit source tracking and a better understanding of biogeochemical transformations as they occur from initial diversion or infiltration to final discharge. Our use of stable isotope tracers provided new and valuable insight into N cycling on Delta islands and a similar application of isotopic tracers would likely be useful in conjunction with the aforementioned suggested monitoring programs for better insight into N sources and transformations.

Beyond nutrients, work on contaminants in the Delta suggests farmed Delta islands may also be a source of a number of ecologically consequential pesticides, herbicides, and fungicides, transported in dissolved forms and/or sorbed on soil particulates (De Parsia et al., 2019; Kuivila & Hladik, 2008; Weston et al., 2019). While challenging, new studies should directly investigate the possibility of delivery of these contaminants via island drains in the Delta. Current-use pesticides and related toxicants delivered with island drainage may be a missing driver of change in this system, especially given recent findings that show particulate loads from drains are commonly soil-derived and can be seasonally large relative to other major inflows (Richardson et al., in review).

Finally, this study and past work show that Delta islands are spatially heterogenous, both within islands and across islands. This has been seen in studies of (1) gas fluxes, which can be remarkably variable across identical land use types on multiple Delta islands (Hemes et al., 2019), and (2) aqueous fluxes of carbon, nutrients, and trace

metals, with clear site-to-site variability in concentrations as shown in this study and Richardson et al. (in review). Controls on this spatial heterogeneity, which affects system wide assessments of gaseous, aqueous, and particulate fluxes, need to be better resolved for more accurate upscaling of gross and net fluxes.

### **3.5 Summary**

We estimated island specific and upscaled Delta-wide fluxes using monthly nutrient (PON, DON,  $\text{NO}_3^- + \text{NO}_2^-$ ,  $\text{NH}_4^+$ ,  $\text{PO}_4^{3-}$ ,  $\text{SiO}_4^{4-}$ ) and trace metal (total dissolved Fe, Mn, and As) concentrations along with discharge data from three Delta islands. Annual Delta-wide island drainage gross TN contributions were almost 1/6 of previously reported TN loads to the system and totaled  $2.7 \times 10^6$  kg. Island drainage waters were net sources of TN, TDN,  $\text{NH}_4^+$ , DON, PON, total dissolved Mn, Fe, and As, while islands acted as sinks for  $\text{NO}_3^- + \text{NO}_2^-$ ,  $\text{SiO}_4^{4-}$ , and  $\text{PO}_4^{3-}$ . Island drainage net TN and TDN exports were  $1.7 \times 10^6$  and  $6.2 \times 10^5$  kg, respectively. Our results complicate existing nutrient budgets in the Delta, which commonly assume N inputs from island drainage are negligible or net zero, and provide new information on understudied trace metal inputs to the Delta.

We compared a subset of the Delta-wide drainage fluxes with available data for other regionally significant N and P sources to better understand the regional importance of island drainage mass fluxes. Under a post-upgrade scenario, annual island drainage

net TDN and  $\text{NH}_4^+$  loads to the Delta, relative to inputs from the San Joaquin River, the Sacramento River, and SRWTP, increased from 5 to 8% and 4 to 46% based on data from WY 2018 (a dry water year), respectively. Both pre- and post-upgrade  $\text{NO}_3^- + \text{NO}_2^-$  and  $\text{PO}_4^{3-}$  percent contributions from island drainage relative to other major sources were similar, suggesting that the approaching SRWTP upgrade, which will ultimately reduce total N loads while maintaining similar P loads to the Delta, will also shift dominant sources of N species in different ways. Of these sources, island drainage will likely become the dominant source of  $\text{NH}_4^+$ , at least during dry water years, and island drainage net TDN inputs will also be similar in magnitude to post-upgrade TDN inputs from SRWTP for most of the year (fall through spring). This work shows that island drainage is a measurable source of nutrients and trace metals during dry water years and highlights the importance of accounting for temporal variability in existing nutrient budgets. Our understanding of dominant nutrient sources in the Delta may be biased without further consideration of mass fluxes as they relate to seasonal, annual, and interannual time scales in a system with direct water year dependence that is projected to become even more variable in the coming years.

## **Acknowledgements**

We thank Rick Carter, Joel McElroy, and the Nature Conservancy for their assistance in accessing sampling locations, and the California Department of Water Resources, including Juan Mercado and David Mraz, for helping arrange access to sampling locations. We thank Kaylee Glenney, Carolyn Brady, and Rob Franks for their help in the Marine Analytical Lab. This research was supported by grants from the International Association of Geochemistry and the J. Casey Moore Award. Additional support for C. Richardson was provided by the National Science Foundation Graduate Research Fellowship Program (DGE-1329626), and J. Fackrell received support from the California Sea Grant Delta Fellowship (R/SF-84).

## References

- Aiken, G. R., Hsu-Kim, H., & Ryan, J. N. (2011). Influence of dissolved organic matter on the environmental fate of metals, nanoparticles, and colloids. *Environmental Science and Technology*.
- Alpers, C. N., Fleck, J. A., Marvin-DiPasquale, M., Stricker, C. A., Stephenson, M., & Taylor, H. E. (2014). Mercury cycling in agricultural and managed wetlands, Yolo Bypass, California: Spatial and seasonal variations in water quality. *Science of the Total Environment*, 484, 276-287.
- Bachand, P. A., Bachand, S. M., Kraus, T. E., Stern, D., Liang, Y. L., & Horwath, W. R. (2019). Sequestration and Transformation in Chemically Enhanced Treatment Wetlands: DOC, DBPPs, and Nutrients. *Journal of Environmental Engineering*, 145(8), 04019044.
- Bennett, G. L., & Belitz, K. (2010). Groundwater quality in the Northern San Joaquin Valley, California. *U.S. Geological Survey Fact Sheet 2010-3079*, 4 p.
- Bennett, G. L., Belitz, K., & Milby Dawson, B. J. (2006). California GAMA Program—Ground-water quality data in the Northern San Joaquin Basin study unit. *U.S. Geological Survey Data Series 196*, 122 p.
- Bricker, S., Clement, C., Pirhalla, D., Orlando, S., & Farrow, D. (1999). National estuarine eutrophication assessment: effects of nutrient enrichment in the nation's estuaries. NOAA, National Ocean Service, Centers for Coastal Ocean Science, Silver Spring, MD.
- CDWR. (1995). California Department of Water Resources. Sacramento-San Joaquin Delta Atlas: State of California, 121 p.
- Clark, I. (2015). *Groundwater geochemistry and isotopes*: CRC press.
- Cloern, J. E. (2019). Patterns, pace, and processes of water-quality variability in a long-studied estuary. *Limnology and Oceanography*, 64(S1), S192-S208.
- Cooke, J., Joab., C., & Lu, Z. (2018). Delta Nutrient Research Plan. Report by California Regional Water Quality Control Board, Central, 50 pp.
- Dahm, C., Parker, A., Adelson, A., Christman, M., & Bergamaschi, B. (2016). Nutrient dynamics of the Delta: effects on primary producers. *San Francisco Estuary and Watershed Science*, 14(4).
- De Parsia, M., Woodward, E. E., Orlando, J. L., & Hladik, M. L. (2019). *Pesticide Mixtures in the Sacramento–San Joaquin Delta, 2016–17: Results from Year*

*2 of the Delta Regional Monitoring Program (2327-638X).*

- Deverel, S. J., & Leighton, D. A. (2010). Historic, recent, and future subsidence, Sacramento-San Joaquin Delta, California, USA. *San Francisco Estuary and Watershed Science*, 8(2).
- Diamond, J., & Williamson, A. (1983). A summary of ground-water pumpage in the Central Valley of California. 1961-1977: U.S. Geological Survey Water-Resources Investigations Report 83-4037, 70 p.
- do Nascimento, C. A., Pagliari, P. H., Faria, L. d. A., & Vitti, G. C. (2018). Phosphorus mobility and behavior in soils treated with calcium, ammonium, and magnesium phosphates. *Soil Science Society of America Journal*, 82(3), 622-631.
- Downing, B. D., Bergamaschi, B. A., & Kraus, T. E. C. (2017). Synthesis of data from high-frequency nutrient and associated biogeochemical monitoring for the Sacramento–San Joaquin Delta, northern California: U.S. Geological Survey Scientific Investigations Report 2017–5066, 28 p.
- Du Laing, G., Rinklebe, J., Vandecasteele, B., Meers, E., & Tack, F. M. (2009). Trace metal behaviour in estuarine and riverine floodplain soils and sediments: a review. *Science of the Total Environment*, 407(13), 3972-3985.
- Dugdale, R., Wilkerson, F., & Parker, A. E. (2015). The “Ammonium Paradox”: A Summary of More than a Decade of Research into Phytoplankton Processes and Nitrogen Relationships in the Northern San Francisco Estuary. Suisun Synthesis II Report Section 2. Prepared for the San Francisco Bay Nutrient Management Strategy.
- Fregoso, T. A., Wang, R.-F., Alteljevich, E., & Jaffe, B. E. (2017). San Francisco Bay-Delta bathymetric/topographic digital elevation model (DEM): U.S. Geological Survey data release, <https://doi.org/10.5066/F7GH9G27>.
- Hemes, K. S., Chamberlain, S. D., Eichelmann, E., Anthony, T., Valach, A., Kasak, K., et al. (2019). Assessing the carbon and climate benefit of restoring degraded agricultural peat soils to managed wetlands. *Agricultural Forest Meteorology*, 268, 202-214.
- Herath, I., Vithanage, M., Bundschuh, J., Maity, J. P., & Bhattacharya, P. (2016). Natural arsenic in global groundwaters: distribution and geochemical triggers for mobilization. *Current Pollution Reports*, 2(1), 68-89.

- Howarth, R., Chan, F., Conley, D. J., Garnier, J., Doney, S. C., Marino, R., & Billen, G. (2011). Coupled biogeochemical cycles: eutrophication and hypoxia in temperate estuaries and coastal marine ecosystems. *Frontiers in Ecology and the Environment*, 9(1), 18-26.
- Izbicki, J. A., Stamos, C., Metzger, L. F., Kulp, T., McPherson, K. R., Halford, K., & Bennett, G. L. (2008). Sources, distribution, and management of arsenic in water from wells, Eastern San Joaquin ground-water subbasin, California. *U.S. Geological Survey Open-File Report 2008-1272*, 8 p.
- Jassby, A. D. (2008). Phytoplankton in the upper San Francisco Estuary: recent biomass trends, their causes, and their trophic significance. *San Francisco Estuary and Watershed Science*, 6(1).
- Jassby, A. D., & Cloern, J. E. (2000). Organic matter sources and rehabilitation of the Sacramento–San Joaquin Delta (California, USA). *Aquatic Conservation: Marine and Freshwater Ecosystems*, 10(5), 323-352.
- Jassby, A. D., Cloern, J. E., & Cole, B. E. (2002). Annual primary production: Patterns and mechanisms of change in a nutrient-rich tidal ecosystem. *Limnology and Oceanography*, 47(3), 698-712.
- Kendall, C., & McDonnell, J. J. (2012). *Isotope Tracers in Catchment Hydrology*: Elsevier.
- Kraus, T., Carpenter, K., Bergamaschi, B., Parker, A., Stumpner, E., Downing, B. D., et al. (2017). A river-scale Lagrangian experiment examining controls on phytoplankton dynamics in the presence and absence of treated wastewater effluent high in ammonium. *Limnology and Oceanography*, 62(3), 1234-1253.
- Kraus, T. E., Bergamaschi, B., & Downing, B. D. (2017). *An introduction to high-frequency nutrient and biogeochemical monitoring for the Sacramento–San Joaquin Delta, northern California* (2328-0328).
- Kraus, T. E., O'Donnell, K., Downing, B. D., Burau, J. R., & Bergamaschi, B. (2017). Using paired in situ high frequency nitrate measurements to better understand controls on nitrate concentrations and estimate nitrification rates in a wastewater-impacted river. *Water Resources Research*, 53(10), 8423-8442.
- Kuivila, K., & Hladik, M. (2008). Understanding the occurrence and transport of current-use pesticides in the San Francisco estuary watershed. *San Francisco Estuary and Watershed Science*, 6(3).

- Limpens, J., Berendse, F., Blodau, C., Canadell, J., Freeman, C., Holden, J., et al. (2008). Peatlands and the carbon cycle: from local processes to global implications—a synthesis. *Biogeosciences*, 5(5), 1475-1491.
- Luoma, S. N., & Rainbow, P. S. (2008). *Metal contamination in aquatic environments: science and lateral management*: Cambridge University Press.
- LWA. (2014). (Larry Walker Associates). EchoWater Project EIR Water Quality Tech Memo. [https://www.regionalsan.com/sites/main/files/file-attachments/echowater\\_deir\\_app\\_a-d\\_0.pdf](https://www.regionalsan.com/sites/main/files/file-attachments/echowater_deir_app_a-d_0.pdf)
- Marvin-DiPasquale, M., Windham-Myers, L., Agee, J. L., Kakouros, E., Kieu, L. H., Fleck, J. A., et al. (2014). Methylmercury production in sediment from agricultural and non-agricultural wetlands in the Yolo Bypass, California, USA. *Science of the Total Environment*, 484, 288-299.
- McClain, M. E., Boyer, E. W., Dent, C. L., Gergel, S. E., Grimm, N. B., Groffman, P. M., et al. (2003). Biogeochemical hot spots and hot moments at the interface of terrestrial and aquatic ecosystems. *Ecosystems*, 301-312.
- Murrell, M., & Hollibaugh, J. (2000). Distribution and composition of dissolved and particulate organic carbon in northern San Francisco Bay during low flow conditions. *Estuarine, Coastal Shelf Science*, 51(1), 75-90.
- Nadelhoffer, K. J., & Fry, B. (1994). Nitrogen isotope studies in forest ecosystems. In: Lajtha, K., Michner, R. Eds. , *Stable Isotopes in Ecology and Environmental Science.*, pp. 22–45.
- Novick, E., Holleman, R., Jabusch, T., Sun, J., Trowbridge, P., Senn, D., et al. (2015). Characterizing and quantifying nutrient sources, sinks and transformations in the Delta: synthesis, modeling, and recommendations for monitoring.
- Ogilbee, W. (1966). Progress report Methods for estimating ground-water withdrawals in Madera County, California: U.S. Geological Survey open-file report, 42. p.
- Ogilbee, W., & Mitten, H. (1979). A continuing program for estimating ground-water pumpage in California--Methods: U.S. Geological Survey open-file report, 22 p.
- Ostrom, N. E., Knoke, K. E., Hedin, L. O., Robertson, G. P., & Smucker, A. J. (1998). Temporal trends in nitrogen isotope values of nitrate leaching from an agricultural soil. *Chemical Geology*, 146(3-4), 219-227.

- Paerl, H. W., Pinckney, J. L., Fear, J. M., & Peierls, B. L. (1998). Ecosystem responses to internal and watershed organic matter loading: consequences for hypoxia in the eutrophying Neuse River Estuary, North Carolina, USA. *Marine Ecology Progress Series*, 166, 17-25.
- Paerl, H. W., Valdes, L. M., Peierls, B. L., Adolf, J. E., & Harding, L. J. (2006). Anthropogenic and climatic influences on the eutrophication of large estuarine ecosystems. *Limnology and Oceanography*, 51(1part2), 448-462.
- Pellerin, B., Anderson, F., & Bergamaschi, B. (2013). Assessing the role of winter flooding on baseline greenhouse gas fluxes from corn fields in the Sacramento-San Joaquin Bay Delta. *Energy Research and Development Division, Final Project Report. A report prepared for the California Energy Commission.*
- Richardson, C., Fackrell, J., Kendall, C., Kraus, T., Young, M., & Paytan, A. (in review). Lateral carbon exports from drained peatlands: an understudied carbon loss pathway in the Sacramento-San Joaquin Delta, California. *Submitted to JGR Biogeochemistry.*
- Saleh, D., & Domagalski, J. (2015). SPARROW modeling of nitrogen sources and transport in rivers and streams of California and adjacent states, US. *Journal of the American Water Resources Association*, 51(6), 1487-1507.
- Schoumans, O. F. (2013). Description of the phosphorus sorption and desorption processes in lowland peaty clay soils. *Soil Science*, 178(6), 291-300.
- Seitzinger, S., & Sanders, R. (1997). Contribution of dissolved organic nitrogen from rivers to estuarine eutrophication. *Marine Ecology Progress Series*, 159, 1-12.
- Senn, D., & Novick, E. (2014). Suisun Bay Ammonium Synthesis Report. San Francisco Estuary Institute.
- Shiple, H. J., Gao, Y., Kan, A. T., & Tomson, M. B. J. J. o. e. q. (2011). Mobilization of trace metals and inorganic compounds during resuspension of anoxic sediments from Trepangier Bayou, Louisiana. 40(2), 484-491.
- Siegfried, L. J., Fleenor, W. E., & Lund, J. R. (2014). Physically Based Modeling of Delta Island Consumptive Use: Fabian Tract and Staten Island, California. *San Francisco Estuary and Watershed Science*, 12(4).
- Sommer, T., Armor, C., Baxter, R., Breuer, R., Brown, L., Chotkowski, M., et al. (2007). The collapse of pelagic fishes in the upper San Francisco Estuary: El colapso de los peces pelagicos en la cabecera del Estuario San Francisco. *Fisheries*, 32(6), 270-277.

- Stumpner, E. B., Bergamaschi, B. A., Kraus, T. E., Parker, A. E., Wilkerson, F. P., Downing, B. D., et al. (2020). Spatial variability of phytoplankton in a shallow tidal freshwater system reveals complex controls on abundance and community structure. *Science of the Total Environment*, 700, 134392.
- Stumpner, E. B., Kraus, T. E., Fleck, J. A., Hansen, A. M., Bachand, S. M., Horwath, W. R., et al. (2015). *Mercury, monomethyl mercury, and dissolved organic carbon concentrations in surface water entering and exiting constructed wetlands treated with metal-based coagulants, Twitchell Island, California (2327-638X)*. Retrieved from
- Ta, J., Anderson, L. W., Christman, M. A., Khanna, S., Kratville, D., Madsen, J. D., et al. (2017). Invasive aquatic vegetation management in the Sacramento–San Joaquin River Delta: status and recommendations. *San Francisco Estuary and Watershed Science*, 15(4).
- Templin, W. E., & Cherry, D. E. (1997). Drainage-return, surface-water withdrawal, and land-use data for the Sacramento-San Joaquin Delta, with emphasis on Twitchell Island, California; U.S. Geological Survey Open-file Report 97-350, 31 p.
- TetraTech. (2006). Conceptual Model for Nutrients in the Central Valley and Sacramento-San Joaquin Delta. A technical report prepared for the U.S. Environmental Protection Agency and the Central Valley Drinking Water Public Policy Workgroup.
- Ward, A. K., & Paerl, H. W. (2016). Delta Nutrients Forms and Ratios Public Workshop: "Role of Nutrients in Shifts in Phytoplankton Abundance and Species Composition in the Sacramento-San Joaquin Delta" November 29-30, 2016 Sacramento, CA.
- Weston, D. P., Moschet, C., Young, T. M., Johanif, N., Poynton, H. C., Major, K. M., et al. (2019). Chemical and Toxicological Effects on Cache Slough after Storm-Driven Contaminant Inputs. *San Francisco Estuary and Watershed Science*, 17(3).
- Winder, M., & Jassby, A. (2011). Shifts in zooplankton community structure: implications for food web processes in the upper San Francisco Estuary. *Estuaries and Coasts*, 34(4), 675-690.
- Yabusaki, S. B., Wilkins, M. J., Fang, Y., Williams, K. H., Arora, B., Bargar, J., et al. (2017). Water table dynamics and biogeochemical cycling in a shallow, variably-saturated floodplain. *Environmental Science and Technology*, 51(6), 3307-3317.

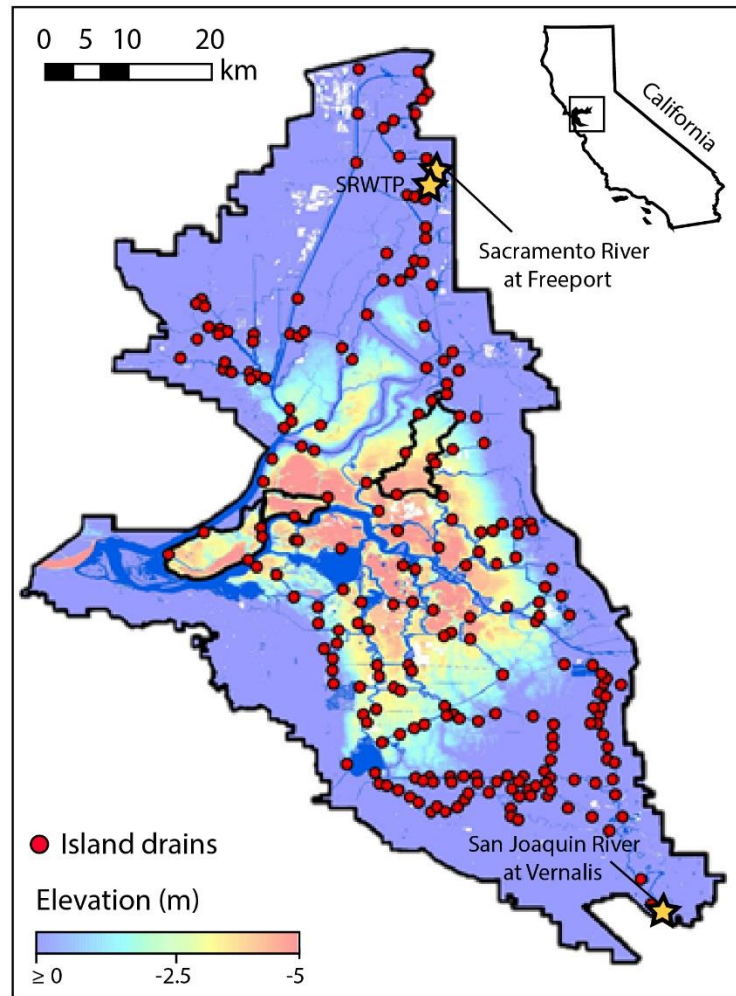


**Figure 3-1. Overview of the Delta and study islands.**

Overview of the Sacramento-San Joaquin Delta with a digital elevation model from Fregoso et al. (2017). The three islands sampled in this study are outlined in black, and island drain locations for the entire Delta are shown as red circles based on a digitized map from CDWR (1995). The Sacramento Regional Wastewater Treatment Plant (SRWTP) effluent location as well as Sacramento River at Freeport (USGS station 11447650) and San Joaquin River at Vernalis (USGS station 11303500) are also shown for reference.

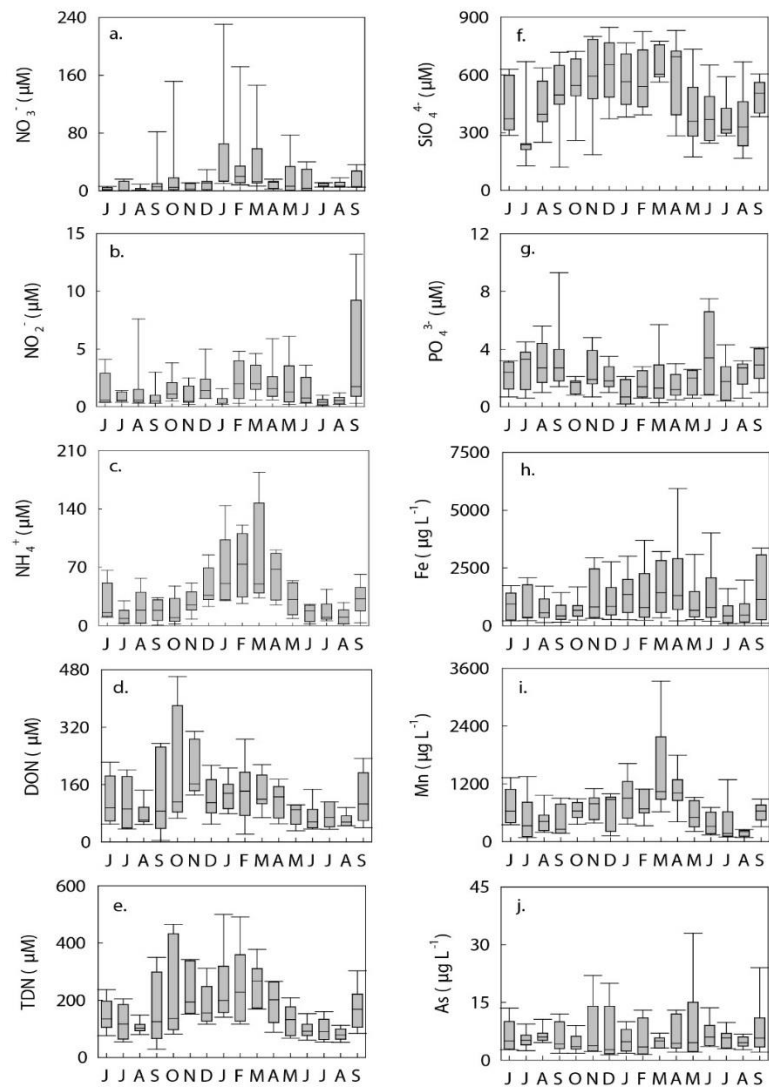


**Figure 3-2. Box plots of monthly island drainage nutrient and trace metal concentrations.**

Box plots of monthly island drainage concentrations for (a) nitrate [ $\text{NO}_3^-$ ] (b) nitrite [ $\text{NO}_2^-$ ], (c) ammonium [ $\text{NH}_4^+$ ], (d) dissolved organic N [DON], (e) total dissolved N [TDN], (f) silica [ $\text{SiO}_4^{4-}$ ], (g) phosphate [ $\text{PO}_4^{3-}$ ], (h) total dissolved Fe, (i) total dissolved Mn, and (j) total dissolved As.

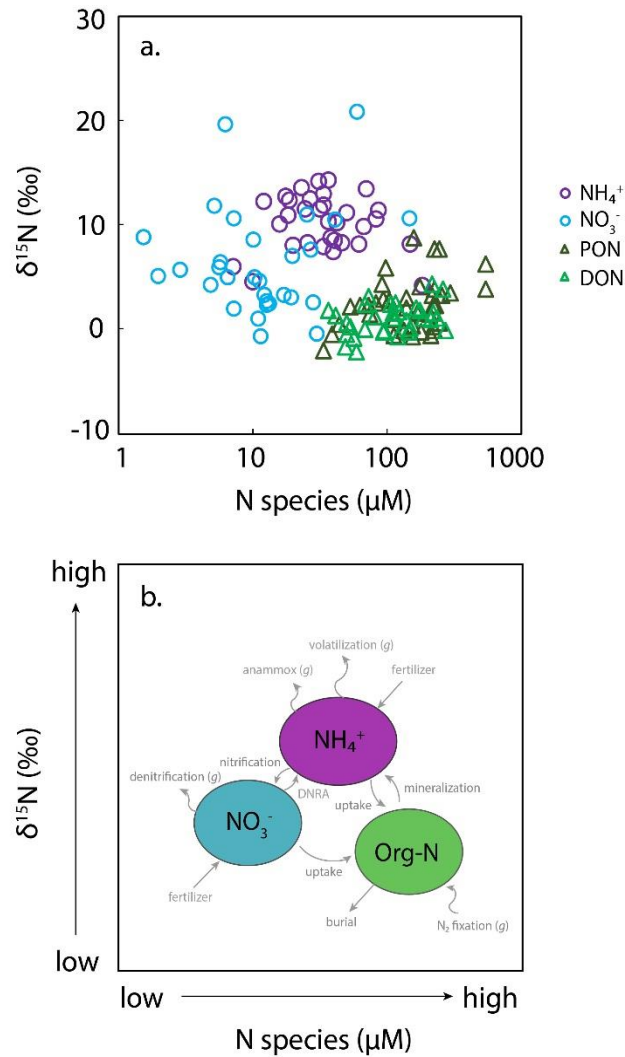


**Figure 3-3. Nitrogen stable isotope values for island drainage.**

(a)  $\delta^{15}\text{N}$  values versus N species concentration for ammonium [ $\text{NH}_4^+$ ] (purple), nitrate [ $\text{NO}_3^-$ ] (blue), PON (dark green), and DON (light green). Circular markers represent inorganic N pools and triangular markers represent organic N pools. (b) Conceptual model of relationship between  $\delta^{15}\text{N}$  values and concentration for major dissolved and particulate N pools on Delta islands. DNRA represents dissimilatory nitrate reduction to ammonium. Grey arrows are qualitative and do not refer to the direction of concentration or  $\delta^{15}\text{N}$  change. Double curved arrows represent conversions to or from various gaseous (g) N forms.

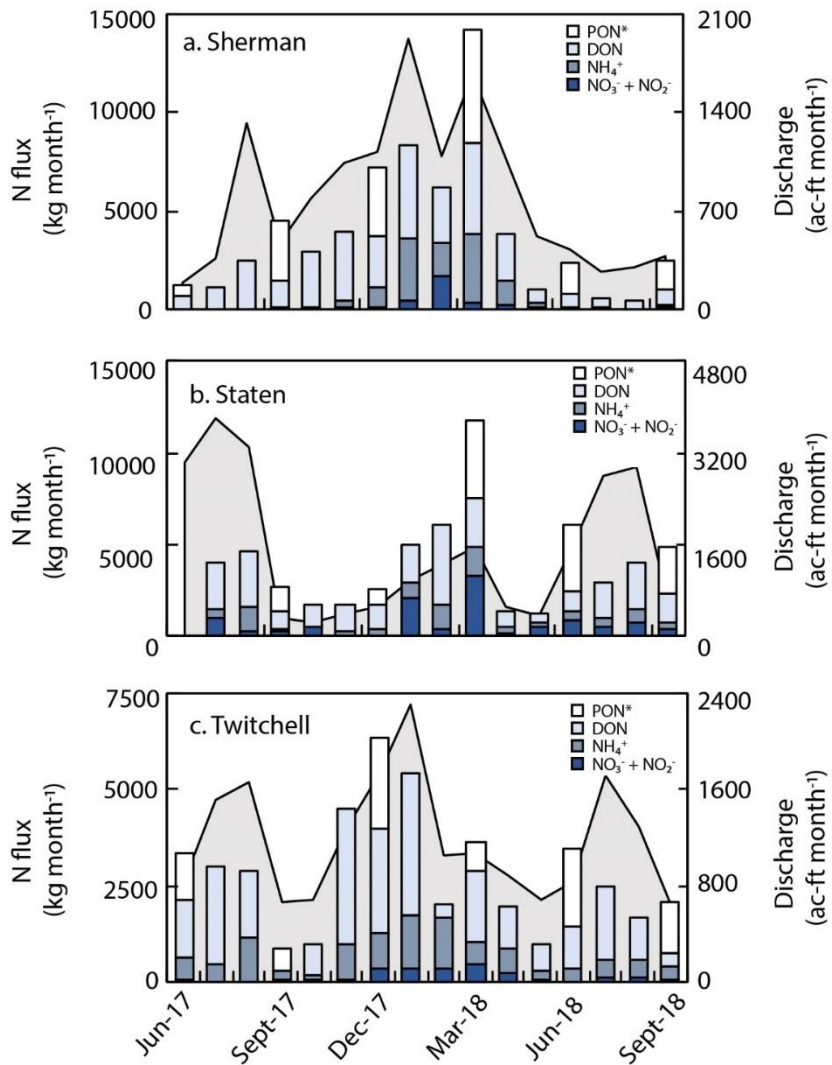


**Figure 3-4. Monthly nitrogen fluxes from each island.**

Monthly gross island drainage nitrogen (N) efflux (bars) and discharge (black line) for (a) Sherman, (b) Staten, and (c) Twitchell islands. Bar color refers to N species (nitrate plus nitrite [ $\text{NO}_3^- + \text{NO}_2^-$ ], ammonium [ $\text{NH}_4^+$ ], dissolved organic nitrogen [PON], particulate organic N [PON]) and asterisk is to indicate that PON data is only available quarterly.

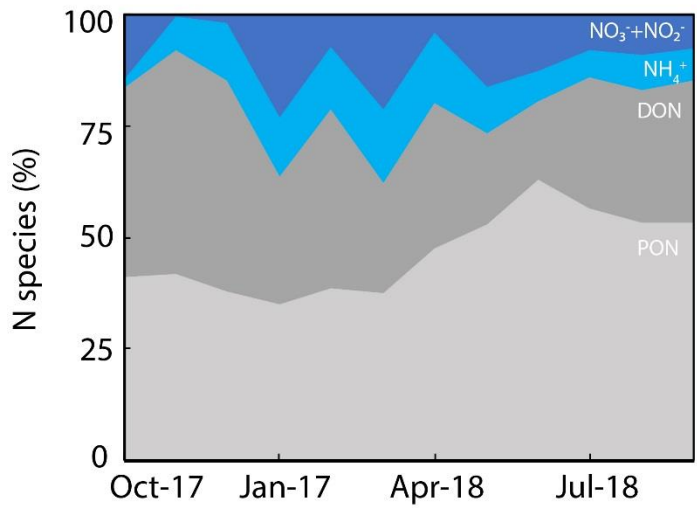


**Figure 3-5. Breakdown of N species comprising total N in island drainage.**

Relative proportion of N species as a percentage of the mean upscaled total nitrogen (TN) flux in Delta island drainage waters (see text for details) for WY 2018.

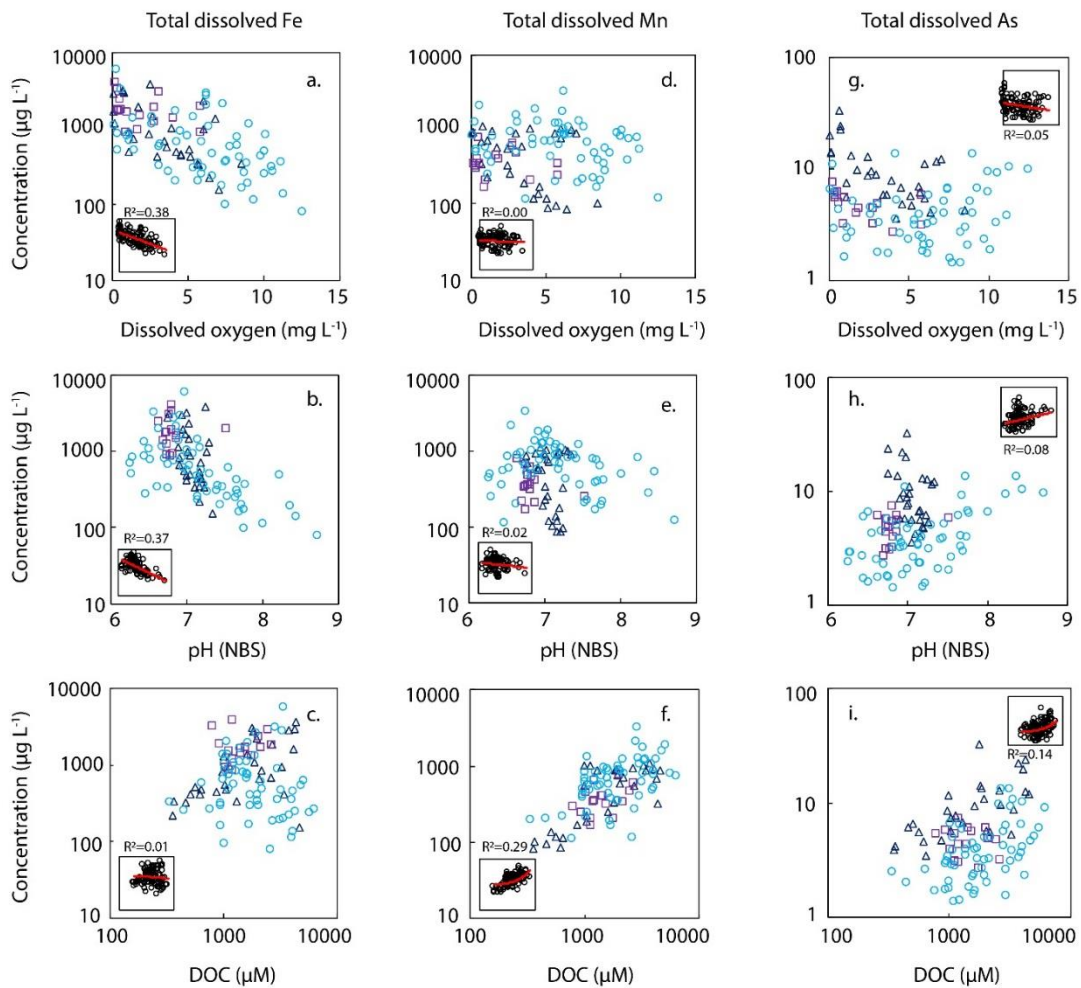


**Figure 3-6. Trace metal geochemistry.**

Island drainage total dissolved Fe, Mn, and As concentrations versus (a, d, g) dissolved oxygen, (b, e, h) pH, and (c, f, i) DOC for all 16 months of sampling across WY 2017 and WY 2018. Inset figures show cumulative  $R^2$  value when considering all sites. Light blue circles, dark blue triangles, and purple squares represent drainage sites on Sherman, Staten, and Twitchell islands, respectively.

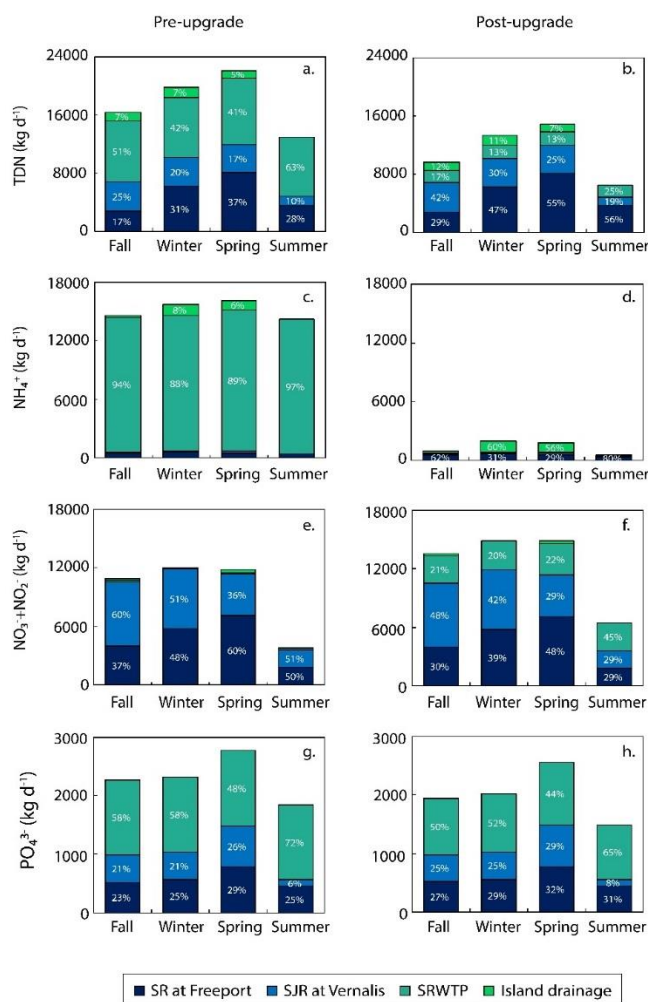


**Figure 3-7. Pre- and post-upgrade regional dissolved N and P fluxes.**

Calculated mean seasonal contributions (kg d<sup>-1</sup>) to the Delta under (a-d) pre-upgrade and (e-h) post-upgrade conditions. Fluxes were calculated using flow and generally monthly concentration data from WY 2018. River sites had some months of missing data, depending on species, and, as such, we present these fluxes as baseline seasonal estimates for WY 2018, a dry year. Pre-upgrade PO<sub>4</sub><sup>3-</sup> fluxes at SRWTP were calculated from three months (Oct-17 to Dec-17) of data in WY 2018 due to limited concentration data, and the decrease in PO<sub>4</sub><sup>3-</sup> fluxes across upgrade scenarios for SRWTP is likely a residual effect of bias in the WY 2018 mean as SRWTP PO<sub>4</sub><sup>3-</sup> fluxes are not expected to change significantly. See Table S4 for percentages.

**Table 3-1. Mean annual river and island drainage geochemistry.**

WY 2018 mean and standard deviation of river and island drainage geochemistry collected monthly between Oct-17 and Sept-18. WY 2017 data are not included so as not to bias the annual mean. \*SH-P4 water year data is incomplete as data collected during net zero discharge months was not included.

		Rivers	SH-P2	SH-P3	SH-P4*	SH-P5	ST-P1	ST-P2	TW-P1
TN ( $\mu\text{M}$ )	mean	65	384	466	230	327	347	366	226
	stdev	46	74	97	115	62	110	134	13
TDN ( $\mu\text{M}$ )	mean	56	183	272	168	113	188	262	128
	stdev	25	87	136	52	44	105	155	49
NO <sub>3</sub> <sup>-</sup> ( $\mu\text{M}$ )	mean	20.9	8.5	22.1	11.8	10.9	45.8	33.0	9.3
	stdev	11.3	10.6	47.4	9.4	5.3	53.9	64.9	7.9
NO <sub>2</sub> <sup>-</sup> ( $\mu\text{M}$ )	mean	0.8	1.5	1.9	0.6	1.0	3.3	2.3	1.1
	stdev	0.5	2.2	1.8	0.1	0.6	3.5	1.8	0.6
NH <sub>4</sub> <sup>+</sup> ( $\mu\text{M}$ )	mean	5.7	53.3	56.4	39.2	24.3	29.1	48.4	35.6
	stdev	4.8	56.4	58.2	18.8	12.6	19.8	23.3	20.2
DON ( $\mu\text{M}$ )	mean	29	119	192	113	75	107	174	80
	stdev	27	35	105	48	32	67	109	40
PON ( $\mu\text{M}$ )	mean	8	218	210	53	204	175	129	105
	stdev	7	28	28	28	49	86	53	51
SiO <sub>4</sub> <sup>4-</sup> ( $\mu\text{M}$ )	mean	250	310	440	790	670	510	540	500
	stdev	60	120	100	60	130	140	170	110
PO <sub>4</sub> <sup>3-</sup> ( $\mu\text{M}$ )	mean	1.7	1.0	1.8	2.5	2.4	2.2	1.6	3.1
	stdev	0.6	0.8	1.3	1.6	0.8	1.9	1.2	1.3
As ( $\mu\text{g L}^{-1}$ )	mean	1.6	3.1	6.1	3.8	2.4	8.5	13.5	4.8
	stdev	0.5	1.2	3.0	3.3	0.8	3.3	9.2	1.4
Mn ( $\mu\text{g L}^{-1}$ )	mean	30	1120	860	780	620	640	600	430
	stdev	30	820	550	710	250	350	380	180
Fe ( $\mu\text{g L}^{-1}$ )	mean	60	820	310	1820	1030	1020	1650	2020
	stdev	60	830	200	2060	740	770	1230	1000
$\delta^{15}\text{N}$ - PON (‰)	mean	4.9	3.0	3.3	0.1	-0.1	3.2	2.4	1.6
	stdev	2.1	3.4	3.2	3.0	0.5	0.9	1.5	1.4
$\delta^{15}\text{N}$ - DON (‰)	mean	1.8	0.1	1.8	0.9	0.3	1.7	1.6	1.8
	stdev	2.1	2.1	2.3	0.4	1.0	0.7	0.5	1.7
$\delta^{15}\text{N}$ - NH <sub>4</sub> <sup>+</sup> (‰)	mean	9.9	9.0	9.8	9.3	9.0	11.9	11.2	10.3
	stdev	5.6	4.3	2.3	1.4	1.8	1.7	2.3	2.4
$\delta^{15}\text{N}$ -NO <sub>3</sub> <sup>-</sup> (‰)	mean	7.0	4.7	3.5	5.2	4.0	12.8	15.2	3.8
	stdev	1.4	3.4	2.3	7.5	1.7	6.6	6.7	3.9
$\delta^{18}\text{O}$ - NO <sub>3</sub> <sup>-</sup> (‰)	mean	-2.8	4.9	6.1	3.4	-1.8	5.9	4.8	2.5
	stdev	3.4	6.4	8.1	7.0	2.1	6.1	6.5	4.3

**Table 3-2. Seasonal gross and net fluxes of nutrients and trace metals from island drainage.**

Seasonal gross and net island drainage nutrient and trace metal fluxes for each island for WY 2018.

	Season	TN	TDN	NO <sub>3</sub> <sup>-</sup> +NO <sub>2</sub> <sup>-</sup>	NH <sub>4</sub> <sup>+</sup>	DON	PON	SiO <sub>4</sub> <sup>4-</sup>	PO <sub>4</sub> <sup>3-</sup>	As	Mn	Fe
Gross		kg d <sup>-1</sup>	kg d <sup>-1</sup>	kg d <sup>-1</sup>	kg d <sup>-1</sup>	kg d <sup>-1</sup>	kg d <sup>-1</sup>	kg d <sup>-1</sup>	kg d <sup>-1</sup>	kg d <sup>-1</sup>	kg d <sup>-1</sup>	kg d <sup>-1</sup>
<b>Sherman</b>	Fall	140	90	3	10	80	50	370	2	0.1	20	20
	Winter	320	200	30	60	110	110	820	2	0.2	60	40
	Spring	340	150	10	50	80	190	660	2	0.2	70	50
	Summer	70	20	1	2	20	50	150	1	0.1	10	10
<b>Staten</b>	Fall	150	60	10	10	50	80	260	2	0.2	10	20
	Winter	170	140	30	30	80	30	610	1	0.4	30	80
	Spring	250	110	40	30	40	140	550	1	0.3	30	20
	Summer	230	100	30	20	60	130	860	7	0.5	10	40
<b>Twitchell</b>	Fall	110	70	2	10	50	40	460	4	0.2	20	70
	Winter	200	120	10	40	70	80	820	5	0.2	20	110
	Spring	90	60	8	20	40	20	570	3	0.1	20	50
	Summer	130	60	3	10	40	70	440	5	0.3	10	100
<b>Net</b>												
<b>Sherman</b>	Fall	70	30	-20	0	30	40	-230	-3	0.0	20	20
	Winter	280	170	10	60	100	110	520	0	0.1	60	40
	Spring	230	50	-30	50	30	180	-80	-5	0.0	60	40
	Summer	-70	-90	-40	-20	-30	20	-1160	-10	-0.4	0	0
<b>Staten</b>	Fall	140	60	10	10	40	80	190	1	0.2	10	20
	Winter	180	150	30	30	80	30	590	1	0.4	30	80
	Spring	190	50	20	20	10	140	60	-3	0.1	30	20
	Summer	60	-30	-30	0	0	100	-680	-7	0.0	10	30
<b>Twitchell</b>	Fall	40	30	-10	10	20	40	100	1	0.1	20	70
	Winter	90	70	-10	40	50	70	350	2	0.1	20	110
	Spring	20	10	-10	10	10	20	150	-1	0.0	20	50
	Summer	10	-10	-20	0	10	50	-370	-2	0.0	10	100

**Table 3-3. Upscaled Delta-wide drainage nutrient and trace metal contributions.**

Delta-wide island drainage flux estimates compared to river flux onto islands for WY 2018 (pre-SRWTP upgrade). Annual load was calculated as the cumulative sum of monthly loads.

	<b>Annual island drainage load</b> (kg)	<b>Island drainage efflux off islands</b> (kg d <sup>-1</sup> )	<b>River influx onto islands</b> (kg d <sup>-1</sup> )	<b>Mean annual net flux</b> (kg d <sup>-1</sup> )	<b>Annual net load</b> (kg)
<b>TN</b>	2.7 x 10 <sup>6</sup>	7390	2880	4510	1.6 x 10 <sup>6</sup>
<b>TDN</b>	1.5 x 10 <sup>6</sup>	4240	2550	1690	6.2 x 10 <sup>5</sup>
<b>NO<sub>3</sub><sup>-</sup>+NO<sub>2</sub><sup>-</sup></b>	3.3 x 10 <sup>5</sup>	910	960	-50	-1.7 x 10 <sup>4</sup>
<b>NH<sub>4</sub><sup>+</sup></b>	3.0 x 10 <sup>5</sup>	830	240	590	2.1 x 10 <sup>5</sup>
<b>DON</b>	9.1 x 10 <sup>5</sup>	2500	1210	1280	4.7 x 10 <sup>5</sup>
<b>PON</b>	1.1 x 10 <sup>6</sup>	3150	330	2820	1.0 x 10 <sup>6</sup>
<b>SiO<sub>4</sub><sup>4-</sup></b>	7.6 x 10 <sup>6</sup>	20770	21210	-450	-1.6 x 10 <sup>5</sup>
<b>PO<sub>4</sub><sup>3-</sup></b>	2.8 x 10 <sup>4</sup>	80	150	-80	-2.8 x 10 <sup>4</sup>
<b>As</b>	4.4 x 10 <sup>3</sup>	10	0	10	2.6 x 10 <sup>3</sup>
<b>Mn</b>	3.7 x 10 <sup>5</sup>	1010	70	930	3.4 x 10 <sup>5</sup>
<b>Fe</b>	5.9 x 10 <sup>5</sup>	1620	200	1420	5.2 x 10 <sup>5</sup>

**Table 3-4. Upscaled Delta-wide seasonal gross and net island drainage fluxes into the Delta.**

Upscaled Delta-wide seasonal mean island drainage gross and net fluxes. The percentage of each seasonal flux relative to the total annual flux is shown in parenthesis.

	<b>Fall</b> (kg d <sup>-1</sup> )	<b>Winter</b> (kg d <sup>-1</sup> )	<b>Spring</b> (kg d <sup>-1</sup> )	<b>Summer</b> (kg d <sup>-1</sup> )
<b>Gross</b>				
TN	3800 (23%)	7030 (38%)	4500 (27%)	1630 (13%)
TDN	520 (22%)	1500 (41%)	1270 (27%)	380 (10%)
NO <sub>3</sub> <sup>-</sup> +NO <sub>2</sub> <sup>-</sup>	360 (14%)	1500 (41%)	1190 (35%)	270 (10%)
NH <sub>4</sub> <sup>+</sup>	2930 (11%)	4040 (45%)	2040 (36%)	980 (8%)
DON	3800 (29%)	7030(40%)	4500 (20%)	1630(10%)
PON	2990 (24%)	4070 (32%)	3330 (26%)	2210 (18%)
SiO <sub>4</sub> <sup>4-</sup>	14930 (18%)	31890 (38%)	22750 (27%)	13500 (16%)
PO <sub>4</sub> <sup>3-</sup>	70 (23%)	70 (23%)	50 (18%)	110 (36%)
As	10 (21%)	20 (39%)	10 (23%)	10 (17%)
Mn	770 (19%)	1620 (40%)	1430 (35%)	200 (5%)
Fe	1200 (19%)	3390 (52%)	1200 (19%)	670 (10%)
<b>Net</b>				
TN	4860 (27%)	6300 (35%)	5030 (28%)	1850 (10%)
TDN	2120 (31%)	2670 (40%)	2020 (30%)	-60 (-1%)
NO <sub>3</sub> <sup>-</sup> +NO <sub>2</sub> <sup>-</sup>	-160 (87%)	-100 (57%)	290 (-161%)	-210 (117%)
NH <sub>4</sub> <sup>+</sup>	160 (7%)	1180 (51%)	1000 (43%)	0 (0%)
DON	1880 (37%)	2360 (46%)	740 (14%)	150 (3%)
PON	2740 (24%)	3620 (32%)	3000 (27%)	1910 (17%)
SiO <sub>4</sub> <sup>4-</sup>	50 (-3%)	-420 (24%)	3930 (-219%)	-5340 (299%)
PO <sub>4</sub> <sup>3-</sup>	-50 (15%)	-120 (37%)	-100 (31%)	-50 (17%)
As	10 (25%)	10 (47%)	10 (21%)	0 (6%)
Mn	730 (20%)	1550 (42%)	1320 (35%)	130 (4%)
Fe	1150 (20%)	3110 (55%)	900 (16%)	530 (9%)

## Supplemental Index

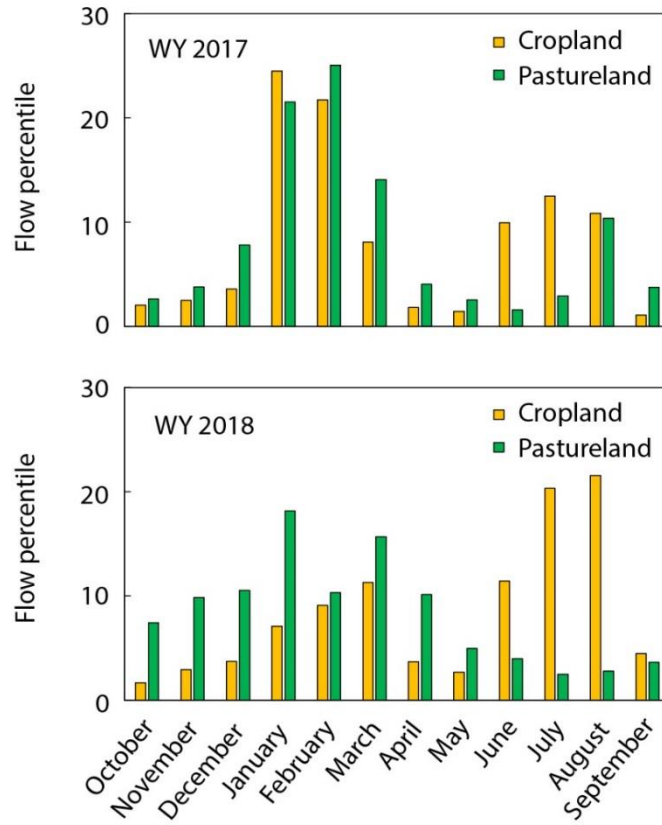


**Figure S1.** Flow percentiles for pastureland and cropland dominated islands for (a) WY 2017 and (b) WY 2018. Sherman Island was used to represent pastureland dominated islands, and Staten Island was used to represent cropland dominated islands.

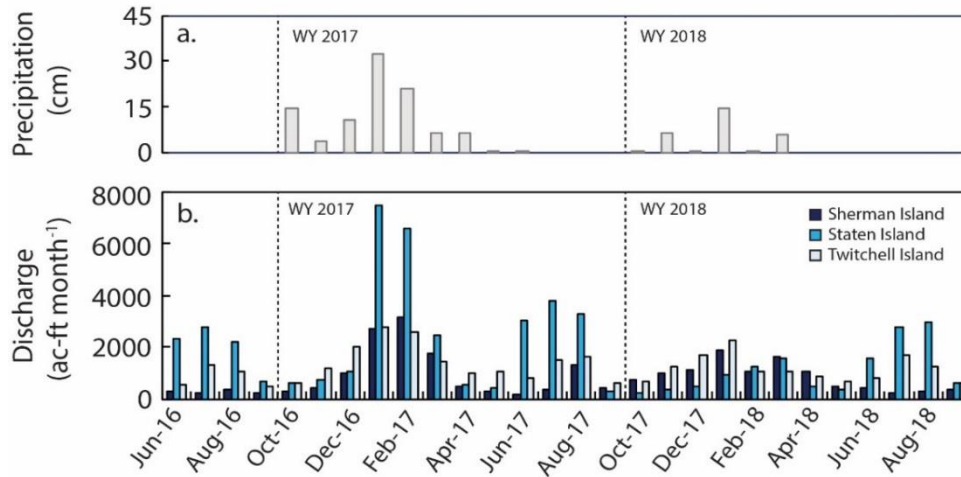


**Figure S2.** (a) Monthly precipitation and (b) discharge from Sherman, Staten, and Twitchell islands. Precipitation data was acquired from Station 242 via the California Irrigation Management Information System (CIMIS). Discharge data was determined using the unit-power consumption method and cross-checked with measured flow meter estimates.

**Table S1.** Regression strength for upscaled TDN versus PON estimates for filling in monthly PON data for drainage and inflow.

	<b>Regression</b>
<b>Drainage - Sherman</b>	$y=0.35x+1460, R^2 = 0.77$
<b>Drainage - Staten</b>	$y=0.59x+1380, R^2 = 0.91$
<b>Inflow - Sherman</b>	$y=0.09x+80, R^2 = 0.86$
<b>Inflow - Staten</b>	$y=0.08x+110, R^2 = 0.46$

**Table S2.** WY 2017 and WY 2018 water budget estimates.

	<b>Inflow</b> (ac-ft yr <sup>-1</sup> )	<b>Outflow</b> (ac-ft yr <sup>-1</sup> )	<b>ET</b> (ac-ft yr <sup>-1</sup> )	<b>Precipitation</b> (ac-ft yr <sup>-1</sup> )	<b>Inflow to Outflow Ratio</b>
WY 2017					
Sherman	30700	12700	34500	16410	2.4
Staten	25100	30420	23400	28700	0.8
Twitchell	28000	17500	15200	4700	1.6
WY 2018					
Sherman	38600	10600	37300	9200	3.6
Staten	28600	13800	23700	8900	2.1
Twitchell	25900	14200	15400	3600	1.8

**Table S3.** A comparison of existing box model estimates for total nitrogen [TN], ammonium [NH<sub>4</sub><sup>+</sup>], and phosphate [PO<sub>4</sub><sup>3-</sup>] annual loads into (IN) and out (OUT) of the Delta.

		<b>SFEI<sup>1</sup></b> (kg)	<b>DSM2<sup>1</sup></b> (kg)	<b>EPA<sup>2</sup></b> (kg)
<b>TN</b>	IN - Rivers	1.3 x 10 <sup>7</sup>	1.4 x 10 <sup>7</sup>	1.8 x 10 <sup>7</sup>
	IN - Island Drainage*	2.7 x 10 <sup>6</sup>	2.7 x 10 <sup>6</sup>	2.7 x 10 <sup>6</sup>
	IN - POTW	6.9 x 10 <sup>5</sup>	7.7 x 10 <sup>5</sup>	n.a.
	OUT - Water Exports	6.3 x 10 <sup>6</sup>	5.9 x 10 <sup>6</sup>	6.0 x 10 <sup>6</sup>
	OUT - River Inflow onto Islands*	1.1 x 10 <sup>6</sup>	1.1 x 10 <sup>6</sup>	1.1 x 10 <sup>6</sup>
	OUT - Suisun	3.7 x 10 <sup>6</sup>	4.7 x 10 <sup>6</sup>	6.7 x 10 <sup>6</sup>
	<b>IN - Total</b>	1.6 x 10 <sup>7</sup>	1.8 x 10 <sup>7</sup>	2.0 x 10 <sup>7</sup>
	<b>OUT - Total</b>	1.1 x 10 <sup>7</sup>	1.2 x 10 <sup>7</sup>	1.4 x 10 <sup>7</sup>
	<b>Missing (IN - OUT)</b>	32%	34%	32%
<b>NH<sub>4</sub><sup>+</sup></b>	IN - Rivers	3.6 x 10 <sup>6</sup>	4.6 x 10 <sup>6</sup>	n.a.
	IN - Island Drainage*	3.0 x 10 <sup>5</sup>	3.0 x 10 <sup>5</sup>	n.a.
	IN - POTW	7.3 x 10 <sup>4</sup>	1.5 x 10 <sup>5</sup>	n.a.
	OUT - Water Exports	2.9 x 10 <sup>5</sup>	2.6 x 10 <sup>5</sup>	n.a.
	OUT - River Inflow onto Islands*	8.8 x 10 <sup>4</sup>	8.8 x 10 <sup>4</sup>	n.a.
	OUT - Suisun	1.0 x 10 <sup>6</sup>	2.9 x 10 <sup>5</sup>	n.a.
	<b>IN - Total</b>	4.0 x 10 <sup>6</sup>	5.1 x 10 <sup>6</sup>	n.a.
	<b>OUT - Total</b>	1.4 x 10 <sup>6</sup>	6.4 x 10 <sup>5</sup>	n.a.
	<b>Missing (IN - OUT)</b>	65%	88%	n.a.

<sup>1</sup>Estimates from Novick et al. (2015)

<sup>2</sup>Estimates from TetraTech (2006)

**Table S4.** Calculated mean seasonal contributions as a percent of the total seasonal contribution to the Delta from the Sacramento River (SR) at Freeport, the San Joaquin River at Vernalis (SJR), net island drainage, and SRWTP under pre-upgrade and post-upgrade conditions. See Figure 7 for graphical version. Post-upgrade SRWTP fluxes, used to calculate percentages, were based on predicted effluent concentrations available from LWA (2014). SRWTP only reports TP, but existing data show PO<sub>4</sub><sup>3-</sup> is over 95% of TP generally.

	Season	SR at Freeport	SJR at Vernalis	Island Drainage	SRWTP
<b>Pre-upgrade</b>					
<b>TDN</b>	Fall	17%	25%	7%	51%
	Winter	31%	20%	7%	42%
	Spring	37%	17%	5%	41%
	Summer	28%	10%	0%	63%
<b>NH<sub>4</sub><sup>+</sup></b>	Fall	4%	1%	1%	94%
	Winter	4%	1%	8%	88%
	Spring	3%	1%	6%	89%
	Summer	3%	0%	0%	97%
<b>NO<sub>3</sub><sup>-</sup>+NO<sub>2</sub><sup>-</sup></b>	Fall	37%	60%	1%	2%
	Winter	48%	51%	-1%	1%
	Spring	60%	36%	2%	1%
	Summer	50%	51%	-6%	5%
<b>PO<sub>4</sub><sup>3-</sup></b>	Fall	23%	21%	-2%	58%
	Winter	25%	21%	-5%	58%
	Spring	29%	26%	-4%	48%
	Summer	25%	6%	-3%	72%
<b>Post-upgrade</b>					
<b>TDN</b>	Fall	29%	42%	12%	17%
	Winter	47%	30%	11%	13%
	Spring	55%	25%	7%	13%
	Summer	56%	19%	-1%	25%
<b>NH<sub>4</sub><sup>+</sup></b>	Fall	62%	12%	19%	8%
	Winter	31%	6%	60%	4%
	Spring	29%	11%	56%	4%
	Summer	80%	6%	0%	14%
<b>NO<sub>3</sub><sup>-</sup>+NO<sub>2</sub><sup>-</sup></b>	Fall	30%	48%	1%	21%
	Winter	39%	42%	-1%	20%
	Spring	48%	29%	2%	22%
	Summer	29%	29%	-3%	45%
<b>PO<sub>4</sub><sup>3-</sup></b>	Fall	27%	25%	-2%	50%
	Winter	29%	25%	-6%	52%
	Spring	32%	29%	-4%	44%
	Summer	31%	8%	-4%	65%

## **CONCLUSIONS**

This dissertation presents three studies on hydrological and biogeochemical processes in riverine and estuarine systems of central California. Broadly, results from these chapters show how multi-tracer datasets are informative for understanding both water movement and related biogeochemical processes in complex environments.

Integrating our understanding of hydrological and biogeochemical processes is critical to improving on current water resources management strategies.